To the Graduate Council:

I am submitting herewith a thesis written by Thomas W. Wise entitled "Significance of Solution Cleavage in the Chapman Ridge Anticline, Tennessee". I recommend that it be accepted in partial fulfillment of the requirements for the degree of Master of Science, with a major in Geology.

D. H. Roeder
Major Professor

We have read this thesis and recommend its acceptance:

Fred B. Keller

John B. Higgins

Accepted for the Council:

L. Evans Roth

Vice Chancellor
Graduate Studies and Research

SIGNIFICANCE OF SOLUTION CLEAVAGE IN THE CHAPMAN RIDGE ANTICLINE, TENNESSEE

A Thesis

Presented for the

Master of Science

Degree

The University of Tennessee, Knoxville

Thomas W. Wise

December 1980

ACKNOWLEDGMENTS

I wish to express my sincere gratitude to Dr. Dieterich H. Roeder, Professor of Geology, for his guidance and friendship. A special thanks is also extended to my committee members, Dr. Higgins and Dr. Keller for all their time and helpful advice in the preparation of this paper. Funding for this thesis was provided by the National Science Foundation.

ABSTRACT

The Lenoir Limestone of Middle Ordovician age contains a coarse set of axial planar solution cleavage exposed in the Chapman Ridge anticline southeast of Knoxville, Tennessee. Three scales of folding are recognized in the anticline: F_1 domal warping, F_2 parasitic folding and F_3 internal folding. F_1 and F_2 folds are externally rotated by F_3 folding. Cleavage is axial planar to each level of folding and demonstrates progressive deformation and preservation through rotation. Distribution of cleavage within the F_1 anticline is inhomogeneous. Cleavage develops in four intensity types (none, low, moderate, high) on the basis of its qualitative attributes and its mean spacing. Shortening can be determined from thin section analysis and reaches 50% in rocks with "high" cleavage intensities. Examination of cleavage intensity demonstrates a fold controlled stress distribution. Cleavage is not found in similar outcrops of Lenoir which have undergone simple thrusting without folding. Regional placement of solution cleavage is with frontal zone fabrics of a polyphase folded fault system. Overprinting of fold controlled cleavage by the emplacement of the Dumplin Valley thrust sheet conclusively places the Dumplin Valley fault kinematically younger than domal warping of the F_1 anticline.

TABLE OF CONTENTS

LIST OF TABLES

LIST OF FIGURES

FIGURE PAGE

FIGURE PAGE

LIST OF PLATES

CHAPTER I

INTRODUCTION

"Pressure solution" by definition is a purely diffusive mass transfer (Elliott, 1973), as opposed to a dislocation mass transfer, wherein shear forces alter the shape of grains (Figure 1). The general idea that crystals dissolve in areas of large compressive stress, with migration and reprecipitation in areas of lower stress, was first documented with good thin section evidence by Sorby (1863). Elliott (1973) called the mechanics of this particle migration "diffusion creep". A reflection of selective dissolution and reprecipitation is evident in a type of cleavage known as "pressure solution cleavage" or simply "solution cleavage".

Cleavage of this type is generally found to occur perpendicular to the maximum compressive strain axis λ_3 (Dieterich, 1969) and in most cases perpendicular to the maximum stress axis, σ_1, (Groshong, 1975). Cleavage oriented perpendicular to λ_3 and not at angles approaching 45°, as would be expected in shear fractures, is used as evidence documenting the occurrence of solution transfer. Also used as evidence of a dissolution origin of this cleavage is the occurrence of truncated or bisected fossils with shortening evident perpendicular to cleavage selvages. The selvages themselves are interpreted by Groshong (1975) and others as insoluble residual material. These clay selvages mark boundaries of dissolution surfaces which might otherwise go unnoticed. The lack of cataclastic boundaries along truncated fabrics (as would occur if the cleavage had a shear origin) is also cited in support of solution transfer.

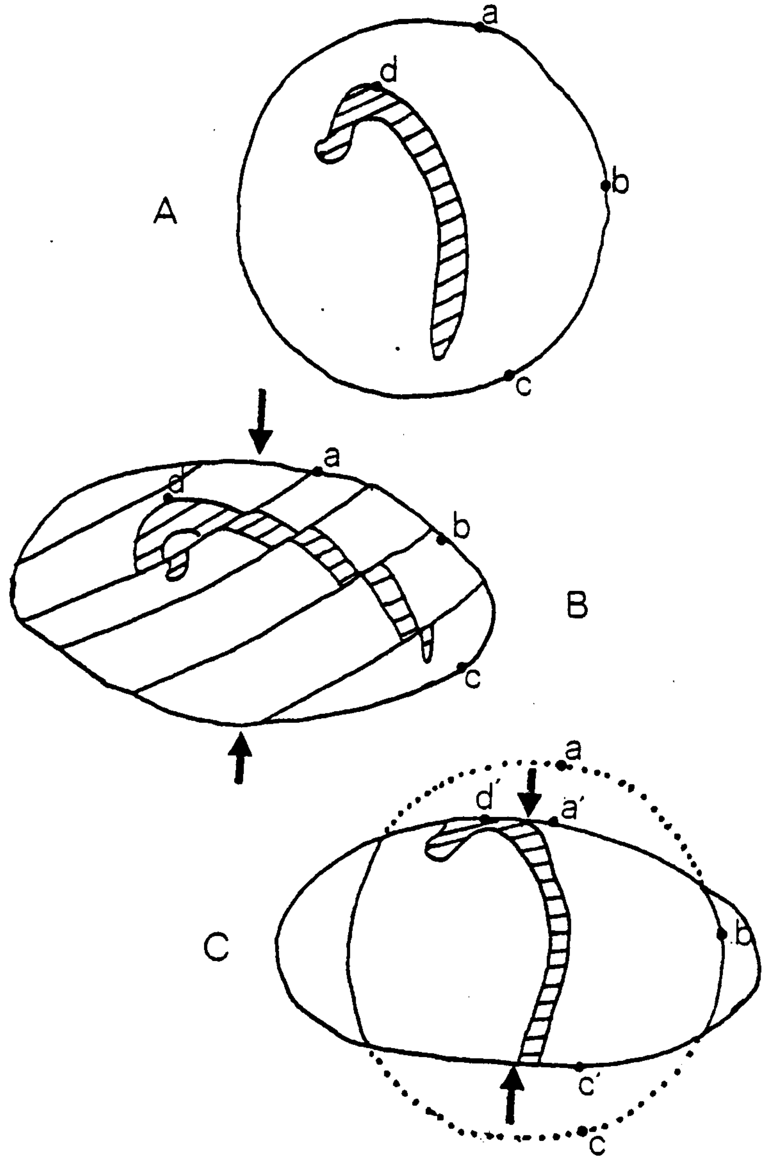

Figure 1. Illustration of dislocation mass transfer and diffusion mass transfer.

A. Undeformed grain with trilobite fragment and marker points a, b, c and d.

B. Deformation by dislocation mass transfer. No mass loss has occurred.

C. Deformation by diffusion mass transfer. Note a, c and d have been displaced by residuals a', c' and d'.

Arrows indicate direction of maximum stress (modified from Elliott, 1973).

Study of rock fabrics can be conducted along three size scales: microscopic, which concentrates on characteristics visible only with the aid of a microscope; mesoscopic, which deals with outcrop or hand speciment size fabrics; and megascopic, which analyses fabrics on a regional scale. All three catagories will be employed for a comprehensive understanding of solution cleavage in the study area.

On a microscopic scale, 45 thin sections were prepared from outcrops of various lithologies across the study area. Then through the use of truncated fabrics and all suitable strain markers, a finite strain analysis was performed to determine stress axes and establish a minimum finite shortening. Methods of analysis were similar to those employed by Alvarez (1976) and Gray (1979). Due to the friable nature of the lithology studied, good field samples were not obtainable from all outcrops, and impregnation was often necessary before thin sections could be made.

Throughout this text cleavage is referred to as having various levels of intensity. Ranking levels correspond with different degrees of cleavage development, and are based on a classification of solution cleavage by Alvarez (1978). The classification system proposed by Alvarez is for an argillaceous limestone, but of a much less "dirty" limestone than the Lenoir. Alvarez's classification system has, therefore, been modified for use in this study area. Parameters used for classifying solution cleavage are listed in Table 1.

Mesoscopically this investigation involved detailed field observations and analysis. Mesoscopic fabrics were plotted on a lower hemisphere equal area net (Schmidt net), and relationships were then analyzed following methods outlined in Turner and Weiss (1963).

TABLE I

CHARACTERISTICS OF SOLUTION CLEAVAGE INTENSITY TYPES

Intensity Type	Symbol	Characteristics	Average Distance Between Cleavage Planes	Shortening Due to Cleavage (Alvarez, 1978)
None	⊙	No signs of residual planes; No compressive fabrics.	0 cm	0%
Weak	●	Not immediately noticeable; Surface discrete; Suture or "stylolite" type surfaces.	5 cm	0-4%
Moderate	✪	Distinct anastomosing nature; Little calcite veining developed; Bedding is distinguishable.	1-5 cm	4-25%
High	★	Bedding distorted; often beyond recognition; Abundant calcite veins; Cleavage forms a sigmoidal pattern.	0.5 cm	>25%

Megascopically, two balanced cross sections were constructed perpendicular to the regional strike and extending from the North Carolina-Tennessee border to Pine Mountain, Tennessee (Figure 2). Correlation along strike to the north and south of the study area was done with cross sections constructed by Roeder, Gilbert and Witherspoon (1978).

A. Location

The field area lies within the Valley and Ridge province, and the focus of research is on a large sigmoidal anticline (herein termed the Chapman Ridge anticline) located near the confluence of the French Broad and Holston rivers to form the Tennessee River. The anticline is exposed extensively along Chapman Highway south of Knoxville, Tennessee and other scattered locations (Figure 3). The Chapman Ridge anticline lies between the Knoxville thrust fault to the northwest and the Dumplin Valley thrust fault to the southeast and is part of a complex folded-fault structure. Areas associated with thrusts of a different kinematic age of deformation but of the same lithologic type were also examined (Figure 3). Detailed mapping is limited to exposures in the Knoxville and Shooks Gap quadrangles.

B. Fabric

Research focused on a coarse set of axial plane fracture cleavage found in varying intensities across the anticline. Cleavage is confined stratigraphically to the Lenoir Limestone exclusive of the Mosheim Member. The Lenoir Limestone is of Middle Ordovician age. The quadrangle scale anticline, (F_1), plunges gently to the southwest. Superimposed on it is a series of megascopic folds, (F_2).

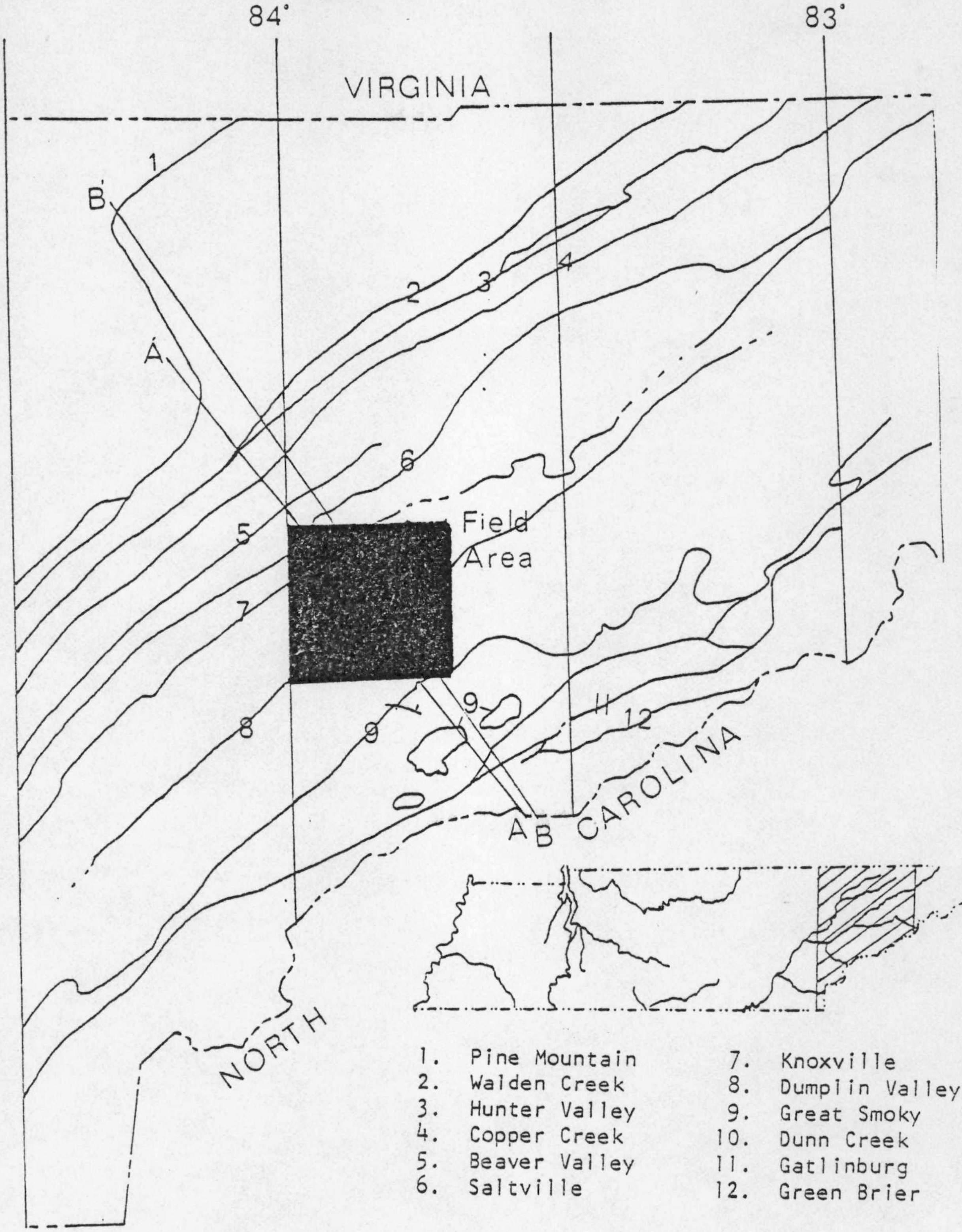

Figure 2. Location map showing field area with major faults (numbered) and profile lines (lettered).

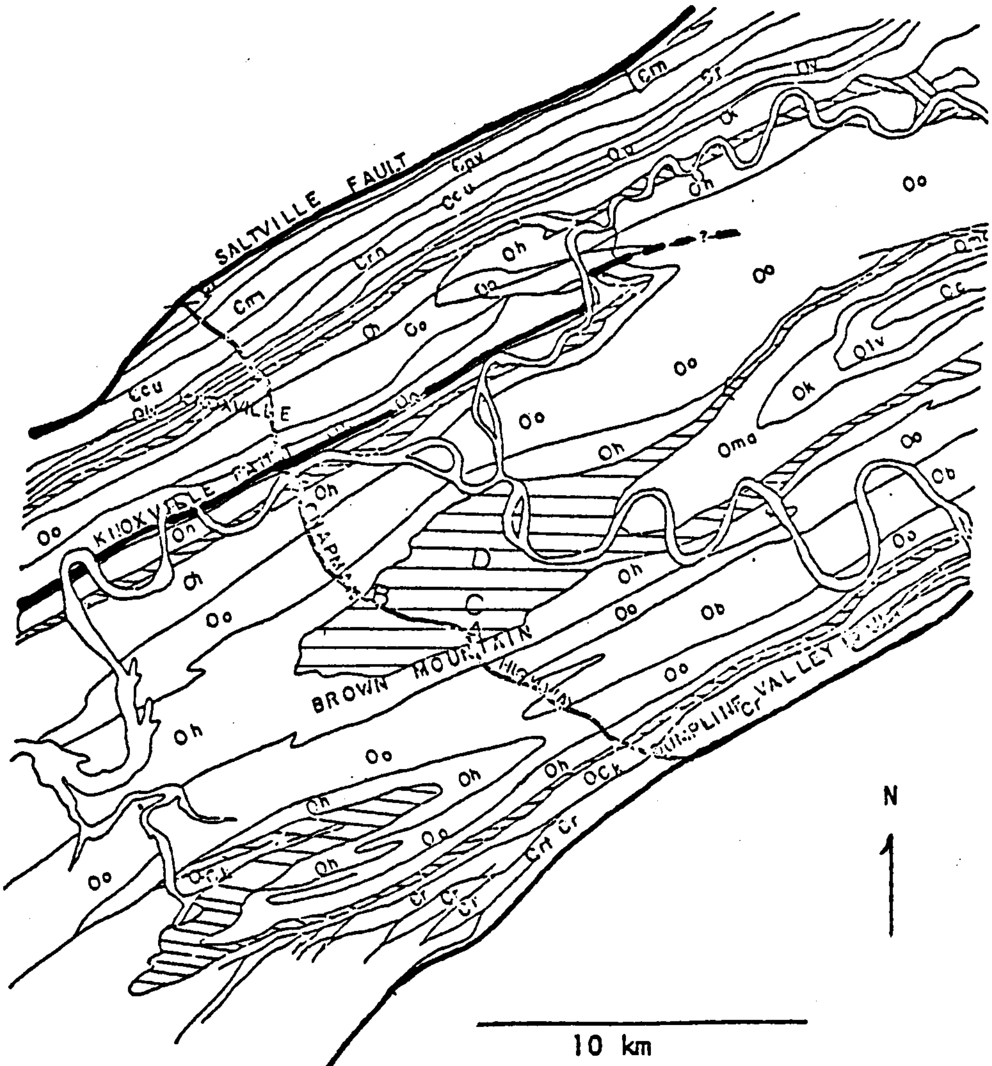

Explanation

Ordovician	Omt	Martinsburg Shale
	Oo	Ottosee Shale
	Ocr	Chapman Ridge Sandstone
	Oh	Holston Formation
	Ol	Lenoir Limestone
	On	Newala Formation
	Olv	Longview Dolomite
Cambrian	Ꞓrt	Rutledge Limestone
	Ꞓr	Rome Formation

Figure 3. Regional geologic map of the study area. Outcrops of the Lenoir Limestone are indicated by ruled areas. Letters indicate outcrops sited in the text.

The F_2 folds are of a parasitic origin and vary from tight chevron folds on the south limb to a much broader train of buckle folds across the crest of the F_1 fold. Roeder (1978) suggests the anticline is a transitional form between domal and polyphase folded-fault structures.

CHAPTER II

STRATIGRAPHIC FRAMEWORK

The regional stratigraphy of the Valley and Ridge thrust belt has been worked out and summarized to a large extent by Harris and Milici (1977). Much of the following information (See Figure 4) is taken from that paper, along with the Knoxville and Shooks Gap quadrangles (Cattermole, 1955) (Figure 4).

Figure 5 is a reconstructed stratigraphic wedge for Tennessee. The wedge was constructed by Roeder (1978) and compiled after Harris and Milici (1977) and published geologic quadrangle maps. The western end of the shelf wedge in Tennessee shows a pronounced thinning of lithologies. This end, being composed primarily of marine and non-marine clastics of Cambrian to Devonian age, is interpreted by Silberman (1971) to be of a horst and graben infilling origin. Thick accumulations of the Conasauga and Knox Group are composed of platform carbonate deposits. On the east end of the reconstruction an acute wedge of Tellico-Sevier Shale is interpreted as representative of a thin foredeep complex of Middle Ordovician age (Roeder, Gilbert and Witherspoon, 1978; Benedict and Walker, 1978).

A. Knox Group -- Ordovician System

Chepultepec Dolomite

The Cheputepec is a light colored dolomite with thinly interbedded sandstones and siltstones. It is distinguished from the Copper

			FORMATION	THICKNESS
ORDOVICIAN	MIDDLE ORDOVCIAN		BAYS FORMATION	335 m
			OTTOSEE SHALE	300m +
			CHAPMAN RIDGE SANDSTONE	0-150 m
			HOLSTON FORMATION	0-110 m
			LENOIR LIMESTONE MOSHEIM MEMBER	120-200 m 0-20 m
	LOWER ORDOVICIAN	KNOX GROUP	NEWALA FORMATION	210-300 m
			LONGVIEW DOLOMITE	110 m
			CHEPULTEPEC DOLOMITE	270-290 m

Figure 4. Generalized stratigraphic column (Cattermole, J.M., 1958).

Figure 5. Stratigraphic wedge of Tennessee and Virginia thrust belt (Roeder, Gilbert and Witherspoon, 1978).

Ridge Dolomite below by a light colored oolitic chert layer. The approximate thickness is estimated at 250-270 meters in the study area.

Longview Dolomite

The Longview Dolomite is composed of light colored, fine grained dolomite and blue limestone. It is characterized as having abundant secondary angular chert fragments formed along fracture and bedding planes. The approximate thickness is 100 meters.

Newala Formation

The Newala is a dense gray dolomite and blue-brown limestone. It is laterally equivalent to the Kingsport and ranges in thickness from 190-270 meters.

B. Middle Ordovician System

Lenoir Limestone

The Lenoir is the lower formation of a wedge of strata interpreted to be of a foredeep origin. The Lenoir is subdivided into two units: the Mosheim Member, in most areas forming the lower boundary between the Knox Group and Middle Ordovician lithologies, and the main body of the Lenoir.

Mosheim Member. The Mosheim Member of the Lenoir Limestone is a "dove-gray", fine-grained limestone and is occasionally replaced by coarse-grained limestone "marble". It varies in thickness from 0-18 meters and is found to laterally interfinger with the main body of the Lenoir.

Lenoir Limestone (Main Body). The Lenoir is an argillaceous limestone with abundant bioturbated horizons. Fresh exposures yield a mottled appearance of dark gray to brown. Abundant clay impurities in the study area are concentrated on irregular bedding surfaces which weather rapidly on exposure and give the Lenoir a distinct nodular or friable appearance. The Lower Mosheim-Lenoir boundary is distinct, but the upper Lenoir-Holston boundary is more gradational, with interbedding of sandy bioclastic and silty limestones. Thickness across the study area varies from 120-185 meters.

Holston Formation

The Holston is a coarse-grained limestone-marble. Extensive exposures at quarry sites reveal a thickness variation of the Holston from 15 to as much as 108 meters. The thickness variations are largely the result of small scale faults and lithologic variations associated with the faulting during Holston deposition.

Chapman Ridge Sandstone

The Chapman Ridge is a calcareous sandstone with interbedded shale and silty-shale layers. The thickness of the Chapman Ridge Formation varies significantly, and both gradational and sharp boundaries exist between the Chapman Ridge and Ottosee Formations. The Ottosee and Chapman Ridge Formations are found to intertongue in some areas.

Ottosee Shale

The Ottosee Shale is laterally equivalent lithologically to the Sevier-Tellico Shale to the south and is generally 340 meters in thickness. Despite the implications of the name, the Ottosee is quite heterogeneous and is composed of a mixture of shale, limestone, sandstone, marble and siltstone. The various rock types grade into and interfinger with one another both vertically and laterally throughout the Ottosee Formation. The Ottosee in the vicinity of the study area is primarily a shale or shaley limestone.

Bays Formation

The overlying Bays Formation is a sandstone to silty-mudstone and interfingers laterally with the Moccassin to form the top of the foredeep wedge.

CHAPTER III

MICROSCOPIC ANALYSIS

Methods

Microscopic examination involved the preparation of forty-five thin sections from throughout the Lenoir and neighboring lithologies. Slides were taken in three orientations to cleavage for a dimensional analysis. Slides were cut in planes parallel to cleavage and perpendicular to bedding, perpendicular to cleavage and perpendicular to bedding, and parallel to cleavage and parallel to bedding (Figure 11, page 26 Orientations perpendicular to bedding and cleavage were most useful for both strain and intensity ranking. Due to the extremly friable nature of the Lenoir, good sampling was difficult and impregnation of samples with resin was often necessary before thin sections could be prepared.

Petrology

The Lenoir Limestone within the limits of the study area is divided into two lithologically distinct parts: The Mosheim Member which rests unconformably on the Knox Group, and the main body of the Lenoir. The observed cleavage is confined to the main body of the Lenoir and does not penetrate the underlying Mosheim Member or the overlying Holston Formation.

The main body of the Lenoir Formation, herein referred to as the "Lenoir", is a silty limestone which mesoscopically shows a nodular or "mottled" appearance. Microscopically, the more consolidated nodules are composed of relatively pure, fine-grained or fossiliferous and micritic limestone and have a medium gray color. The less consolidated and thus easily weathered internodular matrix consists predominantly of clay and silt constituents, which give the rock a dark brown coloration. The lithologic variations are interpreted to be horizons of bioturbation and mark bedding in areas where cleavage has not completely destroyed it.

Cleavage

Mesoscopically, cleavage commonly appears uniformly distributed within the rock, but on a microscopic scale cleavage is distinctly heterogeneous. The cleavage planes anastomose in three dimensions and show highly variable spacing between argillaceous zones and more pure limestone nodules. Argillaceous zones, generally containing 1 to 15% subrounded quartz grains and 5 to 10% clay matrix, show a dense concentration of cleavage planes spaces 0.1 to 0.5 mm apart. Nodules contain generally less that 1% quartz, virtually no clay or mud, and have cleavage spacings from 0.45 to 1.8 mm apart.

Cleavage or selvage planes are composed of insoluble residues left after solution removal of the more soluble carbonate materials. These residual films are termed "clay carbon parting" by Nickelsen (1972). During pressure solution, dissolved calcite migrates to zones of lower compressive stress and reprecipitates in the form of veins, pressure "beards" and intergranular cement. Migration is probably of a localized nature.

Physically, selvages usually anastomose with amplitudes of 0.01 to 0.20 mm and are rarely longer than 4.5 mm. Cleavage is most pronounced as a single planar selvages and is concentrated to a greater density along boundaries of fossils or limestone nodules.

Cleavage occurs in three distinct patterns and variable spacing scales (Figure 6). Selvages are found to form a fanning pattern with

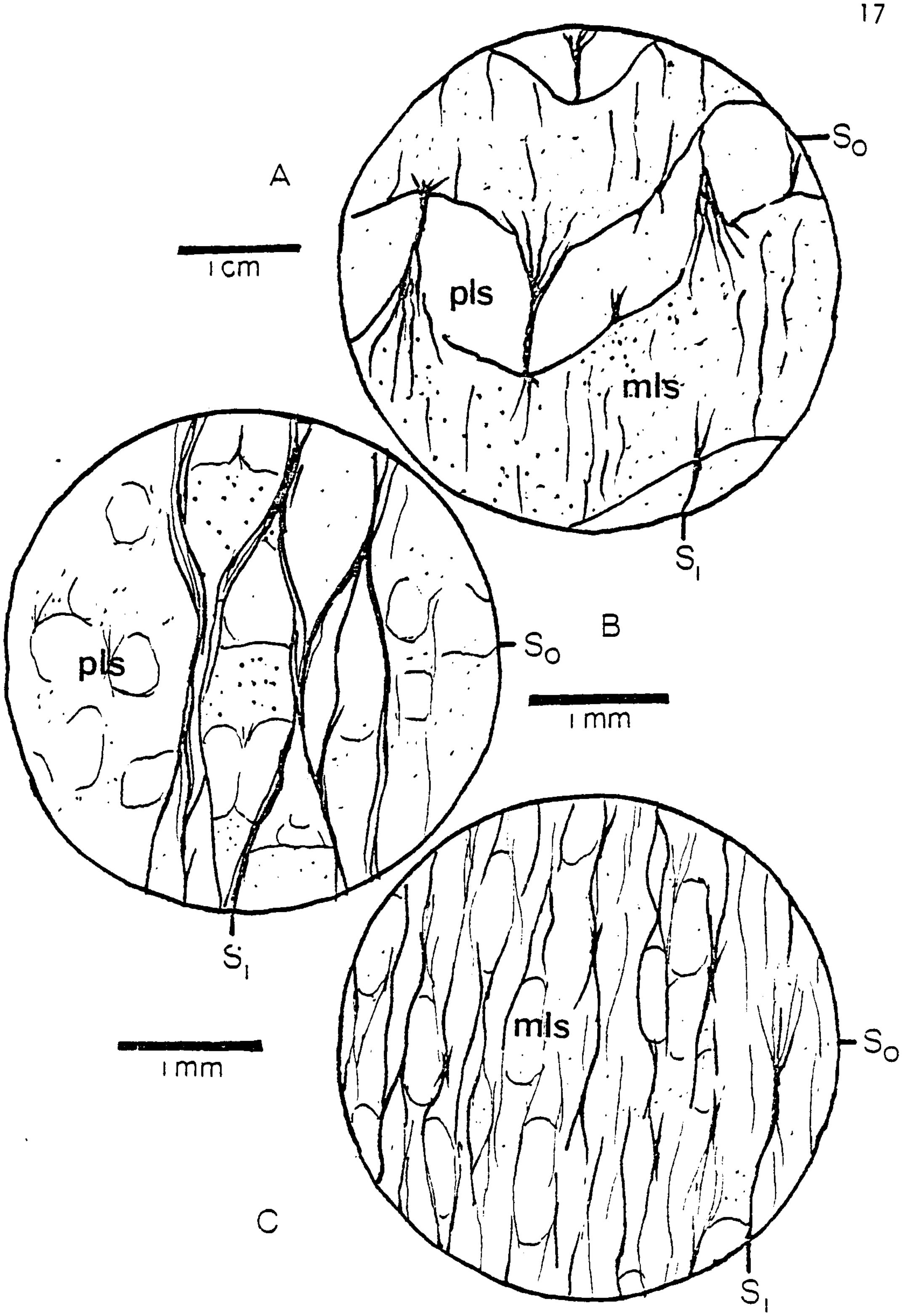

Figure 6. Three sketches of cleavage in photomicrographs.
Type 1. Fanning cleavage (S_1) in small folds of limestone rich beds (pls).
Type 2. Anastomosing cleavage around a nodular matrix.
Type 3. Equidimensional cleavage in a clay rich zone (mls).

a thick concentration of partings between nodules that splays into wider spaced but more distinct selvages within the matrix (Figures 6A, 7A). Type 2 cleavage (Figure 6B) in nodular areas develops as thick concentrations of selvages weaving between nodules in a braided fashion. As a third type, equidimensional selvages are often observed across argillaceous zones and are associated with lithologically uniform areas of the rock (Figures 6C and 7B).

Small single selvages were not found to noticably weaken the rock. However, concentrations of selvages cause breakdown of the rock. Also, it is generally noted that the greater the concentration of selvages observed microscopically, the more prominent the cleavage is in hand specimens. This observation proved valuable in contouring intensities across the study area without microscopic analysis of each outcrop.

Solution cleavage is the result of an unequal distribution of differential motion. Stress is interpreted by many (Ramsay, 1969; Nickelsen, 1972) to be oriented with the maximum compressive stress axis roughly perpendicular to cleavage planes. Nickelsen (1972) used single crystal pelmatozoan plates on a U-stage to determine principal stress axes and concluded that σ_1 is oriented perpendicular to cleavage.

Intensely cleaved areas show grains oriented with their long axes subparallel to maximum strain and often perpendicular to bedding. Similar rotational evidence is seen in both geopetal structures and orientations of the long axes of fossils. Granular rotation in argillaceous zones was observed to develop a general trend of elongate quartz grains or linear fossils oriented parallel to cleavage planes. Geiser (1974) demonstrated with rose diagrams of quartz grain orientations in cleaved zones a distinct

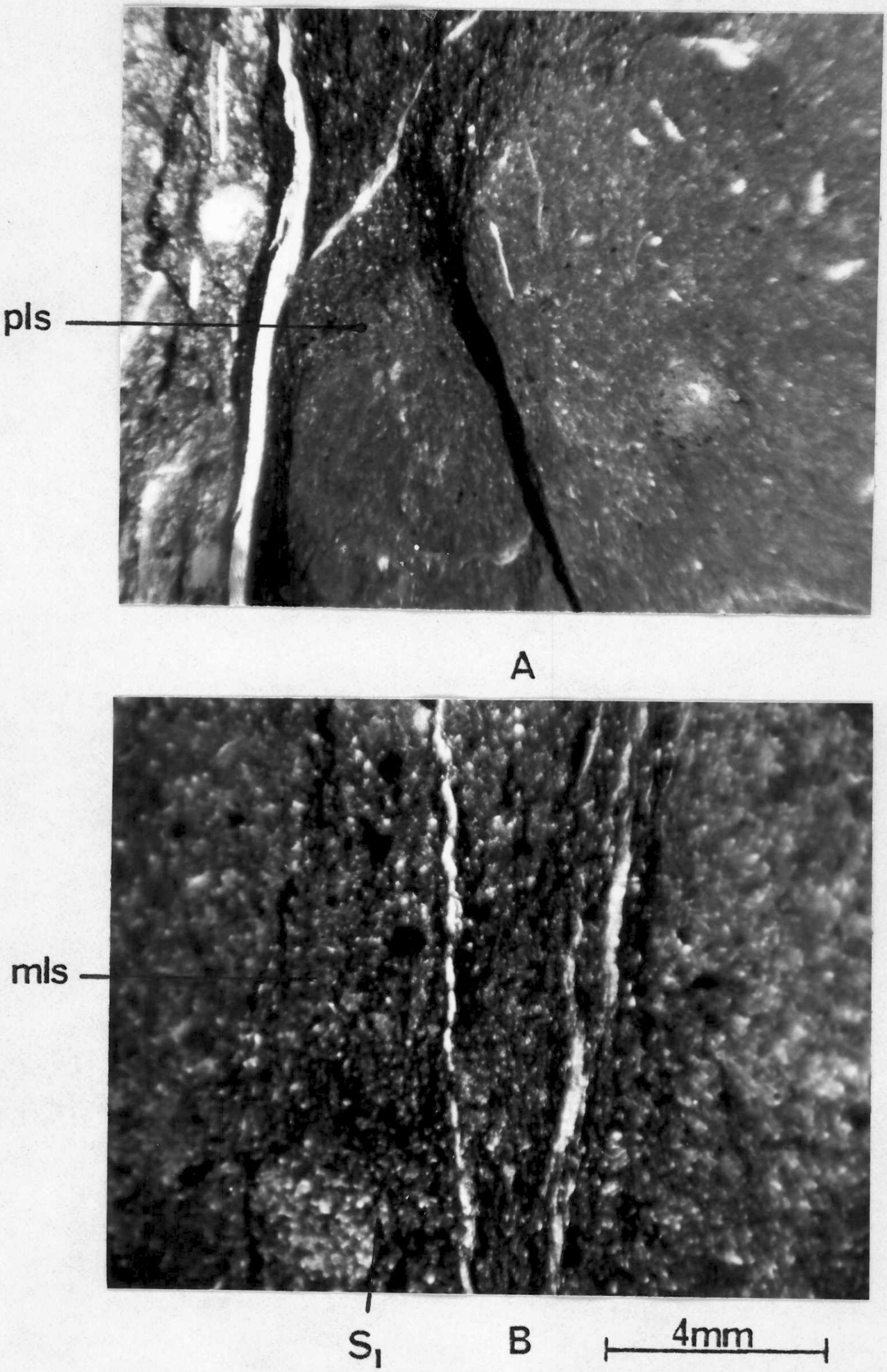

Figure 7. Photomicrographs of fanning and equidimensional selvages.

A. Photomicrograph showing fanning nature of cleavage marked by black areas. Vertical vein (white zone) is a V_2 vein and oblique vein is a V_3 vein.

B. Photomicrograph of anastomosing V_3 vein and equidimensional selvages.

lineation parallel to S_1 cleavage. (Similar analysis was not feasible in the study area.) Williams (1972) and Ramsay (1977) suggest the importance of rotation in the early development of cleavage. No alignment was observed in sections cut parallel to cleavage, which suggests a tabular shape for the strain ellipsoid. Hobbs, Means and Williams (1976, p. 27) have described this type of strain as simple or uniform flattening. Uncleaved areas show the long axis of "nodules" as parallel with bedding.

Pressure Beards

Durney and Ramsay (1973) and Elliott (1973) have all described fibrous crystal fillings, commonly referred to as pressure shadows. Several nearly circular chert nodules show a well developed set of pressure shadows or "pressure beards". Each pressure beard shows a minimum of two different extension orientations. Figure 8 illustrates a typical pressure shadow around a spherical chert mass encountered in the Lenoir. During progressive deformation the matrix is pulled away from the chert nodule along the directional line of greatest principal extension; the potential void is simultaneously filled with new crystallizing calcite. Changes in the principal incremental strain direction, therefore, lead to curving fibers of calcite which are in uniform optical continuity throughout (Ramsay, 1977). Sharp bends in crystal fibers indicate sudden changes in incremental strain, whereas smooth curves indicate a gradual change. By making measurements of the length of fibers in a specific direction and comparing these to the diameter of the chert sphere, it is possible to determine the incremental strain in specific directions (Figure 9A). All pressure beards studies in the Lenoir show fiberous crystal growth with two or three orientations of greatest principal extension. The

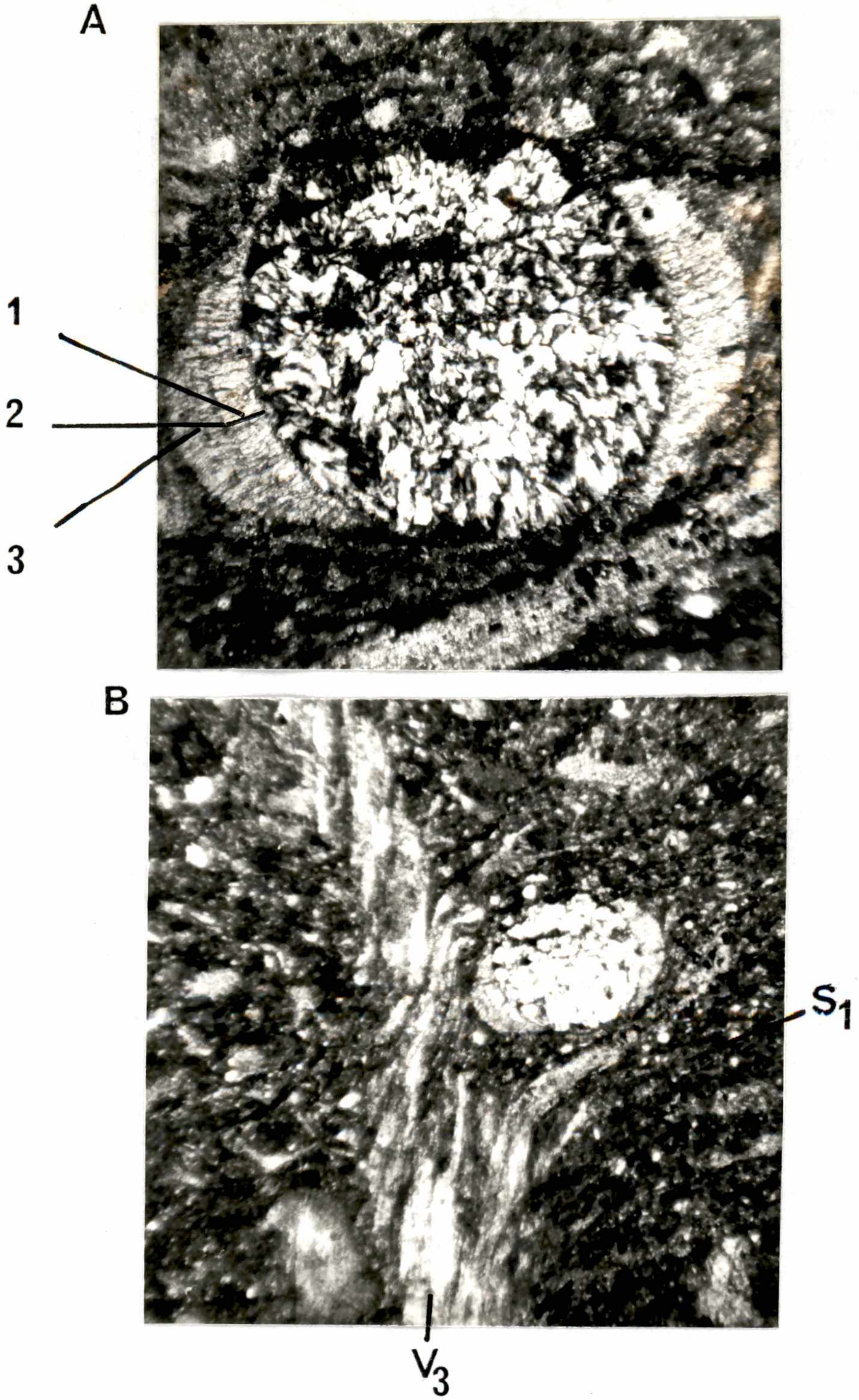

Figure 8. Photomicrographs of typical pressure shadows in the Lenoir Limestone.

A. A photomicrograph of typical pressure shadow around a chert nodule (round feature). Three distinct orientations (labled 1, 2, 3) of λ_1 are visible.

B. Photomicrograph showing relationship of chert nodule to V_3 veining. Chert nodule is .9 mm in diameter.

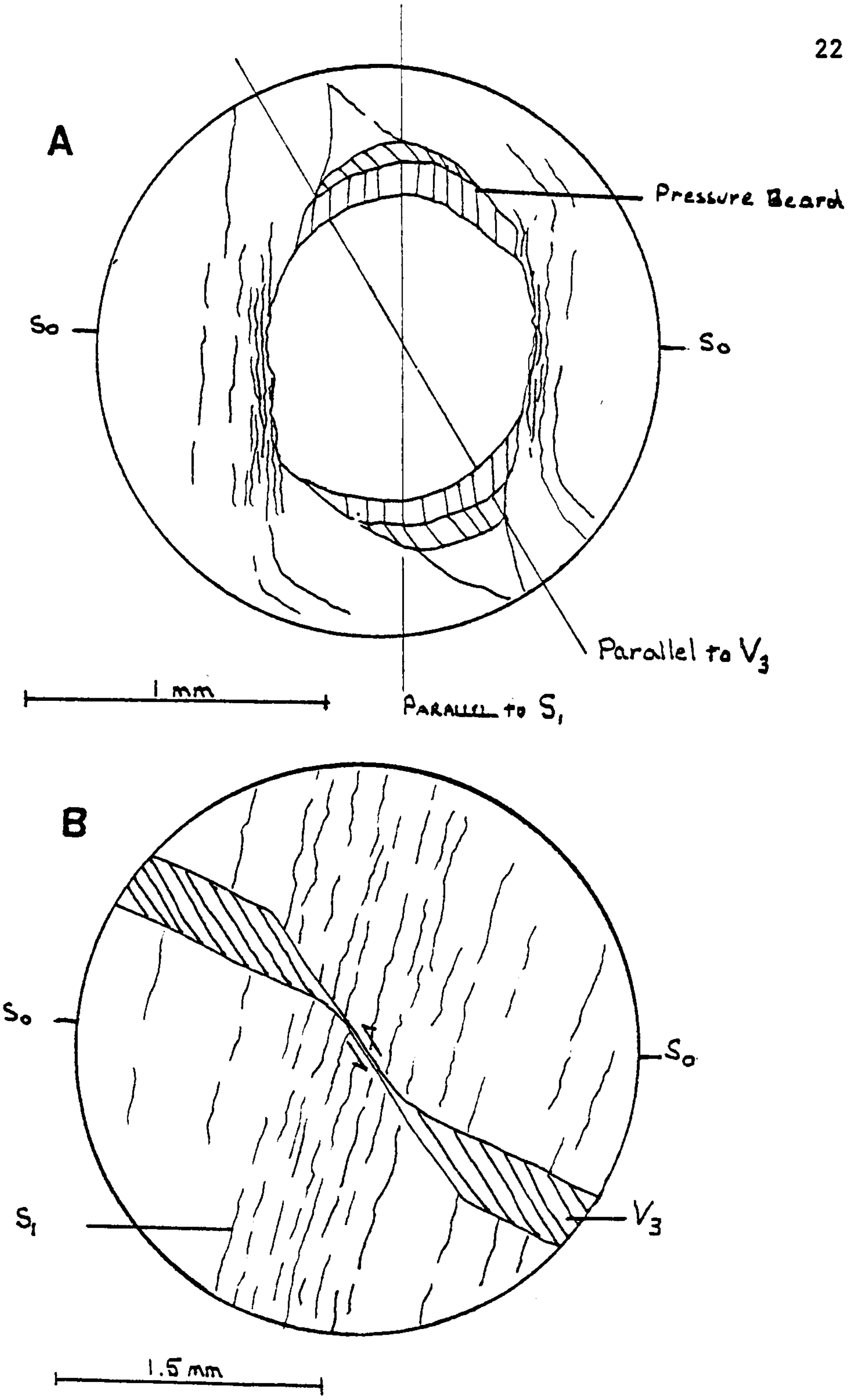

Figure 9. Two sketches of photomicrographs.

A. Sketch of a photomicrograph showing orientation of pressure beard with respect to cleavage (S_1). The first beard orientation parallels the dominant S_1 direction. The second beard orientation parallels V_3 veining. Note the dog-leg of S_1.

B. Sketch of a photomicrograph. S_0 is bedding, S_1 is cleavage and V_3 is shear veining.

fibers closest to the chert (Figure 8) nodule parallel the maximum extension direction of solution cleavage. Later bends in the pressure beards reflect a shift in stress axes due to shear veining.

Veins

In outcrops of the study area with more intense cleavage, substantial calcite veining is evident. A lack of veining in less deformed areas is again presented as evidence of localized transport of dissolved calcite. Calcite veins consist of three distinct types.

Small, mostly microscopic veins (V_1) are found oriented roughly perpendicular to cleavage planes. These veins are filled with fibrous calcite crystals (Figure 10) oriented perpendicular to the fracture wall and demonstrate synkinematic growth during fracture development. These fabrics are not common but are interpreted to be extension fractures allowing expansion in the λ_1 direction.

A second more intense vein fabric (V_2) is found parallel to selvage planes (Figure 10). These veins are often one to ten mm in length, doubly terminating and branching. V_2 veins anastomose, though with a smaller amplitude than cleavage selvages. The veins are filled with fibrous calcite and show the longest crystal axes oriented perpendicular to the fracture wall. Central sutures of residual clays and silts are common. These veins are found to cut selvages in most cases. Some veins, however, are themselves cut by cleavage residues (Figure 7B). For this reason, V_2 veins are interpreted to form synkinematically with cleavage development.

The third and largest type of vein (V_3) again shows fibrous calcite crystals. V_3 veins, however, are oriented at some angle other

A

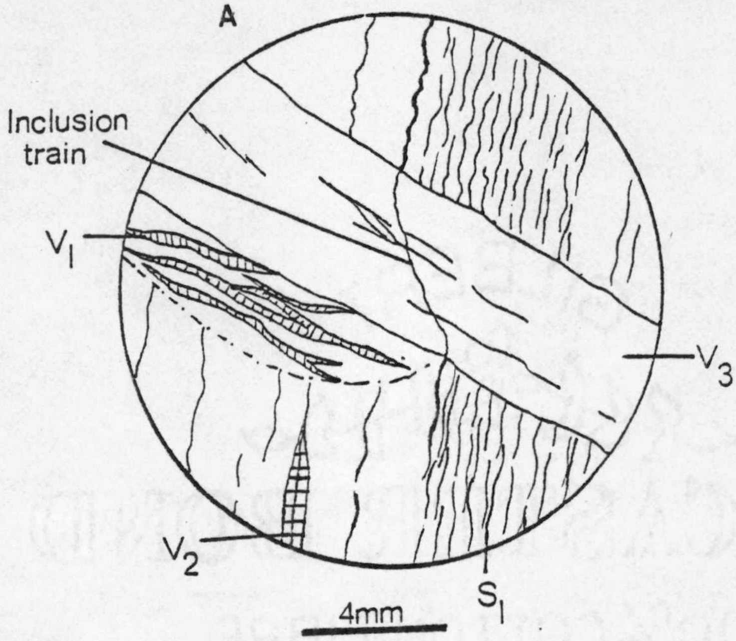

B

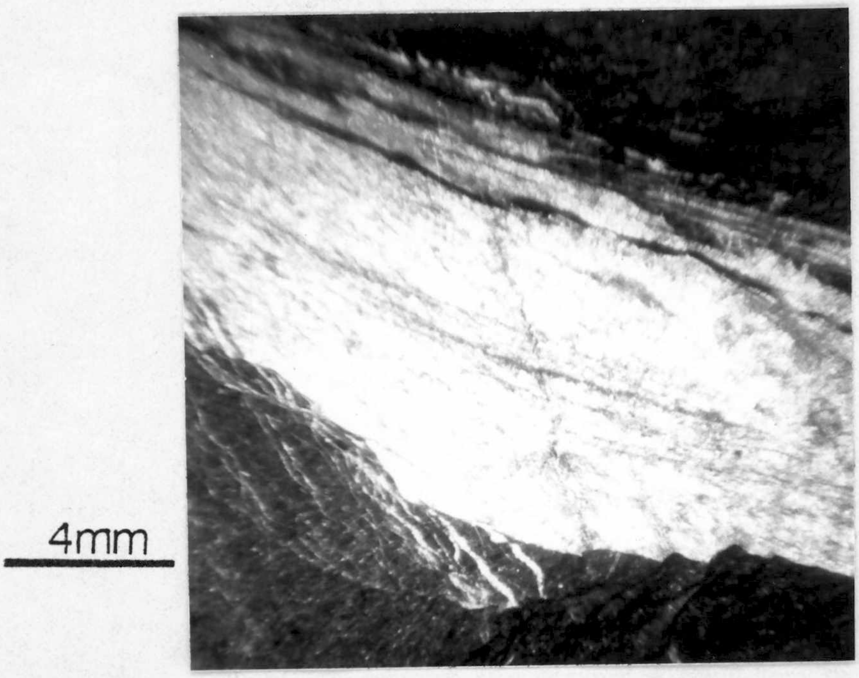

Figure 10. Photomicrograph and enlarged sketch of internal fabrics. Relationships are described in the text. S_1 is cleavage, V_1 is tension gashes, V_2 is veining concordant to cleavage and V_3 is a shear vein.

than 90^{o} to cleavage planes and internal calcite crystals are found to grow in imbricate thrusts. These veins are interpreted to be of a compressional shear origin (Figure 11). They are from one to two meters or more in length and often contain inclusion trains of residual materials originating from selvages (Figure 10). Some thin V_3 veins are bisected and show apparent offset due to solution cleavage, and in areas of intense cleavage are buckled into tight folds. Type V_3 veins are also found to truncate cleavage planes, which could be interpreted to be the result of thick V_3 veins forming impermeable barriers for migrating fluids. This, however, seems to be unlikely due to the sharp boundaries found between V_3 veins and cleavage. Some type of penetration or degradation would be observed if the first interpretation were correct.

Figure 9B is a sketch of a photomicrograph from an intensely cleaved zone of the Lenoir. A V_3 vein appears to be truncated by S_1 cleavage. However, due to the orientation of V_3 fibers and a poorly visible offset of selvage density zones, this kinematic sequence seems questionable. A more likely history would be that V_3 veining post-dates S_1 selvages and grows along a plane indicated by arrows of offset.

Microscopically all three vein types cut each other and cleavage; therefore, no specific fabric can be clearly said to form before any other (Figure 11). Orientations of pressure shadows and frequencies of specific cross-cutting relationships yield a general preference of fabric development in time. Pressure shadows have always been found to first parallel cleavage, and cleavage is predominantly cut by V_3 veins. Inclusion trains across V_3 veins also indicate a late stage of vein development. V_1 tension gashes are only rarely found to be cut by cleavage and are also placed in the later stages of development. V_2

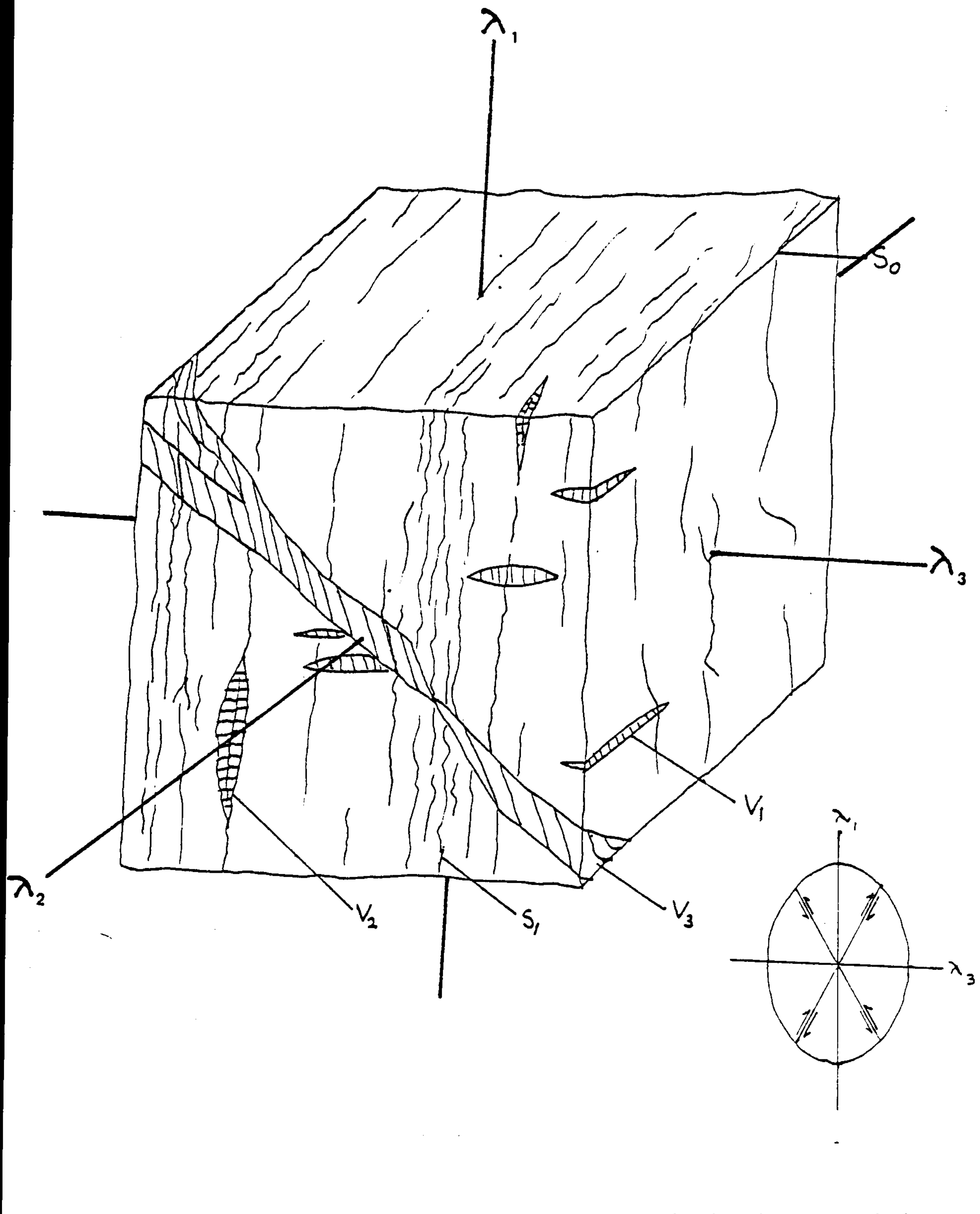

Figure 11. Block diagram of cross-cutting relationships. Ruled lines are fibrous calcite veins (V_1, V_2, V_3). Cleavage and V_2 veins are poorly visible along the surface parallel to cleavage. Strain ellipsoid is seen in the lower right corner. S_0 = bedding, S_1 = cleavage.

veins are mutually cut by V_1 and V_3 veining and are placed kinematically early.

Fibrous V_2 veins are kinematically a problem in that they are parallel to cleavage and yet show fibrous growth and thus maximum extension along the same direction as S_1 shows maximum compression. Two completely opposing stress fields with a mutually cross-cutting nature obviously indicate a multigenerational sequence of compressional and extensional events. Such a history is difficult to develop.

Kinematically, however, due to the lack of calcite veins in low intensity cleavage zones, S_1 is placed first and is later followed by the development of V_2 veins. This event is dominated by ductile deformation of perhaps alternating compressive and extensional events. As the rock continues to lose fluid, brittle deformation in the form of V_1 and V_3 veins begins to develop. V_2 and S_1, however, do not stop developing but are probably limited to channels of increased fluid content, hence the psuedo-dewatering feature.

Alvarez and Engelder (1976) suggest that similar fabric relationships in the Scaglia Rossa in Switzerland are also due to progressive deformation. It has been demonstrated that progressive deformation may rotate an extension fabric such that it no longer coincides with the extension strain axis and thus a new fabric develops (Durney and Ramsay, 1973). This process was undoubtedly instrumental in the development of fabrics seen in the Lenoir.

Discussion:
Cleavage -- Dissolution or shear?

Until recently, cleavage of all types was largely thought to have a shear deformational origin (Groshong, 1975). In the last ten years, however, detailed work has shown that oriented cleavage develops perpendicular to the maximum principle compressive strain axis (Dieterich, 1969; Wood, 1974). Since this original discovery extensive research has led to substantial evidence in support of a dissolution instead of a shear origin of cleavage. The Lenoir Limestone contains many such relationships which prove that it is, in fact, a "pressure solution" cleavage.

The first and most obvious factor supporting a dissolution origin is that cleavage planes lack signs of cataclastic movement. Selvages are curved or even sutured, neither of which lend themselves to shear displacement. Also, there is no sign of gouge or fragmented material as would be associated with shear planes. Delicate fossil fragments, especially trilobites, are often truncated by smooth surfaces with no signs of mechanical deformation (Figure 12A). Embayments of cleavage planes are also common and support a dissolution theory.

Fabric offsets, which at first glance may appear to support a shear origin, are instead, extensively used in support of dissolution. Linear veins or fossils which are cut at any angle other than 90° often demonstrate offsets which appear to be the result of shear (Figure 12B). However, based on methods demonstrated by Groshong (1975), offsets which show a normal fault-like displacement (using the linear fabric as a datum) are explainable by dissolution removal. (See Appendix for methods used.) Offsets which show a reverse fault-like displacement are found to a lesser extent, but can only rarely be explained by a dissolution origin.

Many of these offset fabrics have proven useful, not only in support of dissolution, but also as a valuable tool for a generalized

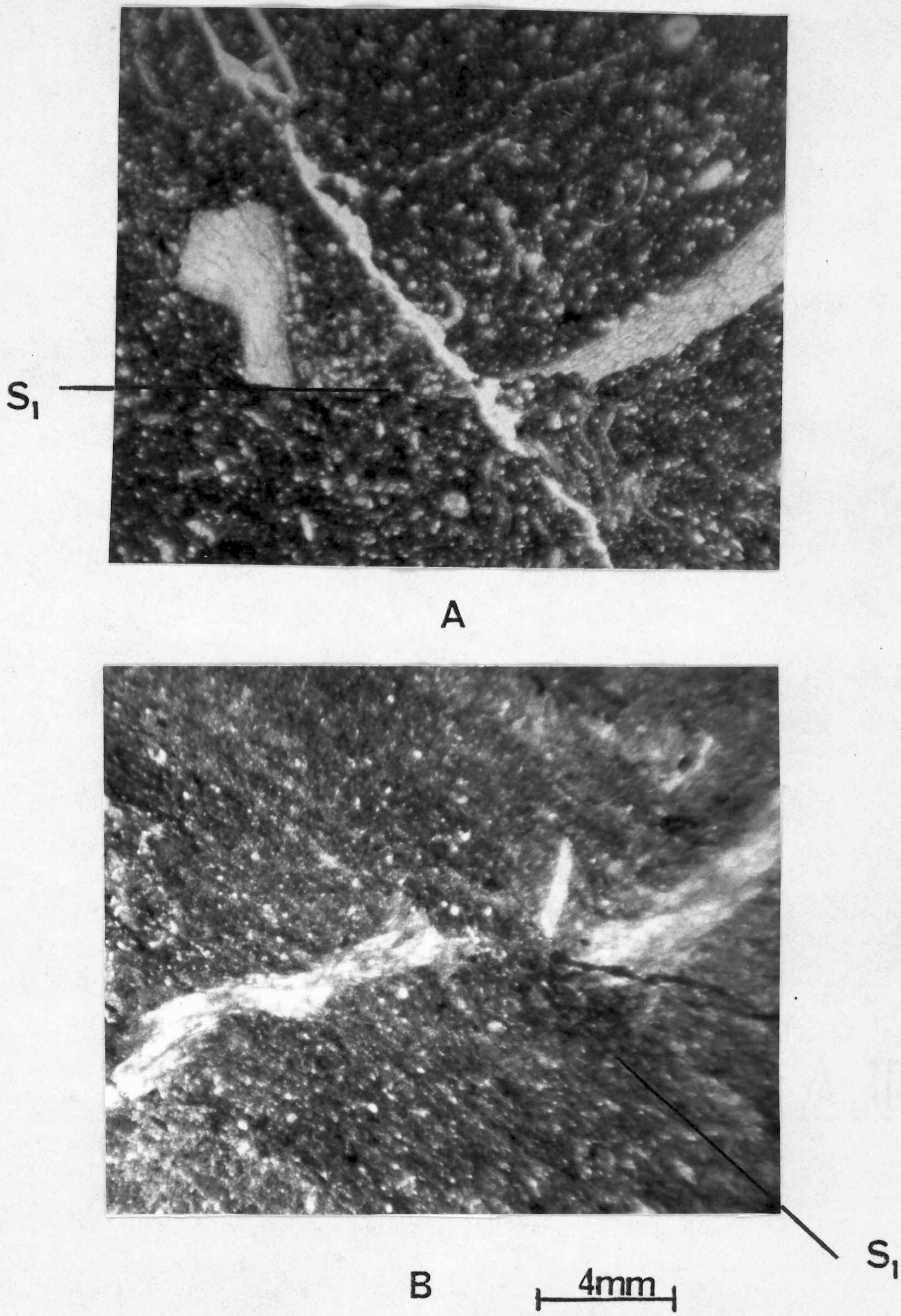

Figure 12. Photomicrographs of the Lenoir Limestone
A. Sutured truncation of trilobite hook.
B. Fibrous calcite vein with apparent shear offset.

finite strain analysis. The analysis is "generalized" in that figures obtained are only a "minimum" finite shortening due to dissolution. Unfortunately, a lack of distinct bedding planes precludes the calculation of bulk or total strain.

Discussion:
Consolidated Origin of Cleavage

Another major controversy associated with pressure solution is the question of whether dissolution is a soft sediment phenomenon or is associated with the consolidated rock. Water as a means of dissolving and transporting materials is not questioned. Rather, the degree of the sediments consolidation at the time of cleavage development is of interest.

Geiser (1974) stresses the importance of primary structures such as burrows in channeling dewatering fluids. He further cites the association of cleavage with these lines of fluid escape as evidence of a soft-sediment origin. No similar primary structures that seemed to control the development of cleavage were seen in the study area. Cleavage selvages are, however, seen to wrap around large nodules or fossils. Also, though the maximum development of cleavage is found perpendicular to bedding a greater development of selvages is found on the stratigraphic bottom side of structures than is revealed on the stratigraphic top. This would suggest an upward migration of fluids similar to dewatering.

Substantial evidence supporting a consolidated formation of cleavage is also observed. For example, cleavage is found to bisect and offset all calcite vein types. In order for cleavage to cut vein fabrics, especially V_1 and V_3 veins, which are associated with brittle deformation, the rock must have been largely consolidated at the time of cleavage development. Also, if individual selvages are traced out, they are almost always found to be doubly terminated within the length of a 3 inch thin section. Such a short channel of dewatering seems highly. The attitude of cleavage to bedding also supports a consolidated origin. Cleavage is axial planar to observed folds and thus kinematically placed at or later than fold development.

This study proposes that many relationships observed by Geiser and this author are "pseudo-dewatering" structures. Lateral pressure due to tectonic forces, as with vertical forces due to overburden, produce a hydraulic gradient with a generalized upward migration of fluids toward areas of lower pore pressure. This upward migration of fluids would predictably follow burrow holes because of a greater porosity in those zones. Upward migration of fluids, even though the rock is essentially solid, can account for the "pseudo-dewatering" fabrics observed. Cleavage, therefore, developed neither as soft sediment deformation nor in rock devoid of water, but in rock consolidated enough to behave brittly, yet still supply sufficient fluids for dissolving rather large quantities of calcite.

Strain Markers

Several attempts have been made at establishing absolute values of strain in pressure-dissolved rock (Geiser, 1974; Groshong, 1975; Alvarez and Engelder, 1976; Beutner, 1977; Alvarez, 1978; Gray, 1979). Both Alvarez and Groshong used the offset of bedding planes which fall at some angle other than 90^{o} to cleavage planes. Bedding, when restored to its planar form by extension perpendicular to cleavage, reveals the amount of material lost to dissolution. From these measurements, finite shortening due to pressure solution can be obtained.

Because bedding within the Lenoir is almost totally obscured by cleavage and weathering, it was necessary to use offsets of internal linear fabrics. Similar methods as those mentioned above were used for calculations. The three main requirements necessary for a good strain marker are as follows:

1. It should be abundant.

2. The marker should deform in equal proportion to the host rock and, therefore, should be made up of similar material.

3. The original shape of the marker should be known (Geiser, 1974).

The most abundant constituent meeting these three requirements were trilobite fragments. Trilobite fragments composed of calcite will deform very much like the limestone host rock. The shape of trilobite sections can also be reasonably well estimated from undeformed examples. Offset calcite veins and other linear fabrics with predictable original forms were also used when possible.

Two different types of fabric truncations were used. The methods used in calculating the finite shortening for each type are discussed below.

(1) In one case, fabrics which have been cut and show apparent offset between parts that were obviously continuous before cleavage were used. Values obtained were total shortening values for single selvages. Requirements for this method are that the shape of the missing segment must be predictable and that the offset be of a normal fault-like displacement using the crosscut fabric as the hypothetical datum and the average cleavage orientation as the hypotetical fault plane.

Calculations used follow methods developed by Alvarez and Engelder (1976) in calculating bedding plane shortening due to pressure solution. The procedures are described in Appendix A (Case I).

(2) The second type of strain markers used were fabrics simply truncated and not bisected. Data from calculations on this type marker were only "minimum" values of shortening due to dissolution and not total shortening values as in Case I. Requirements of this method are again, that the original shape be predictable and that some end of the fabric be removed. Because in many cases, the fabric may have been broken before dissolution occurred, careful consideration needs to be made before selecting strain markers of this type. For this reason, critical bends of fossils with missing sections of the curve proved most useful. Procedures for strain calculations are described in Appendix A. (Case II).

Results of the strain marker analysis are listed in Table II. Measured values of shortening from the Lenoir thin section analysis are listed in the far right column and are correlative with similar studies of solution cleavage by Alvarez (1978). Shortening accomodated by cleavage is listed for each cleavage type.

<u>Assumptions and Drawbacks</u>. Assumed relationships along with errors inherent in the procedures used made values unusable for a bulk strain analysis. The foremost problem in applying these strain markers to bulk strain is that bulk strain is the total shortening due to folding, telescoping and pressure solution. Since bedding surfaces are at best thick and irregular, and in most cases nearly obscured

TABLE II

RESULTS OF FINITE STRAIN ANALYSIS, CHAPMAN RIDGE ANTICLINE

Cleavage Type	Shortening Accomodated by Cleavage (Ranking Percents)	Shortening Values (Alvarez, 1978)	Shortening Values from Lenoir Thin Section Analysis
Weak	0-4%	2% 2% 2% 4%	2.0%
Moderate	4-25%	4% 6% 8% 9% 16% 20%	5.0% 9.8% 15.6% 14.1% 20.0%
Strong	>25%	27% 27% 28% 28% 38% 41% 45% 46% 50%	26.6% 28.4% 36.7% 36.7% 36.2% 38.4% 39.3% 46.2%

by cleavage, neither telescoping nor small scale folding were reliably obtainable.

Strain due to pressure-solution also should be examined. One of the major assumptions for the use of strain markers of pressure-solution is that dissolution occurred perpendicular to selvages. Though this appears to be the dominant mechanism, there are those cases that suggest some forces of shear are involved. Also, the cleavage densities vary strongly, both laterally and vertically, on a microscopic scale. Single selvages found in small fold hinges showed apparent shortening variation from zero to thirty percent within one centimeter of vertical length. However, this analysis has shown that mesoscopic field ranking of cleavage intensity is directly correlatable with microscopic ranking based on percent shortening. Therefore, mesoscopic cleavage classification is a useful tool in generalized studies of pressure-induced shortening.

CHAPTER IV

MESOFABRIC STUDY

INTRODUCTION

Mesoscopic fabric data are rock characteristics such as folds, cleavage and bedding visible in single outcrops. Examination on this scale has been subdivided into spacial relationships, field relationships and Schmidt net analysis.

Spacial Distribution of Cleavage

Cleavage Classification

Ranking of cleavage intensities, as demonstrated microscopically, is a mesoscopic reflection of percent shortening. Mesoscopic ranking is by far a much faster and easier method of strain determination and is thus employed in the following analysis.

Ranking of solution cleavage was first developed by Alvarez (1978). His system, however, was limited in that it was based on nearly pure limestone outcrops. The Lenoir Limestone is a more argillaceous limestone than those classified by Alvarez and thus it was necessary to modify Alvarez's classification system for use in the Lenoir.

Table I (pg. 4) describes the diagnostic characteristics for each cleavage type. Symbols used to represent various levels of development and average distances between cleavage planes are also included. Shortening percentages based on results from Alvarez (1978), though not directly used in this study, are listed here for comparison. Figure 13

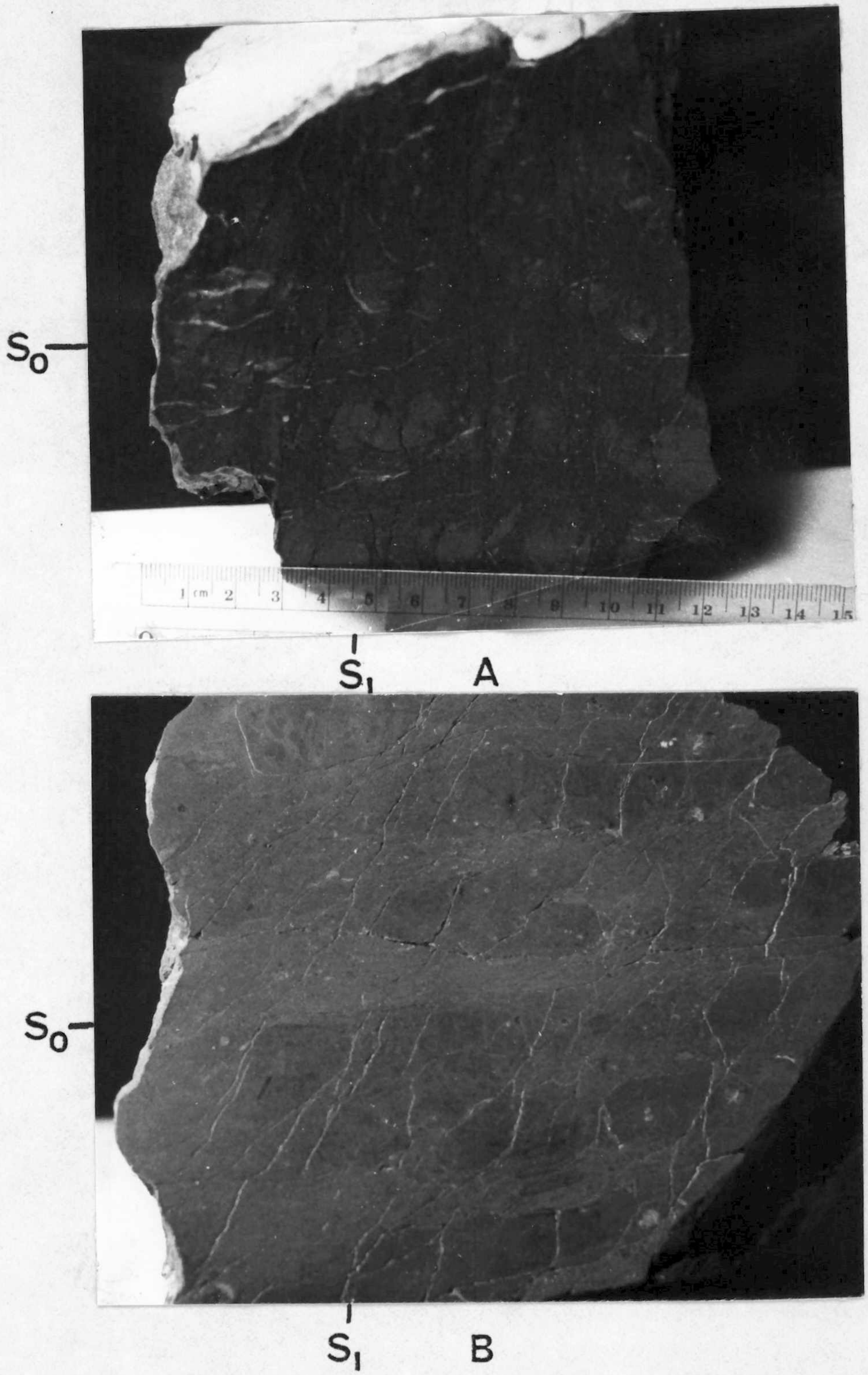

Figure 13. Slabbed samples of high cleavage (A) and low cleavage (B).

demonstrates the visual differences between low and high cleavage in slabbed hand speciment.

Sampling

Sampling was limited to exposures of Lenoir across the Chapman Ridge anticline of the study area. Other outcrops associated with simple thrusting without folding showed no cleavage. Exposures of Lenoir were poorly developed over a 58 square kilometer area in the Knoxville and Shooks Gap quadrangles. A total of 66 stations were used with a minimum of 2 to 3 measurements taken per station. Thin sections were prepared for most suitable outcrops, but a final intensity ranking of cleavage was based on an average for the outcrop. For example, an outcrop of generally uncleaved rocks, but with zones of cleavage, would be given a rank of "low".

Results

The product of this analysis is an areal map of contoured cleavage intensities (Figure 14). The bordering lithologies are the Holston along the flanks of the anticline and the Mosheim in the core. Each outcrop studied is indicated by a symbol and its respective cleavage type. Solid contour lines indicate areas where accuracy is within 0.25 km, and dashed lines indicate less precise determinations. Major anticlines, synclines and faults are indicated with conventional symbols.

Immediately apparent is the distribution of moderate cleavage in a nearly continuous zone on the outside of the fold limbs. Two crescent shaped patterns of high intensity cleavage disrupt this pattern. These areas of the highest cleavage intensity are associated with the shortest wavelength of folding.

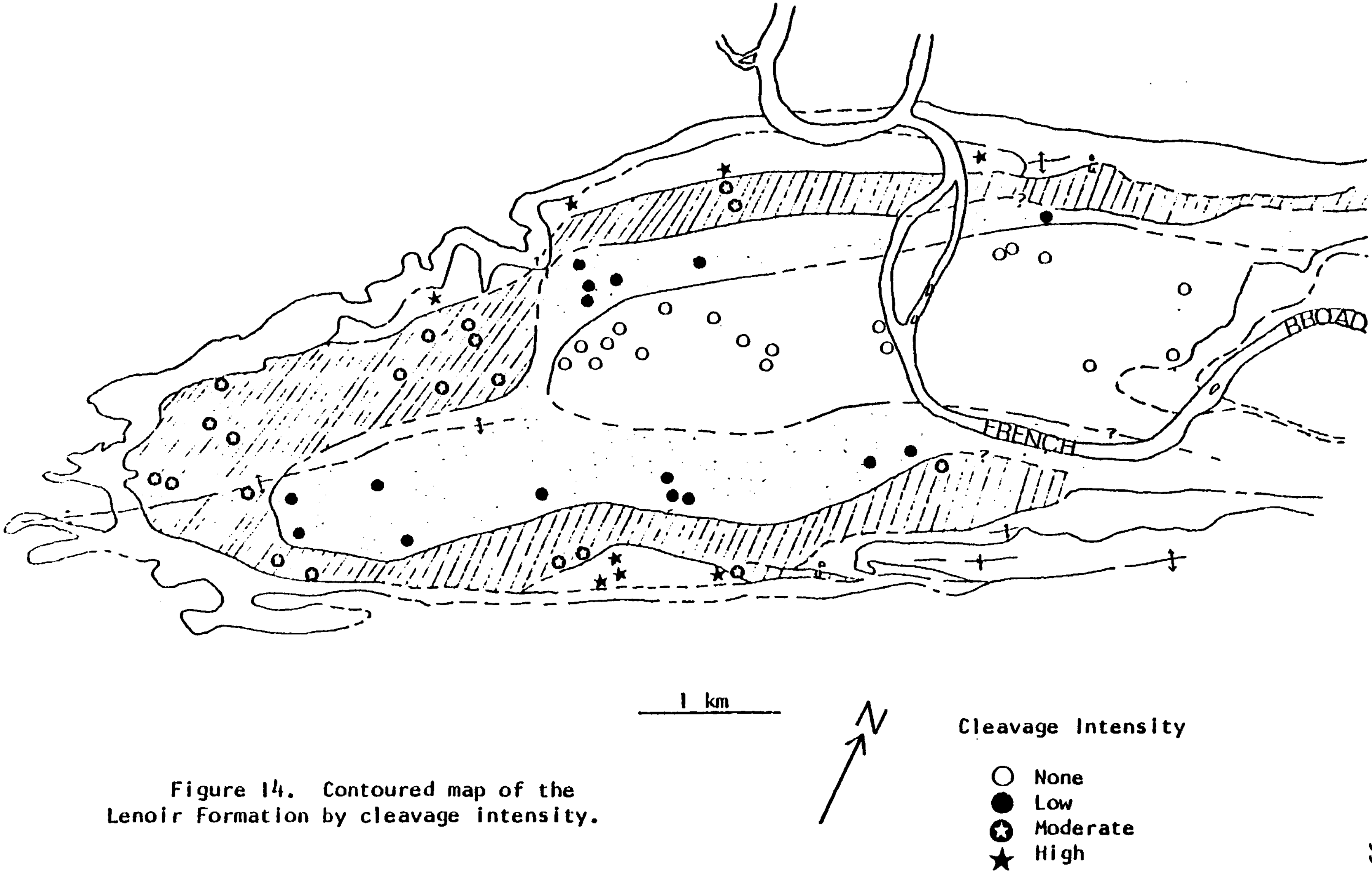

Figure 14. Contoured map of the Lenoir Formation by cleavage intensity.

A belt of low cleavage intensity is found roughly concentric to the moderate cleavage belt. However, no cleavage is developed in the crestal exposures of the anticline. This zone encompasses the widest area and is well exposed along the French Broad River. Dip angles of beds in this zone are rarely greater than ten degrees.

Figure 15 is a map of bedding orientations in the study area. The variable dip directions observed are the result of outcrop scale parasitic folds. Strike directions of bedding are parallel to outcrop patterns when directly adjacent to other lithologies.

Application of Contoured Cleavage to Finite Element Modeling

Recent studies by O. Stephensson (1976) with computer modeling of folds has uncovered interesting results concerning applications of finite element analysis. Stephensson's use of the computer to model the distribution of stress and strain throughout folds subjected to variable parameters may be extremely useful in understanding these "variable parameters" in this fold and other natural folds. The variables available for manipulation are the following: viscosity contrast between beds, bed thickness, percent shortening due to folding and strain rate.

Figure 16 is an example of a fold model which appears very similar to the Chapman Ridge anticline and its internal deformation. This is a multilayered model consisting of three competent layers (thin shaded layers) sandwiched between less competent layers and subjected to a small percent shortening. Incompetent layers are modeled at twice the thickness of the competent layers. The viscosity contrast between layers is assumed at 100 to 1. The contour lines represent stress isopleths, with compressive stress indicated by negative signs.

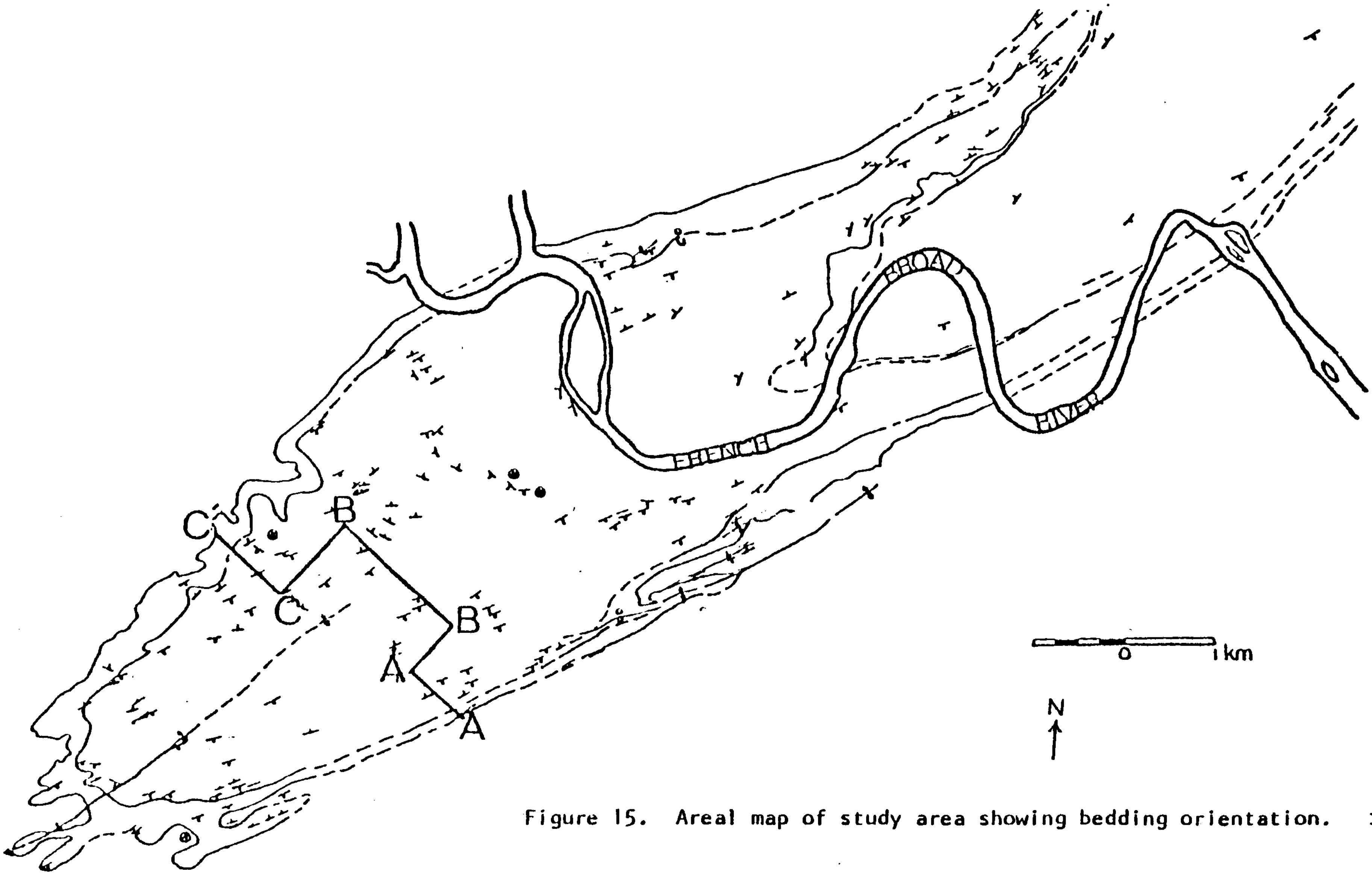

Figure 15. Areal map of study area showing bedding orientation.

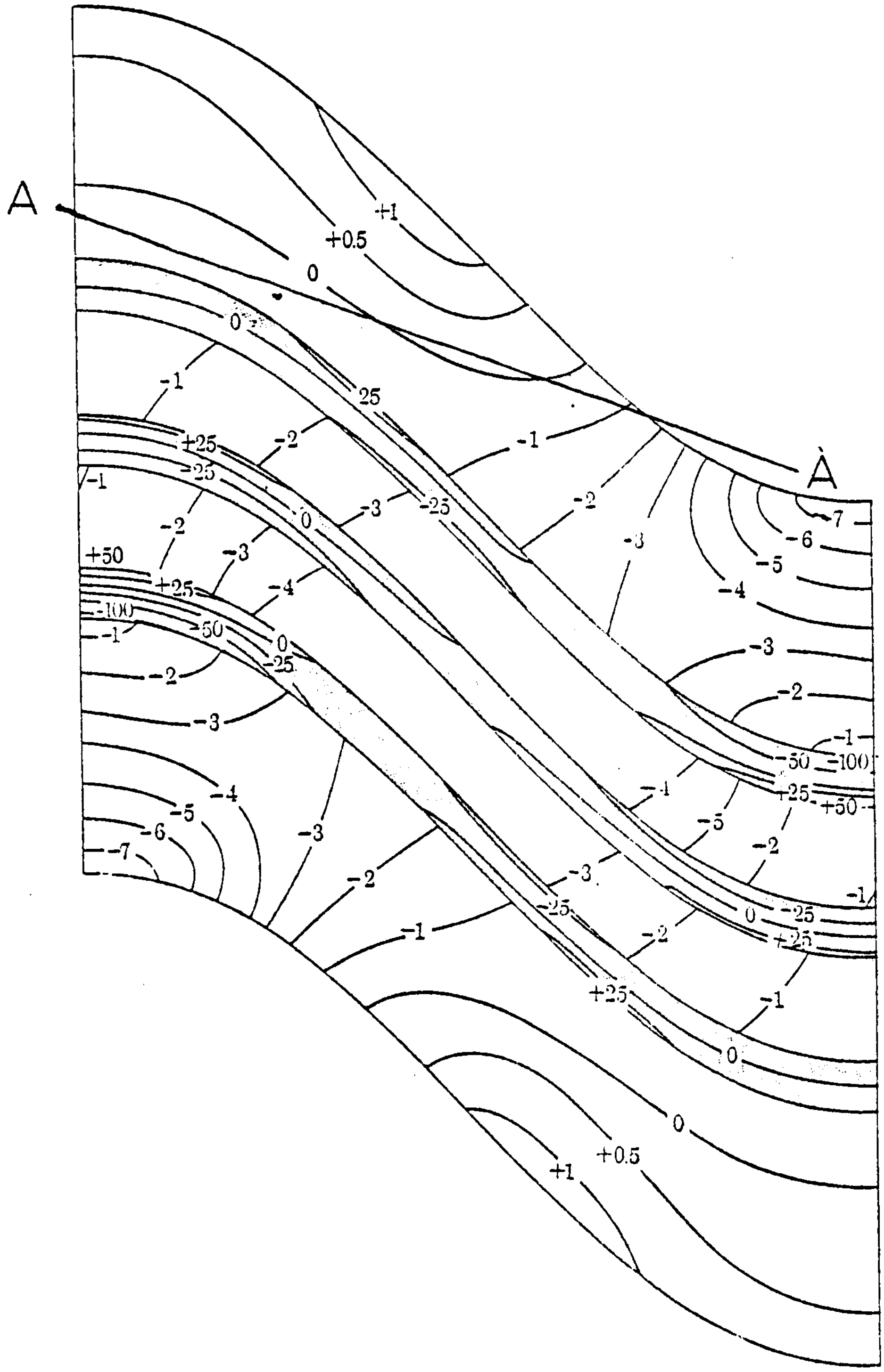

Figure 16. Computer model of multilayered fold (Stephensson, 1976). Line A to A' is the projected line of outcrop for the Chapman Ridge Anticline.

A comparison of Figure 14 with Figure 16 clearly shows qualitative similarities in the boundaries of stress and their configuration. A horizontal projection of cleavage intensities from A to A' as drawn across the model and projecting a small amount of plunge, (Figure 17), would form an outcrop pattern similar to that mapped in the field area. The crest of the hypothetical fold with stress values of 0 to +1 would have no compressional or even minor extensional stress as is apparent by mesofabric analysis of the anticline. The limbs of the anticline show the most intense compressive strain as is the case of the model with high negative values of stress along the limbs. Stephensson (1976) discovered that no region of tension in the outer portion of hinges developed if the viscosity contrast of modeled layers was 5 to 1 or less, so clearly, at the time of folding, the viscosity contrast in the hinges of the Chapman Ridge anticline must have been greater than this.

Field Relationships

Within the scope of single outcrops, solution cleavage proved to be a useful tool in the determination of stress distribution. In the absence of other fabric data, cleavage was the only useful tool. The response of solution cleavage to seemingly small variations in stress made it extremely helpful in the study of local deviations of stress within an area. Comparisons with hypothetical stress induced models also proved to be surprisingly accurate.

Low to moderately intense cleavage (See Table 1, pg. 4) best preserved the orientation of small stresses (Figure 18A). Cleavage of

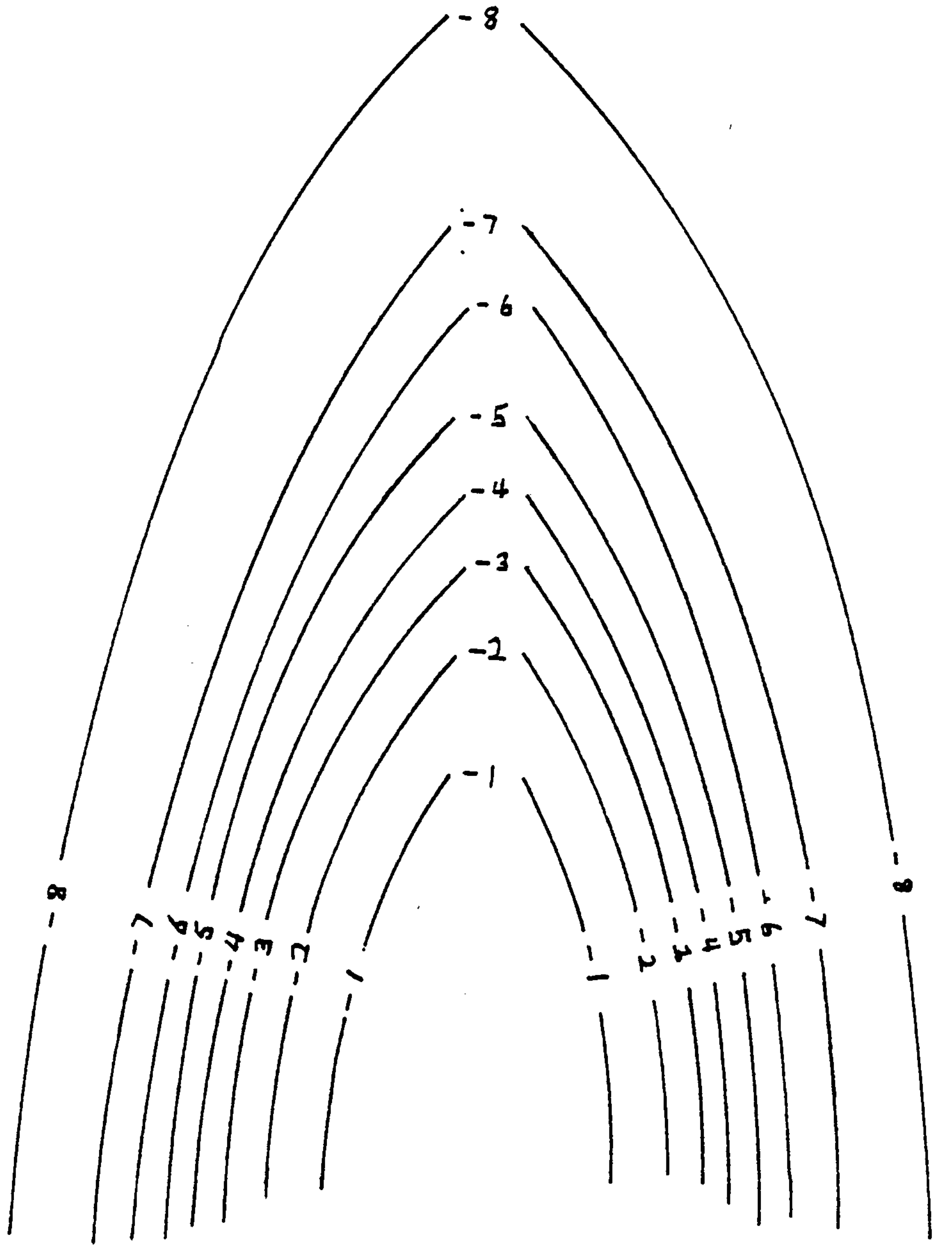

Figure 17. Outcrop pattern of modeled fold in Figure 16 projected into a plunging anticline and eroded to line A-A'. Numbers represent related values of compressive stress.

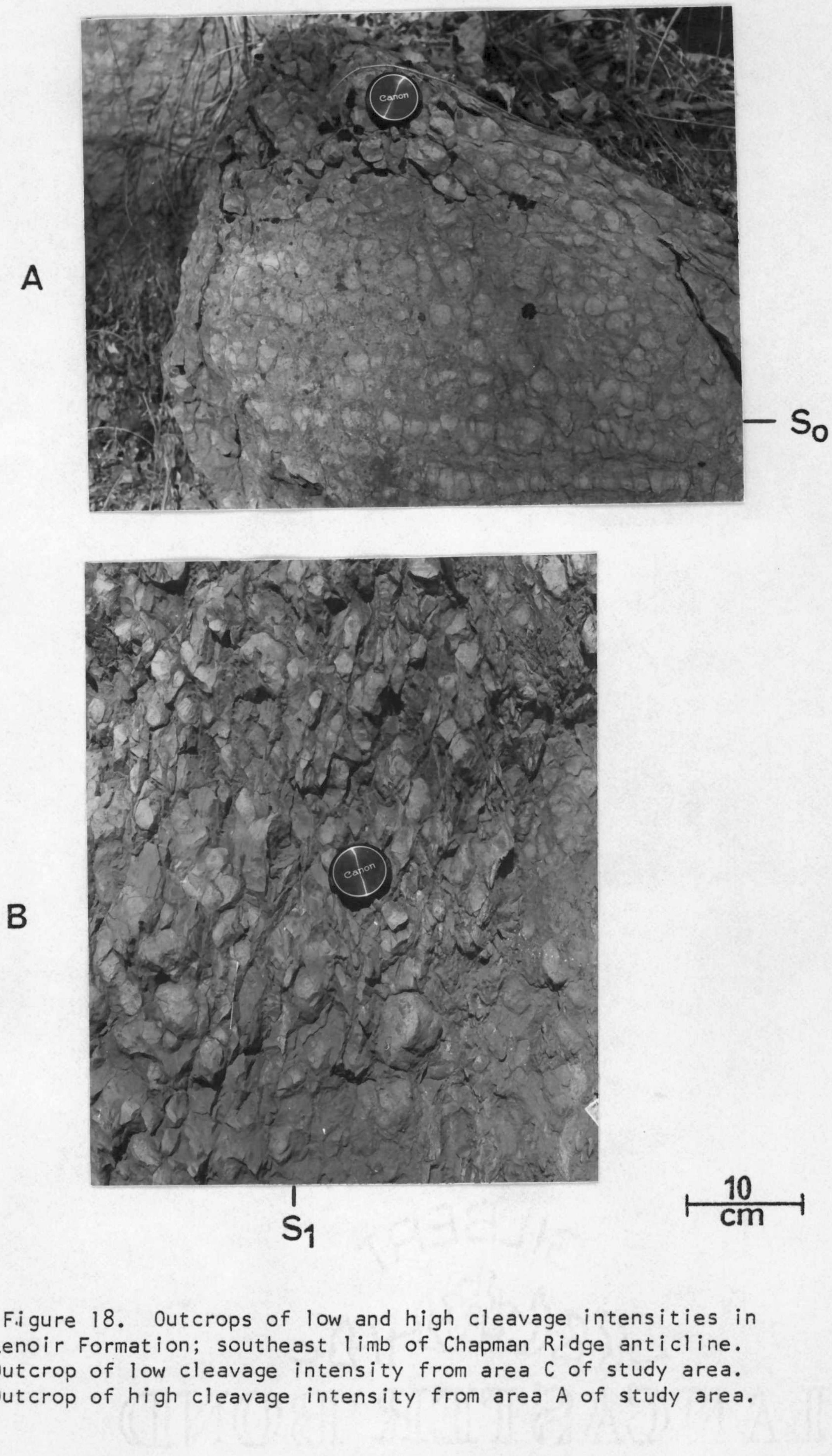

Figure 18. Outcrops of low and high cleavage intensities in the Lenoir Formation; southeast limb of Chapman Ridge anticline.
A. Outcrop of low cleavage intensity from area C of study area.
B. Outcrop of high cleavage intensity from area A of study area.

a high ranked intensity (Table I, pg. 4) was so strongly developed that axial stress was the only record of stress preserved in the rock (Figure 18B). This superimposed fabric was most beneficial in regional interpretation, but offered little information in mesoscopic stress studies. Regional fabric relationships were, therefore, obtained from the more intensely cleaved areas, and the areas with less intense deformation such as outcrop C (Figure 3, pg. 7) were used for local fabric relationships.

Fold Relationships

The axial planar nature of cleavage in the study area precluded any study of cleavage rotation with increased intensity (Alvarez, 1978). Figure 19 is a plot of cleavage spacing versus cleavage-bedding angles for measured outcrops across the study area. Distinct grouping of cleavage at high angles to bedding appears to support a fanning nature of cleavage and, thus, the development of cleavage before folding. It should be noted that this relationship could be an artifact of the generally low dip angles of the gentle to open folds in the study area. Also, cleavage at a low angle to bedding would more likely develop into boudinage rather than the more common solution cleavage. However, the grouping of southwesterly dipping cleavage on the northwest limbs and northwesterly dipping cleavage on the southwest limbs clearly demonstrates a large scale fanning nature of cleavage. Figure 20 is a panorama of outcrop A of the study area (See Figure 3, pg. 7) and distinctly shows the gentle fanning nature of cleavage.

This characteristic cleavage pattern of individual folds resembles the "strain" controlled pattern in Figure 21 more than the "stress"

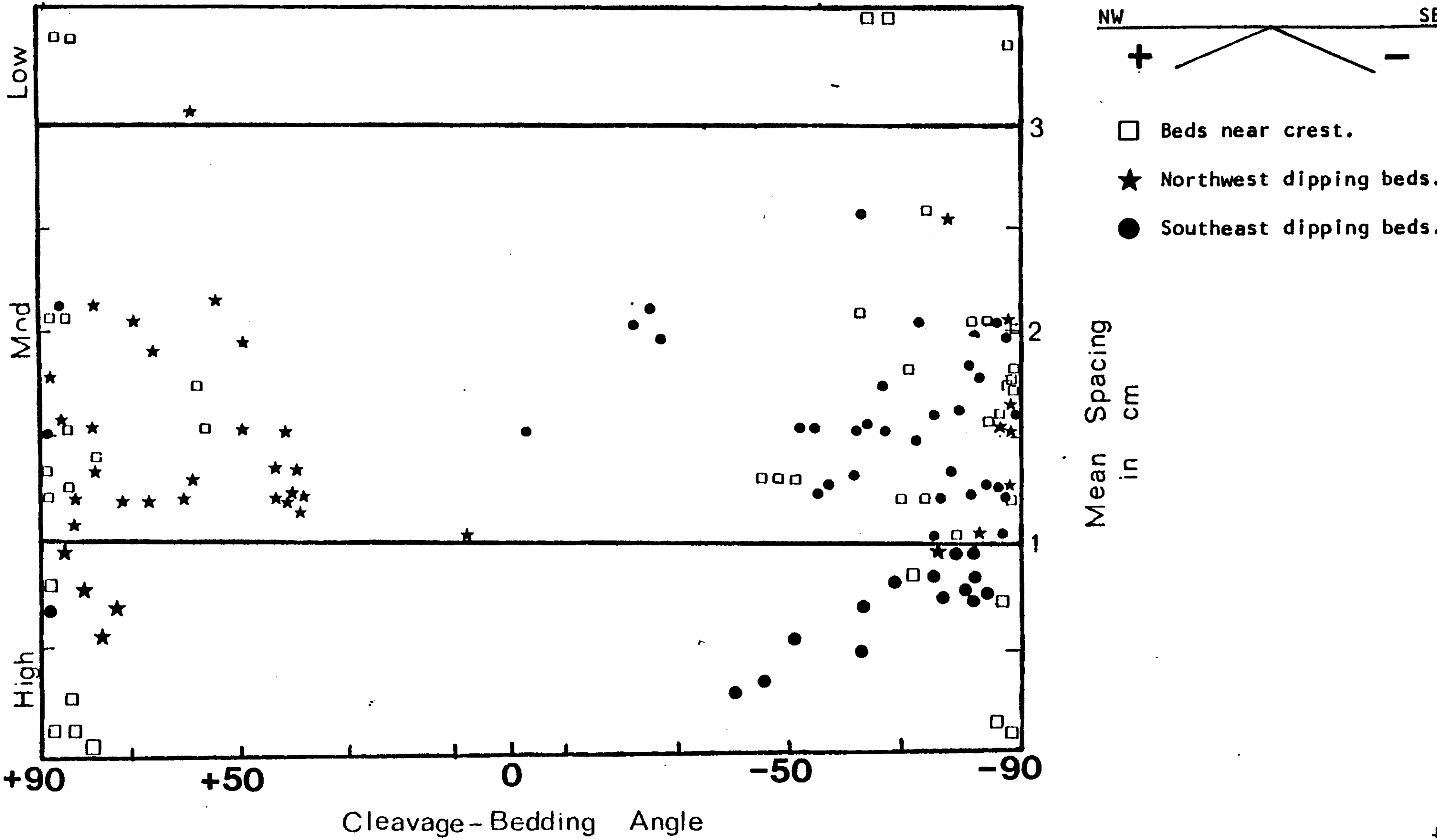

Figure 19. Plot of 128 cleavage spacings versus cleavage-bedding angles for measured outcrops across the study area.

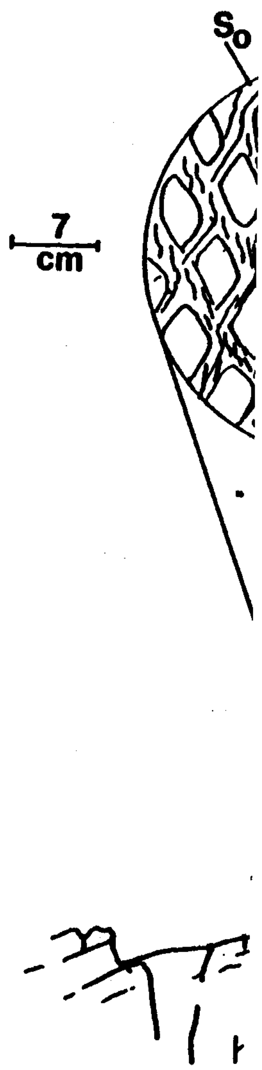

Figure 20. Panorama of outcrop A.

A

B

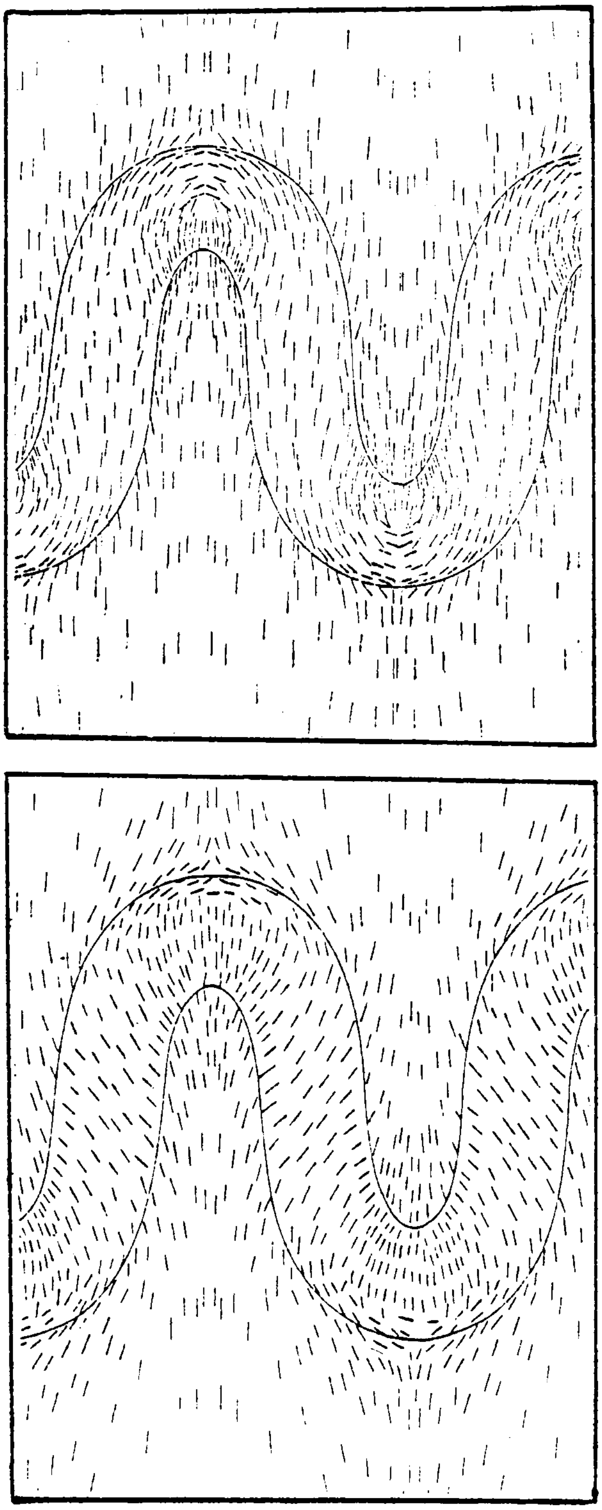

Figure 21. Distribution of stress (A) and strain (B) in a fold by Dieterich (1969). Lines are perpendicular to σ_1 in A diagram and perpendicular to λ_3 in B.

controlled pattern. Cleavage laminae of the limbs, being nearly perpendicular to bedding, exemplifys the preservation of cleavage as it becomes part of the rock. Cleavage develops early in the folding history and is kept as the rock is continually deformed through rigid body rotation. The final orientation of cleavage planes preserved in the rock is almost perpendicular to λ_3, as defined by the finite-element buckle fold model (Figure 16) (Dieterich, 1969), demonstrating a strain controlled development. Similar relationships were observed by Groshong (1975) in hand specimen folds.

Across the study area both folding symmetry and cleavage intensities are variable (Figure 22). F_2 folding of the highest amplitudes and shortest wavelengths occur along the limbs of the anticline (F_1). Broad, gentle mesoscopic F_2 folds are distributed across the crest of the anticline. Fold shortening and cleavage intensity were discovered to be directly related. F_2 folds of the shortest wavelengths along the limbs of the anticline contain the strongest cleavage, the most intense shearing and the most highly developed jointing. Folds of less bulk strain show less intense cleavage and only minor shear development (See Table IV).

Along the southeast limb of the F_1 anticline the most intense folding is observed (Figure 22). Bedding in this area is nearly vertical, and F_2 fold limbs show a distinct thinning. Tight to isoclinal folds are developed near the contact with Holston Formation. Directly adjacent to the Holston-Lenoir contact, boudinage of layers is parallel to axial plane solution cleavage (Figure 23). Weiss (1972) has interpreted this to be evidence of transport. The contact between boudinaged

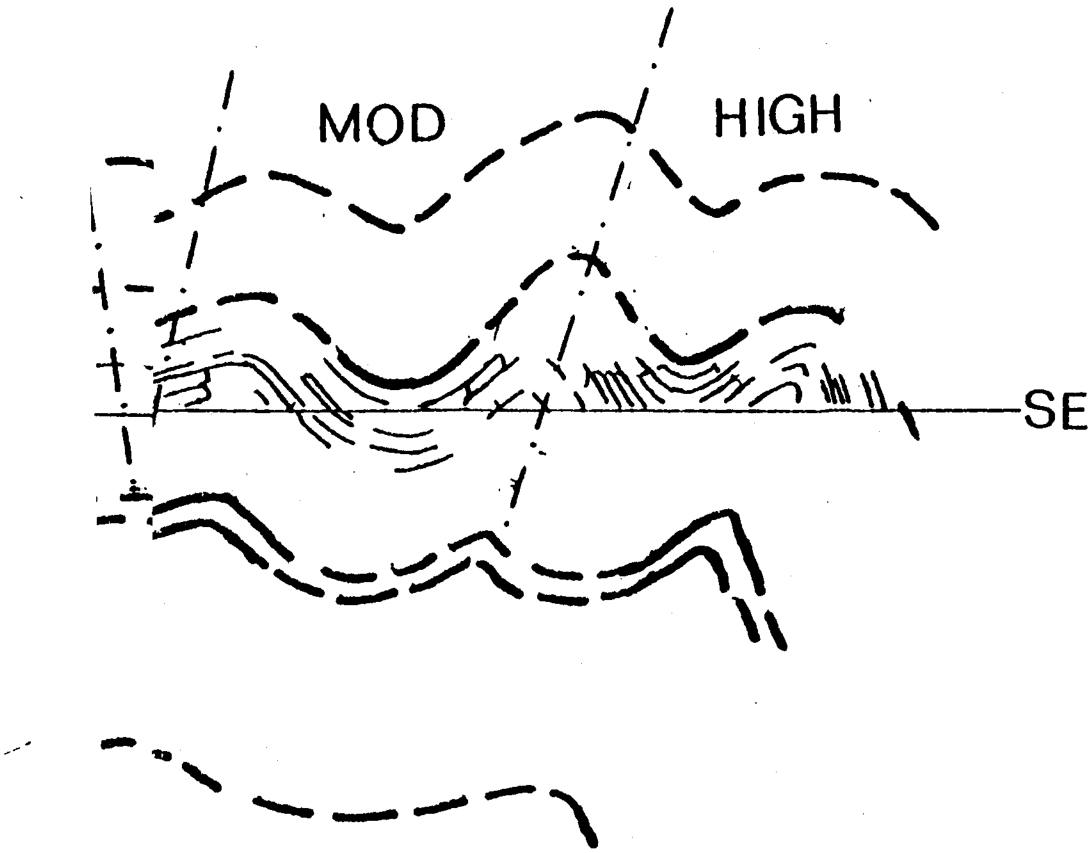

Figure 22. Panaroma of Lenoir anticline from A to A', B to B', and C to C' (Figure 15). See text for explanation.

TABLE III

TERMS USED TO DESCRIBE TIGHTNESS OF A FOLD

Description of Fold	Interlimb Angle-Degrees
Isoclinal	0
Tight	Less than 30
Close	30-70
Open	70-120
Gentle	120-180

TABLE IV

SYMBOLS

Symbols Used on Schmidt Nets	Symbols Used on Maps
○ Low Cleavage	⊕ Horizontal Beds
● Moderate Cleavage	Strike and Dip of Beds
★ High Cleavage	Overturned Bed
λ_3 Principal Strain Axes of Maximum Shortening	Solid Lines are Formation
λ_2 Principal Strain Axes of Intermediate Deformation	Dip Slip Fault
λ_1 Principal Strain Axes of Maximum Extension	Plunging Anticline
A-C Plane	Plunging Syncline
Calculated Fold Axis	○ No Solution Cleavage
	● Low Solution Cleavage
	Moderate Solution Cleavage
	★ High Solution Cleavage

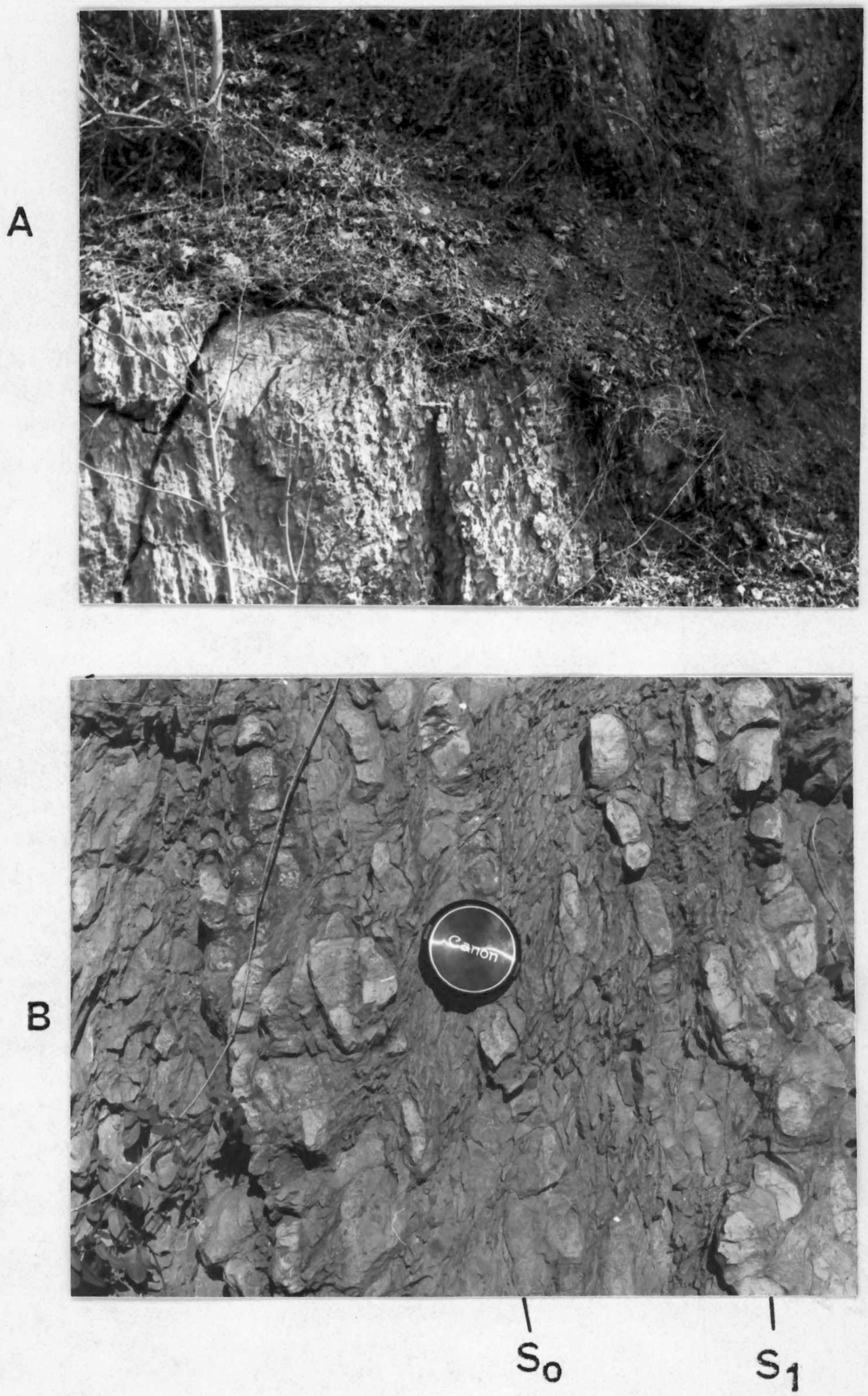

Figure 23. Photographs of southeast flank of the Chapman Ridge Anticline (Outcrop A).

A. Photograph demonstrating boudinaged bedding near southeast Holston-Lenoir contact.

B. Photograph of S_o (bedding) and S_1 (cleavage) attitudes in the Lenoir Limestone.

bedding and steeply dipping, unboudinaged bedding is gradational over five to ten meters. Figure 24 shows the gradational contact between fabric styles with bedding marked by limestone rich nodules steeply dipping to the right of the photograph. Cleavage exhibits wavy patterns but generally dips to the left of the photograph. A possible sequence of events in the development of boudinaged bedding is shown in Figure 25. This sequence involves the rotation and translation of competent beds in an incompetent matrix (Hobbs, Means and Williams, 1976).

Medium-thick beds in the moderate to low cleavage range display several small variations in strain. Cleavage within these mesoscopic F_2 folds show the closest spacing and, thus, the greatest percent shortening in the core of the fold (Figure 26). Cleavage spacing decreases gradationally toward the crest of the fold, and there is no evidence of cleavage toward the top of individual beds. Spacing of solution cleavage varies abruptly from one bed into the next, and evidence of flexural slip along the limbs of these folds is common. Bed-parallel slippage around the fold hinge allows extension at the top of individual beds and compression at the bottom. A close resemblance is seen between these folds and the modeled buckle fold by Hobbs, Means and Williams (1976)

Three possible types of rigid-body folds have been proposed by Groshong (1975) to account for the loss of material due to pressure solution (Figure 27). Figure 27A is a fold with removal of material symmetrical along zones perpendicular to bedding and with increasing amounts of dissolution toward the core. The resultant fold in this case is one with no offset at the top or bottom of the bed. Fold 27B

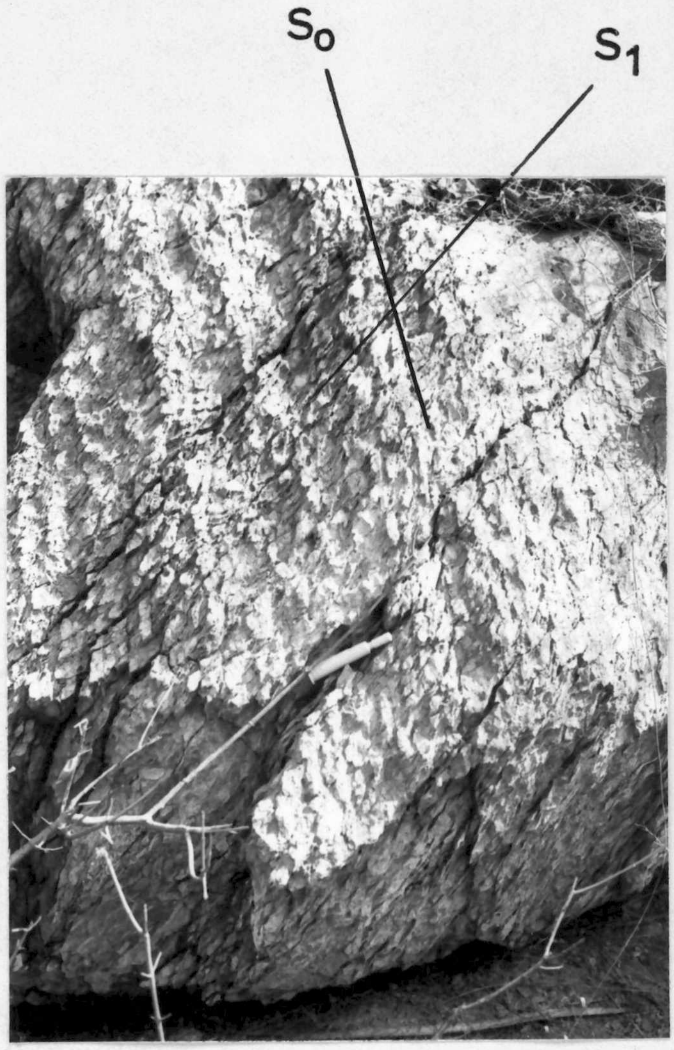

Figure 24. Photograph of gradational contact between boudinaged and unboudinaged areas. Bedding dips steeply to the right. S_o is bedding and S_1 is cleavage.

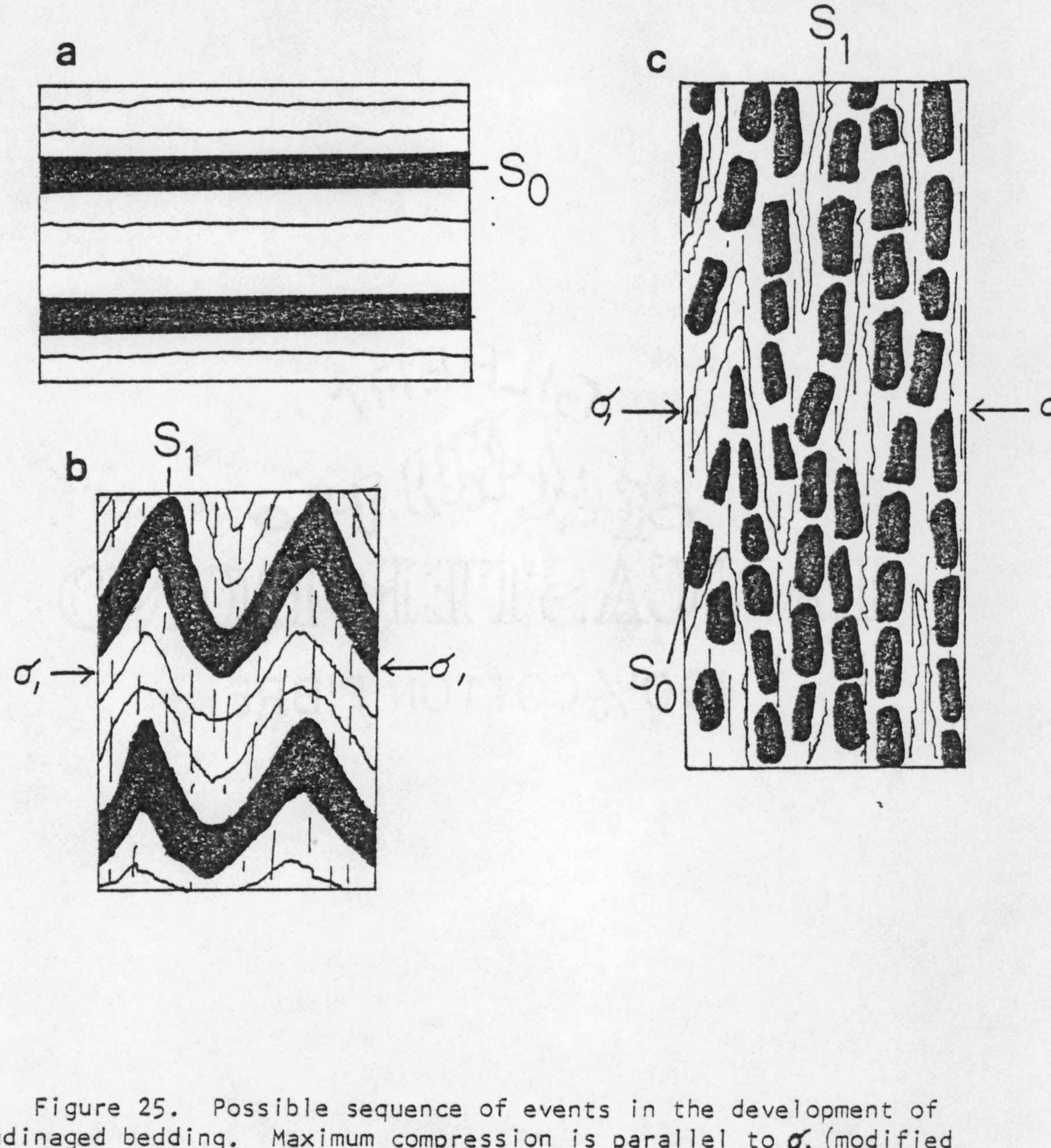

Figure 25. Possible sequence of events in the development of boudinaged bedding. Maximum compression is parallel to σ_1 (modified from Hobbs, Means and Williams, 1976)

A

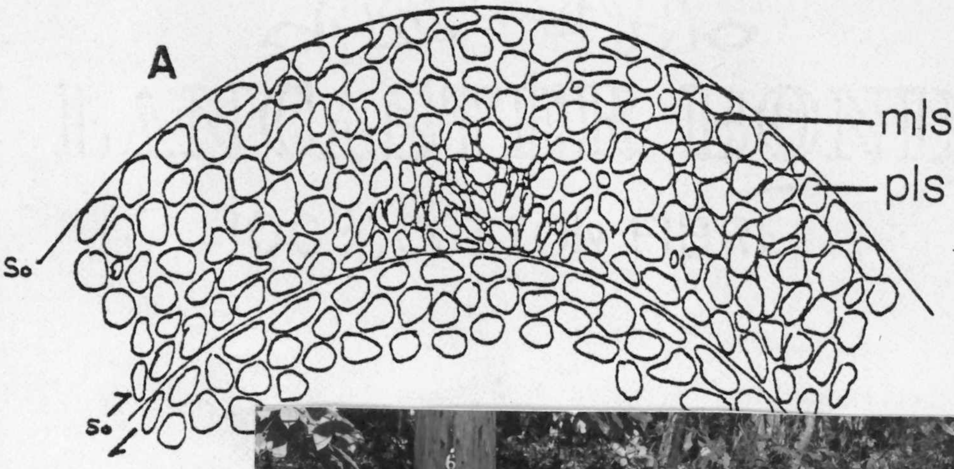

B

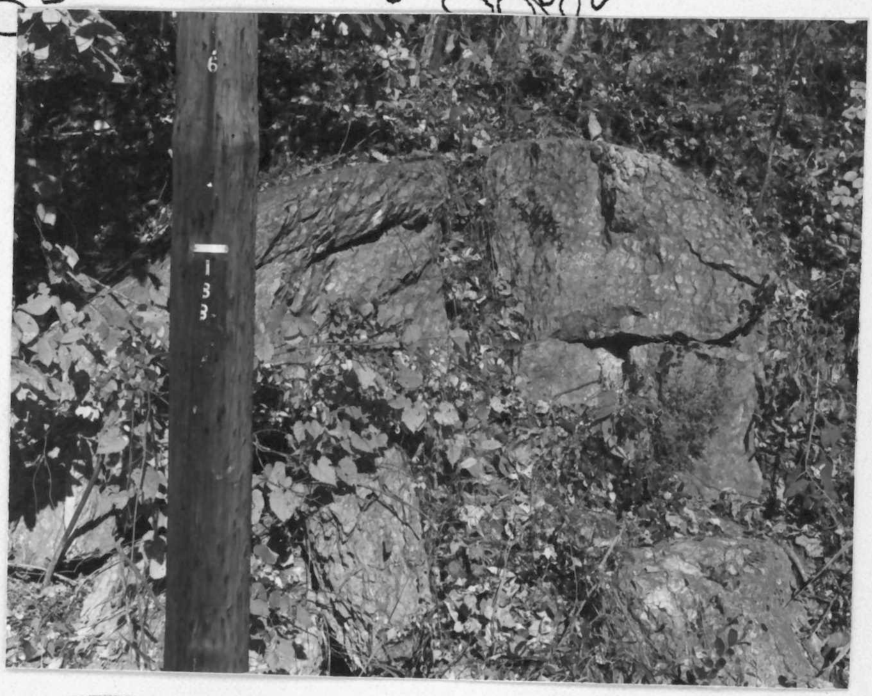

C

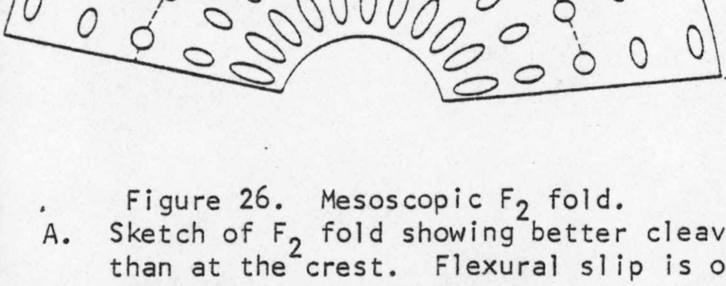

Figure 26. Mesoscopic F_2 fold.

A. Sketch of F_2 fold showing better cleavage development in the core than at the crest. Flexural slip is observed along the limbs.

B. Photograph of mesoscopic F_2 fold. Telephone pole is 30 cm in diameter for scale. Spacing of cleavage is reflected in the limestone nodules.

C. Fold with stress ellipsoids in buckle fold (Hobbs, Means and Williams, 1976).

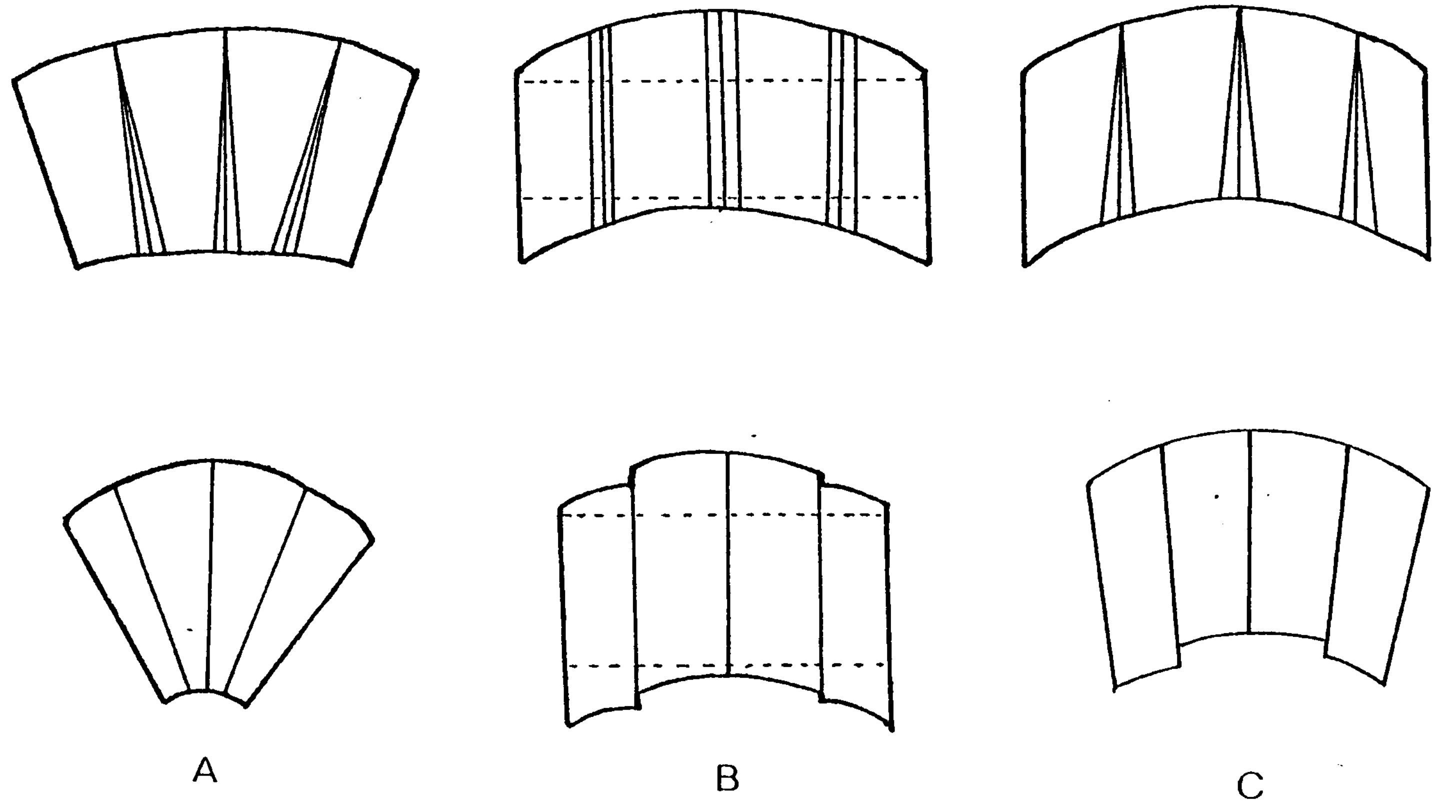

Figure 27. Three possible fold configurations, caused by selective removal of material. Upper diagrams show original folds with areas to be removed indicated by thin lines. Lower diagrams show folds after material is removed.

A. Removal from zones perpendicular to bedding and increasing toward fold core.

B. Removal of constant amount from zones oblique to bedding.

C. Removal of amounts that increase into fold core from zones oblique to bedding (Groshong, 1975).

exhibits removal of material along parallel zones oblique to bedding but with a uniform amount of material lost along the zone. External layering (i.e. bedding) is offset both on the top and bottom; whereas, no offset is created within the bed. Figure 27C demonstrates the third type fold which has been formed by loss of material increasing toward the core and oblique to bedding. Folds with this type of solution loss show the greatest offsets at the bottom and decreasing amounts of offset toward the concave side of the fold. The top bedding surface has no offset. Two or possibly all three of these type folds are observed in the study area.

Mesoscopic F_2 folds show no offset at the top or bottom of individual folded beds and are, therefore, interpreted to be folds of type A with cleavage developing perpendicular to bedding. Hand specimen F_3 folds show a different type of folding. These small, internal folds show no offset along the crest, but reveal distinct displacement at the hinge core. Removal of material is, therefore, oblique to bedding and increasing toward the core. The final orientation of cleavage laminae shows a fanning nature. Similar solution shortening was observed in a hand specimen size buckle fold from a fault zone in the Appalachian Plateau of New York (Groshong, 1975). Bedding planes in intensely cleaved zones are too distorted by cleavage to allow a similar analysis, but due to the gentle fanning nature of cleavage, folds in these realms are thought to be of type C.

Shear Surfaces

Solution cleavage was also determined to be controlled by shear planes. Outcrops, which would otherwise be uncleaved or only moderately cleaved, often showed well developed cleavage in close proximity to shear surfaces. Cleavage here is reflected in the orientation and size of limestone-rich nodules. Nodules in shear zones are oriented in onlap patterns which clearly indicate the direction of slippage (Figure 29). Unfortunately, shear planes of this nature were not found consistently enough to measure orientations accurately.

In some areas, shear planes reflected in cleavage form conjugate pairs (Figure 28). Contemporaneous movement in opposite senses is reflected in the onlap nature of nodules. Shear displacements usually dissipate before intersection or along bedding surfaces. Displacement on shear planes is consistently of the reverse fault sense and is compatable with horizontal compression.

Solution cleavage distribution is also reflected in flexural slip folds. Bedding parallel slippage along fold limbs is marked by onlap relationships similar to those of the conjugate shear sets. In areas of generally low intensity cleavage, well pronounced zones are found associated with bedding slippage. Cleavage selvages showing these "drag" type features were often accompanied by slickensides with similar reverse faulted movement.

Clay Content

The percentage of clay in a rock was microscopically observed to correlate with a decrease in the cleavage spacing and an increase in the density of cleavage mesoscopically. A comparison of cleavage to clay content microscopically was on such a scale that an assumption of uniform stress was reasonably reliable. Further evidence of the effects of clay content was observed along the scale of individual beds.

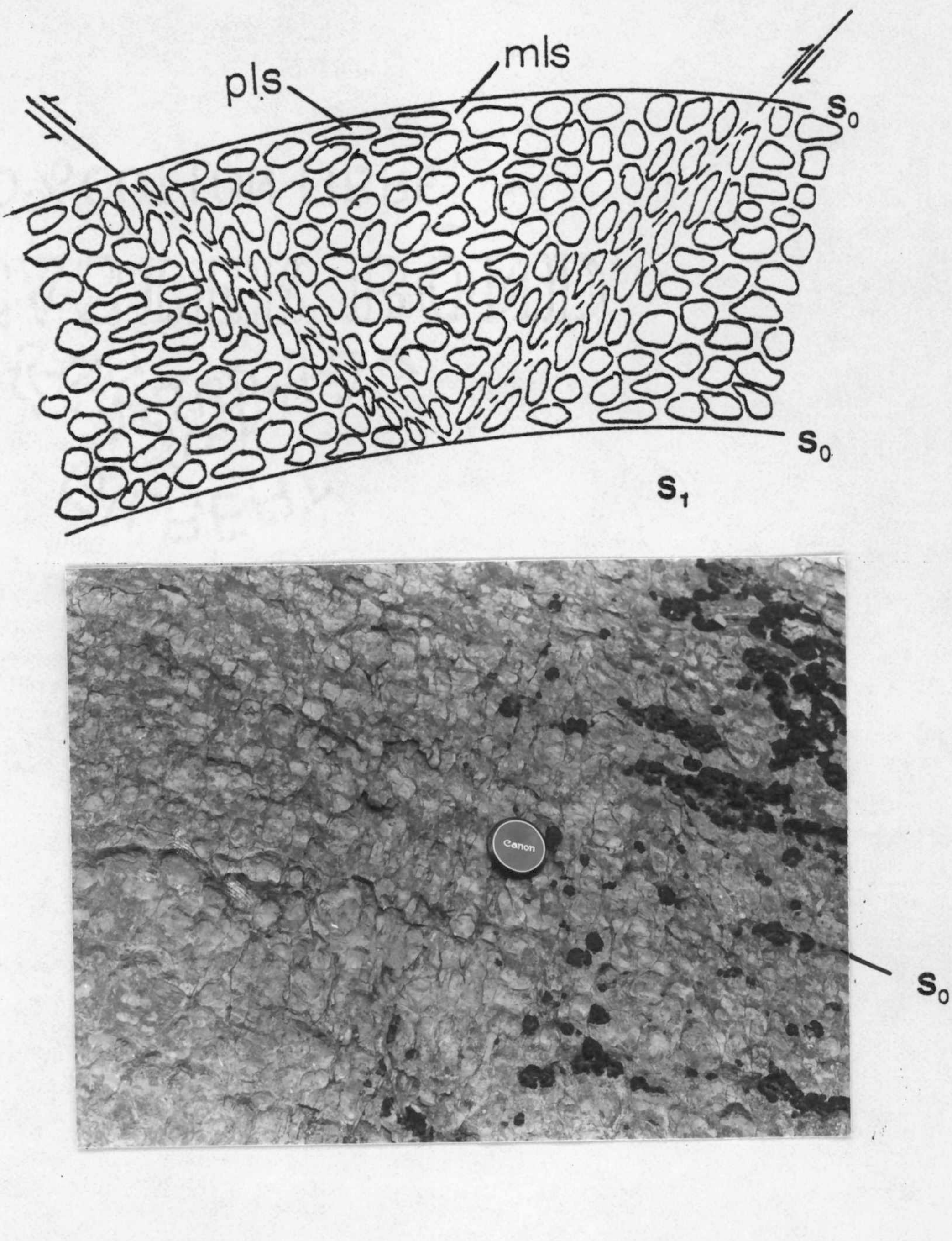

Figure 28. Photograph and field sketch of cleavage developed along shear zones. Limestone rich nodules are labled pls. The muddy limestone matrix is labled mls.

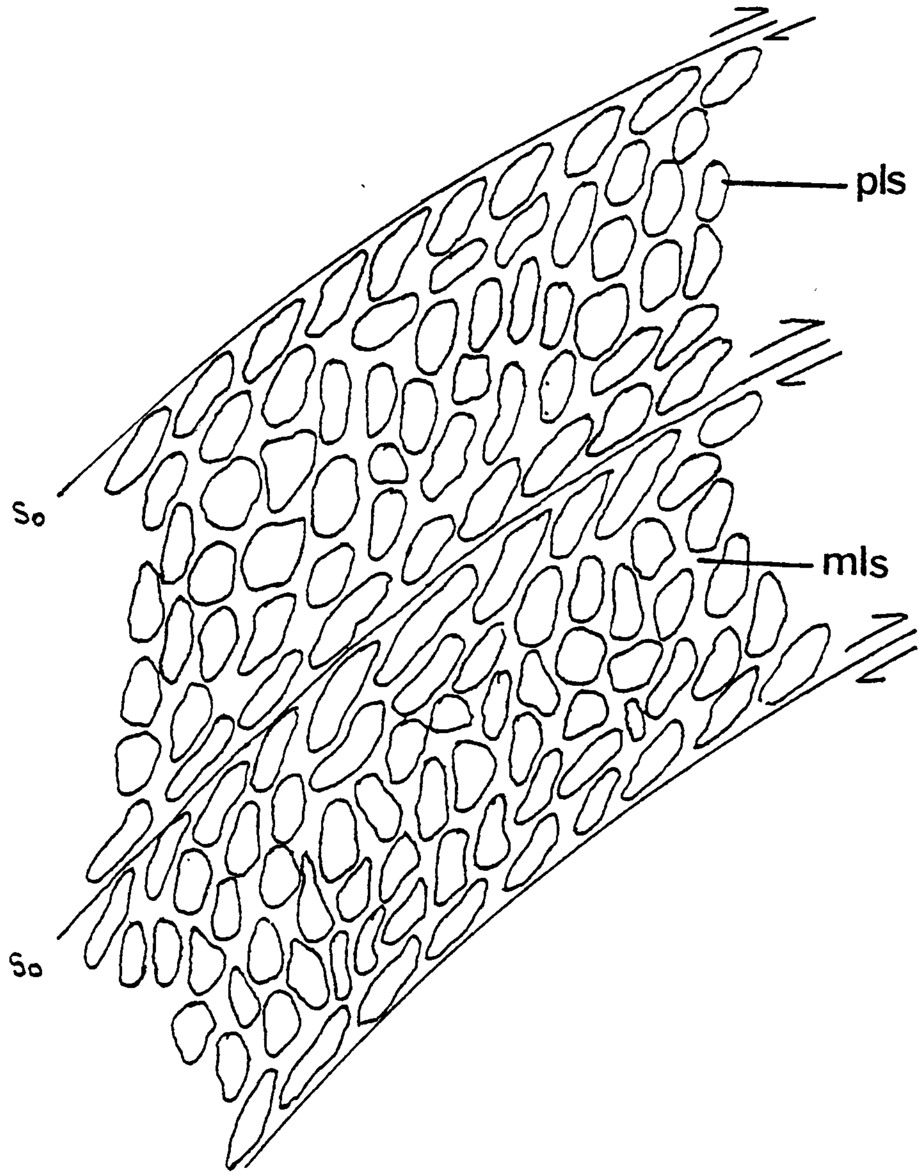

Figure 29. Photograph and field sketch of cleavage reflected in bed parallel slippage.

Two beds within a fold were found to vary in their percentages of limestone-rich zones to clay and slit rich zones (Figure 30). Uniform bulk strain is assumed since the beds are part of the same fold, yet cleavage developed along a shear plane disperses abruptly when crossing bedding planes. Well developed cleavage in the clay and silt rich bed ends within centimeters of entering the less argillaceous bed. Argillaceous limestones, therefore, appear to foster higher intensity cleavage than do areas richer in limestone which have undergone similar stress. Analogous relationships of cleavage to clay content were noted by Alvarez (1978).

Calcite Veining

Abundant calcite veining of shear or brittle origin is associated with the most densely developed cleavage; whereas, less intensely cleaved areas show fewer or no similar fabrics. Calcite veins of this nature are, therefore, cited as evidence that much of the "missing" material involved in dissolution during cleavage development is reprecipated locally. Groshong (1975) suggested that most of the material removed along the cleavage laminae is locally precipitated as cement. Hudson, (1975) further suggested that this "cement" is responsible for the preservation of otherwise friable rocks.

Schmidt Net Analysis

Structural fabrics within the study area were measured in the field and plotted on a lower hemisphere equal area net. The symbols used for various fabrics are listed in Table III. Cleavage and bedding plane attitudes were plotted as pole points to a plane of a given strike

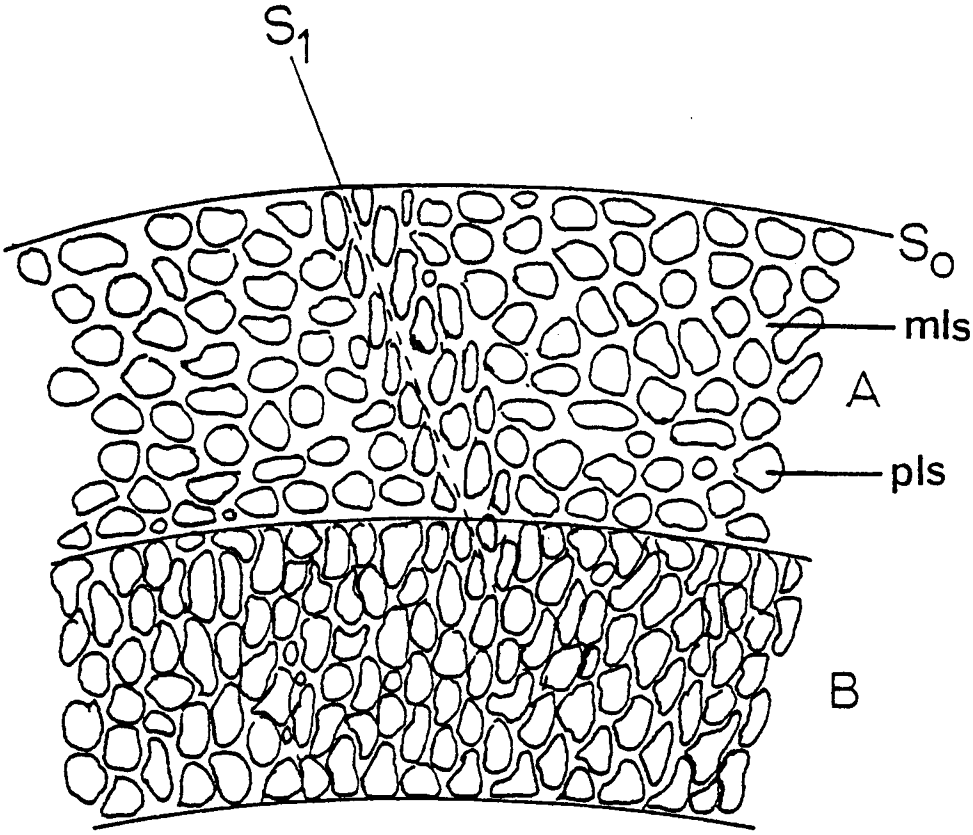

Figure 30. Mesoscopic solution cleavage developed along a shear plane in layer A and dying out in layer B. Layer A has a greater percentage of clay content than B. Limestone rich nodules are designated pls and the muddy limestone matrix is labled mls.

and dip direction. The poles of surfaces were then oriented along a great circle to the Schmidt net called a girdle, pi-circle or a-c plane (Turner and Weiss, 1963). The pole of the pi-circle is the fold axis and equivalent to the lambda 2 (λ_2) direction of a strain ellipsoid (Appendix B). A visual bisectrix which halves the pole points along the great circle and is representative of the fold crest is the lambda 1 (λ_1) direction for that fold. Lambda 3, (λ_3), the direction of maximum shortening in a strain ellipsoid, is found along the great circle or pi-circle at 90^o from the lambda 1 direction. Poles to surfaces are at 90^o from the surfaces themselves. Bedding and cleavage orientations were contoured using density contours when a large number of orientations were measured.

It should be noted that both cleavage planes and bedding planes within the Lenoir were usually undulatory across a single surface. Wide splays of points on the Schmidt net are, therefore, better interpreted as errors in field measurement than as extensive external rotations of the fabric itself. Experimental rotation of pole points around the regional strike increased the spread of data.

Folds

Three groups of macroscopic and mesoscopic folds have been recognized in the study area (Table V). The largest macroscopic or megascopic fold (F_1) consists of a first order domal uplift. This fold forms a large open fold with an exposure nearly three kilometers across and a maximum amplitude of less than 150 meters. Limbs of the fold dip steeply in comparison to the width of the crest. The F_1 fold plunges gently to the southwest, exposing the Lenoir Formation for over eight

TABLE V

STRUCTURAL ELEMENTS IN THE KNOXVILLE THRUST SHEET SOUTH OF KNOXVILLE, TENNESSEE

Folds		Planar Structures	
<u>Macroscopic</u>			
F_1	First-order domal warping concordant with underlying thrust.	S_o	Sedimentary bedding.
		S_1	Pervasive axial plane solution cleavage sub-parallel to F_1 and F_2 folds.
<u>Mesoscopic</u>			
F_2	Second-order parasitic folds across the F_1 fold. F_1 and F_2 folds are coaxial.	S_1	Solution cleavage with variable orientations relative to local stress deviations.
F_3	Third-order hand specimen folds with S_1 subparallel to F_3 fold axes and with material loss increasing toward fold core.		

kilometers along the fold axis, which trends northeast--southwest. The axial plane (Figure 31) of the fold is vertical. Contoured poles to bedding show a large concentration of points in the center of the pi-circle, which (assuming a fairly uniform sampling of the area) demonstrates the anomalous width of the crestal area.

Solution cleavage across the entire anticline has a general strike of N65°E, which is within one degree of the trend of the F_1 fold axis. The overall trend of cleavage is, therefore, inferred to be coaxial and axial planar to F_1 folding (Figure 32). A wide spread of cleavage clearly shows that it is not uniformly axial planar to folding, and develops in response to progressive deformation and local stress variations (Figure 33). Figure 33 is a rose diagram of frequency of cleavage directions. Selvage orientations vary from N50° to N90°, but the bulk of cleavage forms a fairly tight trend. Figure 33 is representative of all cleavage intensities. Plots of each cleavage intensity show only minor rotation from a general trend of N75°E for "low" cleavage to N62°E for "high" cleavage. Figure 34 is a Schmidt net plot of cleavage ranking versus orientation. It demonstrates that there is no grouping of intensities.

F_2 mesoscopic folds are visible in individual outcrops across the F_1 fold. Wavelengths and amplitudes of individual folds vary in the regional dip direction (Figure 22). Due to the generally poor exposure and lack of unique marker beds within the Lenoir, no continuous line of outcrops was available. Therefore, Figure 22 is based on lines A to A', B to B' and C to C' (Figure 15, pg. 41) and is representative of the general fold variation and not a continuous section. Dashed lines

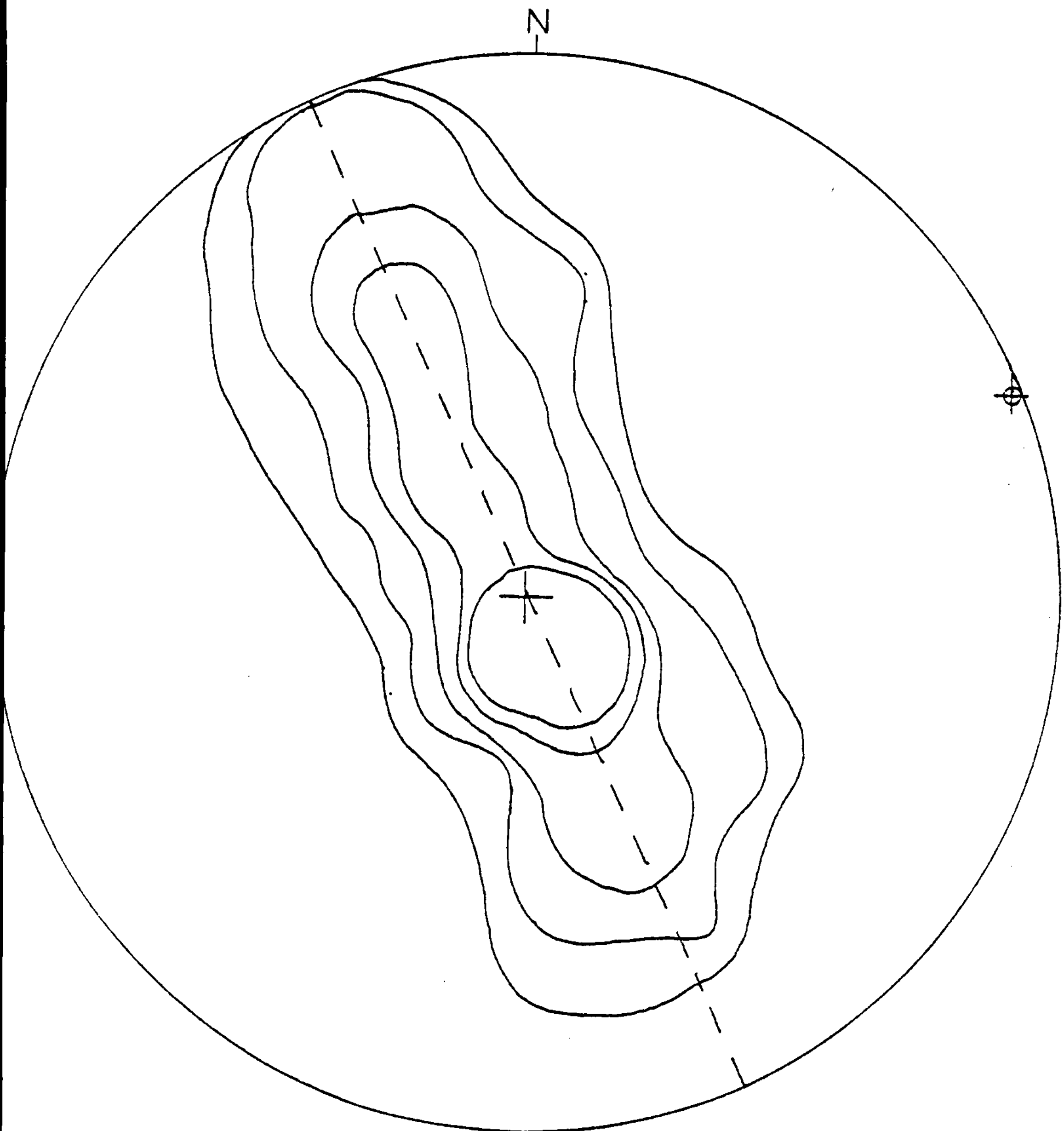

Figure 31. Schmidt diagram: Megascopic F_1 fold; Chapman Ridge anticline. Two hundred twenty poles to bedding contoured at 1, 5, 10, 15 and 20 percent.

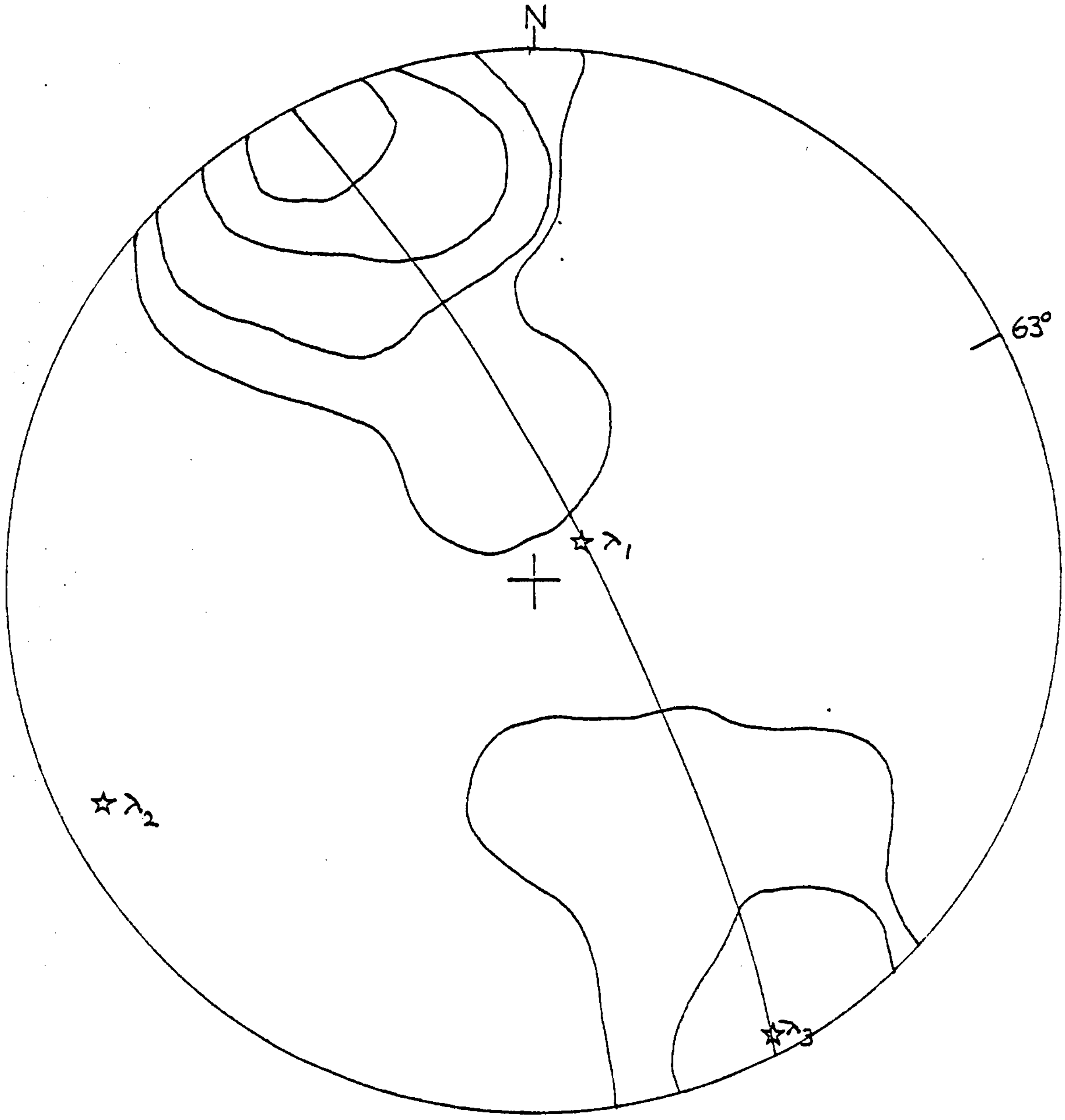

Figure 32. Schmidt net: Megascopic S_1 cleavage. Eighty-three poles to cleavage contoured at 1, 4, 8 and 18 percent.

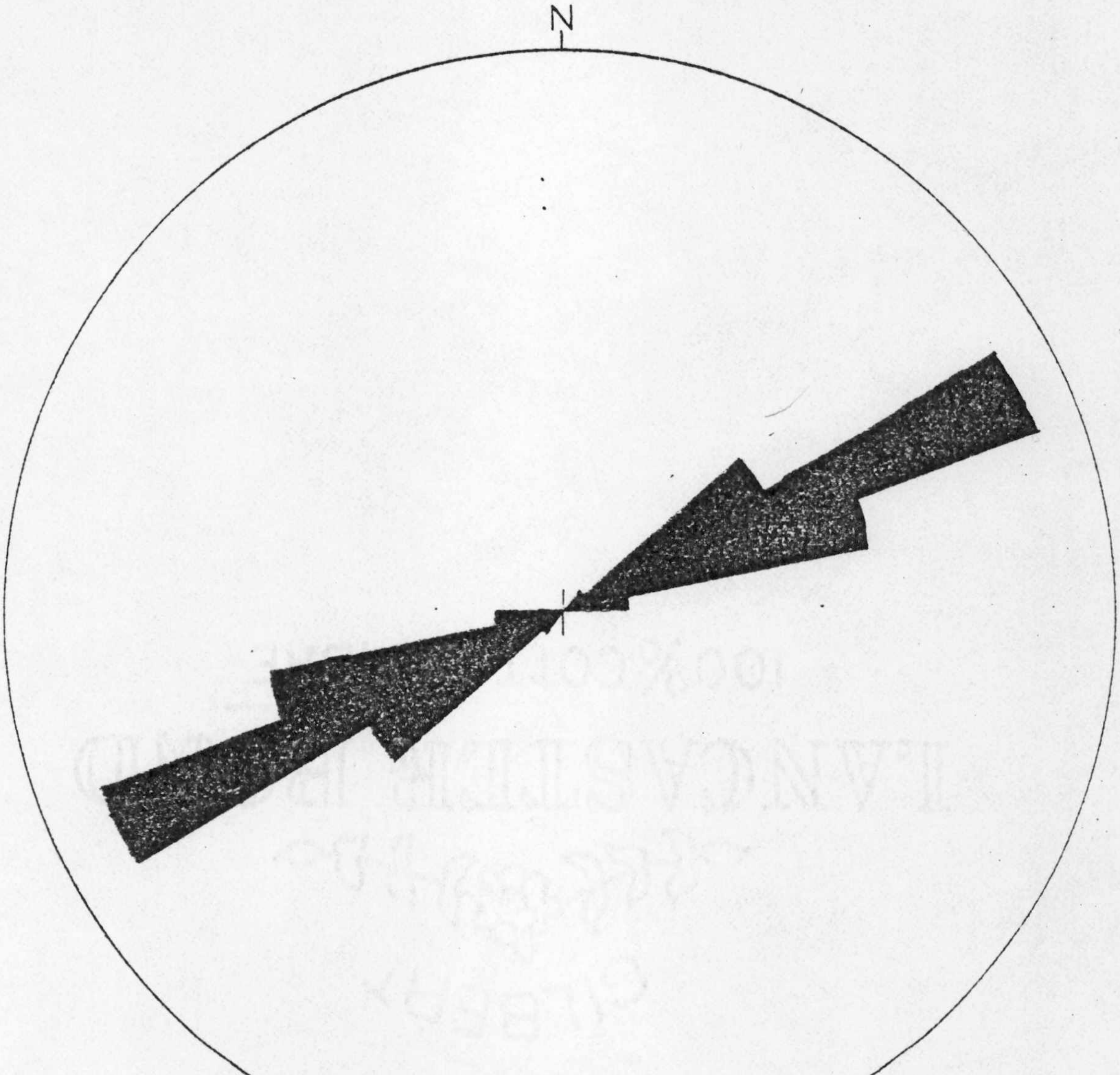

Figure 33. Rose diagram of cleavage orientations.

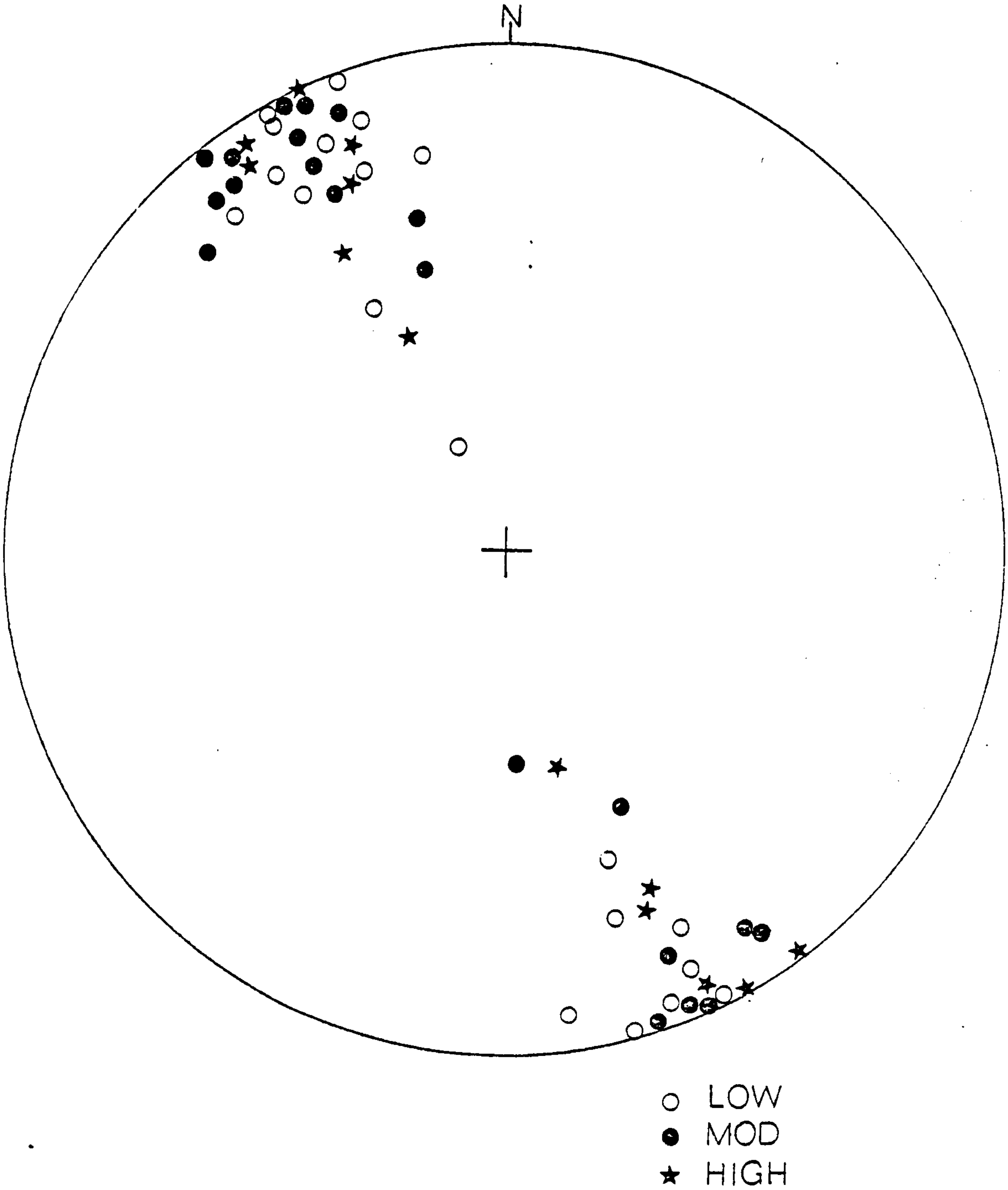

Figure 34. Schmidt net: S_1 cleavage intensity relative to strike and dip.

represent inferred folding patterns, and solid lines depict established folds. Thin lines are scaled field sketches of individual outcrops. Dotted and dashed lines denote zones of varying cleavage intensities.

Area A (Figure 22, pg.51) is dominated by rocks which have a pervasive cleavage. Mesoscopic folds in this plot (Figure 35) have an isoclinal to gentle interlimb angle (Table III, pg. 52 for interlimb angle conventions) and a slightly fanning axial plane cleavage. Fold symmetry is monoclinic with northwest-dipping limbs slightly longer than southeast-dipping limbs. Wavelengths of folds vary from ten meters in folds near the Holston-Lenoir contact to nearly 100 meters further north. Folds are of a concentric type to the northwest end of the outcrop but grade into a highly deformed, boudinaged and isoclinal folds on the southeast end.

The Schmidt net in Figure 35 shows two distinct clusters of poles to bedding in the northwest and southeast quadrants. The dashed line is the a-c plane for F_2 folds in this location. Stars represent strain axes for this set of folds. A slight inclination of the axial plane of the fold and very gentle plunge of the fold axes are evident on the Schmidt net. Tension gashes, feather joints and shear surfaces in-filled with calcite cement are associated with this fold.

Area C (Figure 22) is an exposure of low intensity cleavage approximately 100 meters in length. Rocks of this location are generally poorly cleaved, but occasional conjugate shear pairs develop more pronounced cleavage. Folds typically have a gentle interlimb angle with orthorhombic symmetry. Wavelengths are in the order of 25 to 30 meters. However, departing from this general trend, one fold at the northern extreme of the outcrop has a much tighter interlimb angle and a distinct

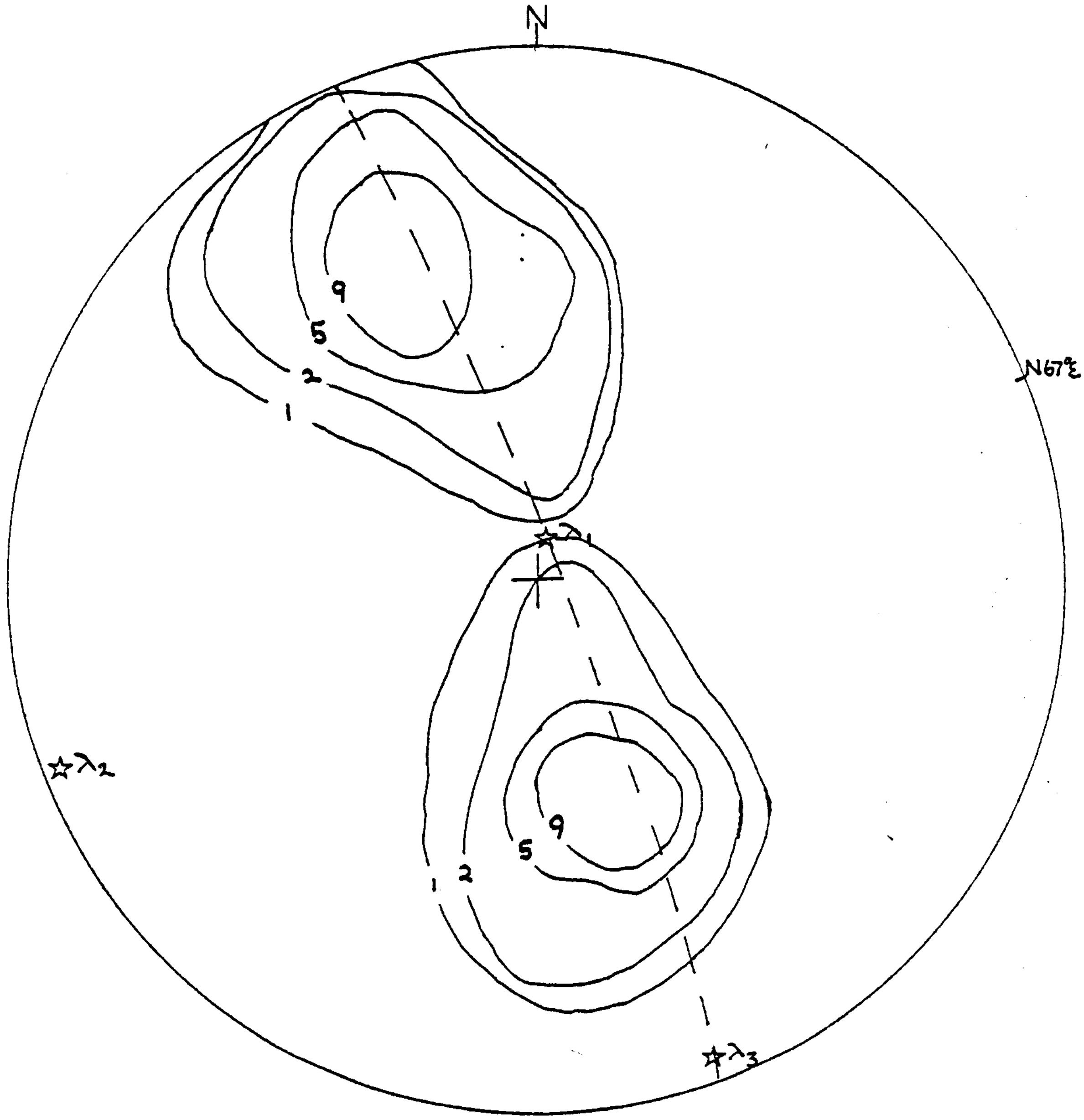

Figure 35. Schmidt net: Mesoscopic F_2 folds. Location: A (Figure 3). Fifty-five poles to S_o bedding contoured. Contours at 1, 2, 5 and 9 percent.

monoclinic symmetry. This anomolous fold is interpreted to be the near surface response to subsurface faulting.

Area D contains no mesoscopic or microscopic cleavage. Wavelengths of folds in this area extend beyond the limits of individual outcrops and are estimated to be in the order of 400 meters. The interlimb angle is gentle, and the rocks are generally more consolidated than in cleaved areas. Low topographic relief, however, limits the extent of exposures. Fold symmetry is orthorhombic, and the average fold axis strikes N61°E. Rocks of this location are well consolidated with no observed slickensides, calcite veining or shear planes. Small outcrops between areas C and D show a gradational change in both fold patterns and cleavage types. The Schmidt net in Figure 36 illustrates the pattern of poles to bedding for F_2 folds near the crest of the F_1 anticline. A slight shift of data toward the northwest quadrangle is developed with an unimodal distribution. The a-c plane, passing nearly through the origin and the unimodal grouping, represent a fold with a horizontal fold axis but an inclined axial plane.

Area B consists of very thick to massive beds of argillaceous limestone. Bedding planes are infrequent but distinct when present. Although area A and B warrant the same cleavage ranking by definition, A contains, by far, the most intense cleavage in the study area.

The Schmidt net for poles to bedding (Figure 37) in area B again shows a nearly horizontal fold axis. A bimodal distribution of pole points with a shift to the southeast quadrant depicts an axial plane to a fold which dips steeply to the southeast. Fold symmetry for this area is also monoclinic with longer limbs dipping to the northwest and shorter limbs dipping to the southeast. The interlimb angle is open.

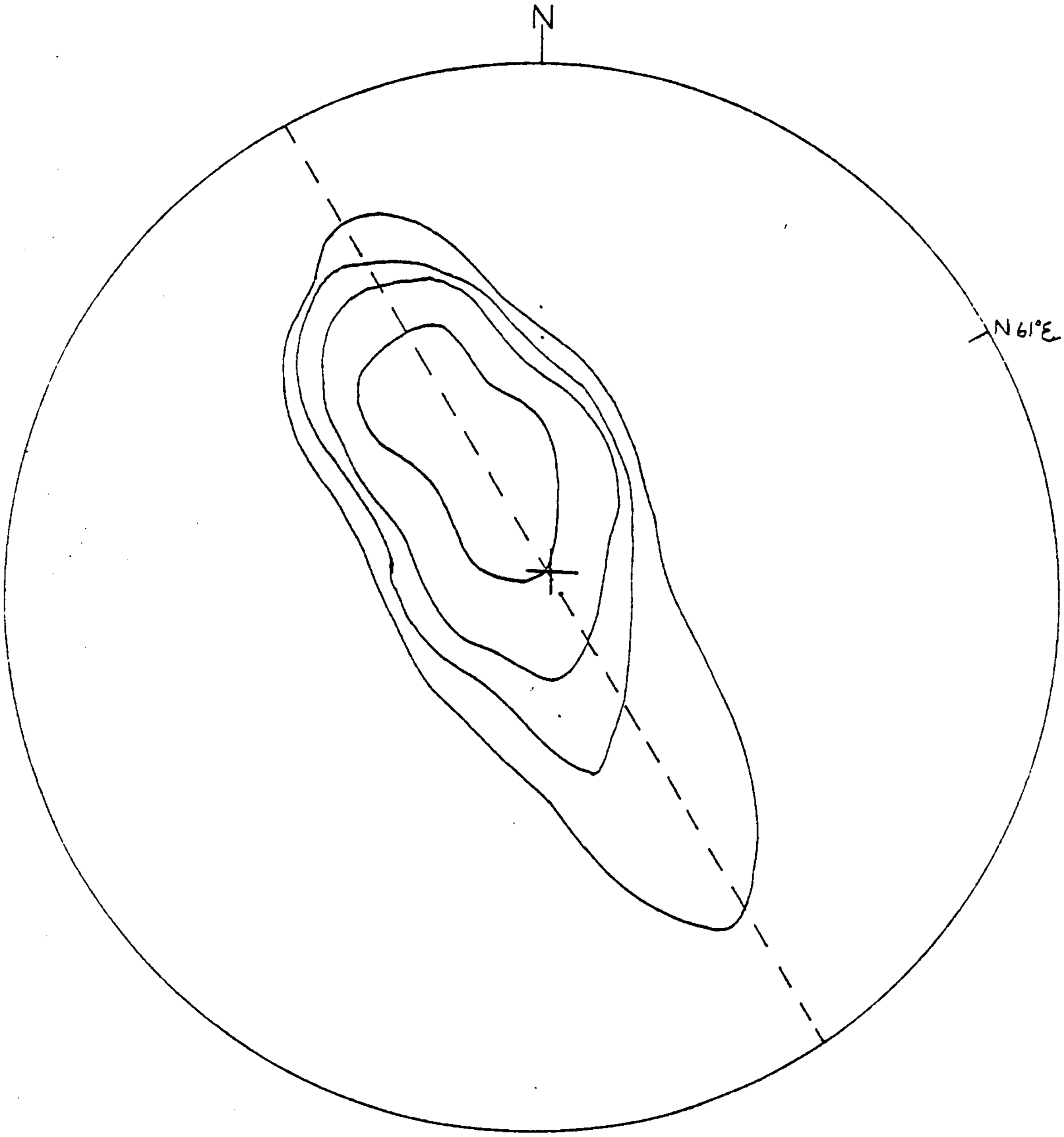

Figure 36. Schmidt net: Mesoscopic F_2 folds. Location: D (Figure 3). Fifty-three poles to S_o bedding contoured at 1, 4, 8 and 18 percent.

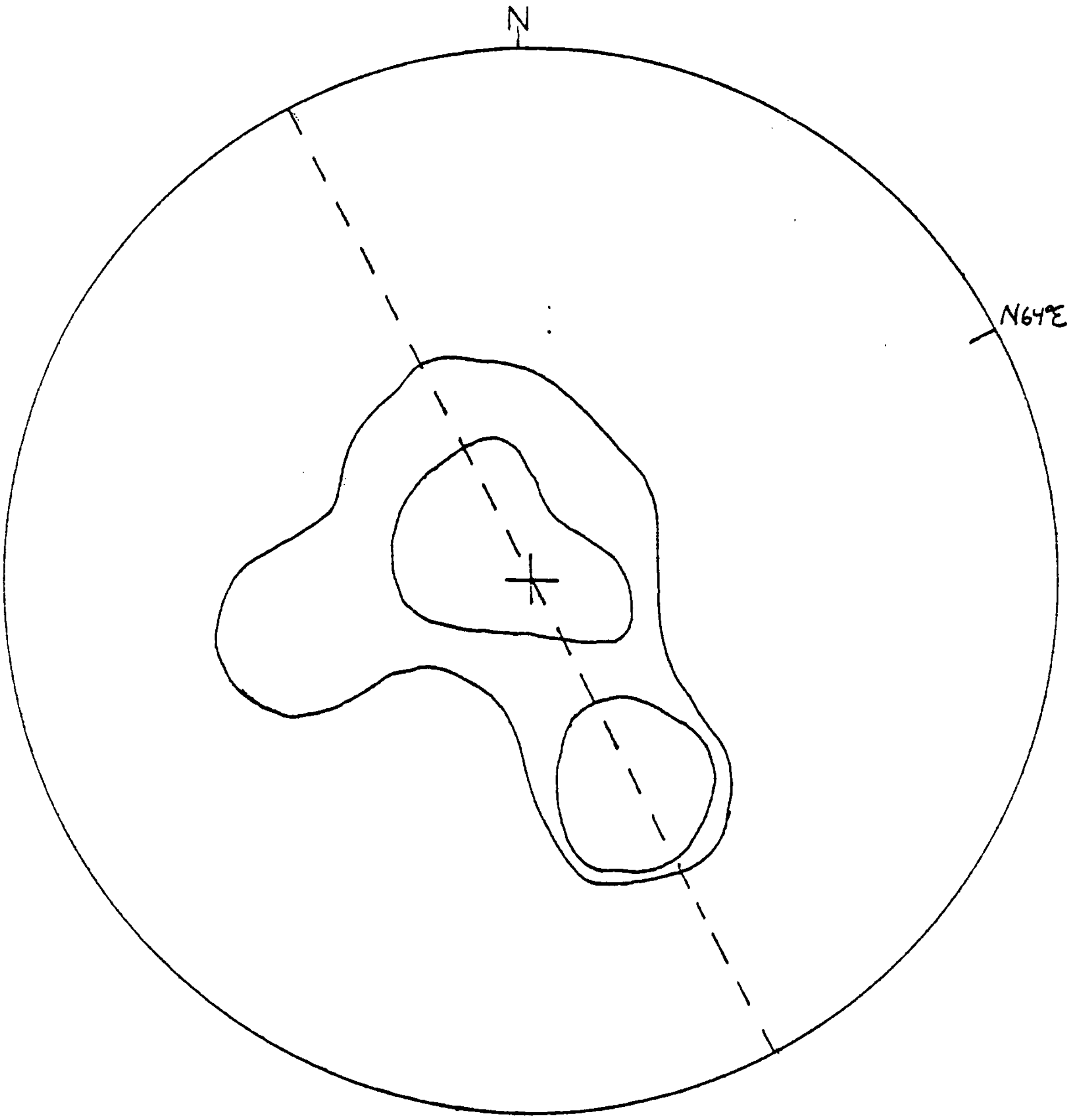

Figure 37. Schmidt net: Mesoscopic F_2 folds, location B. Thirty-seven poles to S_o bedding contoured at 3 and 14 percent (Figure 3).

F_2 folds on the crest and both limbs of the Chapman Ridge anticline illustrate a fanning of axial planes. However, the fold axes or the lambda 2 strain axes of F_2 folds are consistently within two or three degrees of the megascopic F_1 fold axis. Lambda 1 and lambda 3 vary between F_1 and F_2 folds but are interpreted to be of the same deformational event. Folds generated when the anticline was young, undergo some rotational deformation as is depicted by monoclinic fold symmetry, but most of the original F_2 orientation is preserved. It might be suggested that F_2 folds formed before the F_1 fold, but had this been the case, one would expect a uniform distribution of fold wavelengths across the studied anticline.

Cleavage is also coaxial to both F_1 and F_2 folds. An average strike of solution cleavage which is very close to the strike of all folds and strain axes that fall within eight degrees of the F_1 fold axis, supports this conclusion. Within the limits of errors in measuring undulatory surfaces, F_1 and S_1 are coaxial and thus, of the same deformational event.

F_3 folds (Figure 6A) are the smallest recognized folds in the study area. Folds of this scale are internal within major beds. These "internal" folds are visible as a wave type train of limestone-pure nodules in an otherwise clay or silt-rich matrix. Undeformed exposures of Lenoir display alternating layers of limestone-pure and detrital-rich beds and are the result of bioturbation horizons. These discontinuous horizons are parallel to recognized bedding planes.

Folding on the F_3 scale is confined to zones of the study area which contain cleavage. Realms with low cleavage development have only undulatory folding of these horizons while greater cleaved areas have much more pronounced F_3 folding. In zones with very high cleavage intensity, F_3 folding tends to be obliterated and unrecognizable. In the most intensely disrupted area near the southeast end of the anticline, F_2 mesoscopic folds are so greatly distorted that only F_3 boudinaged folding remains.

Because F_3 folds do not form bedding planes, it is impossible to accurately measure and plot fold elements. F_3 folds have a wavelength range of five to ten cm. Interlimb angles vary with cleavage intensity from gentle in poorly cleaved zones, to isoclinal in boudinaged regions. Average laminae orientations for the rock as a whole are not related to internal folding, but cleavage often shifts locally to perpendicular with respect to bioturbation horizons.

Axial planes of F_3 folds are not accurately measurable with standard field techniques. The fact, however, that F_3 folds are themselves folded by F_2 folds is strong evidence that F_3 folds formed early in the development of F_2 folds. If only the limbs of the study area were examined, one would quickly conclude that F_3 predates all other folding. However, when the crestal area of the anticline is considered with the fact that there is no F_3 folding in this zone, one needs to reevaluate the kinematic sequence. The close relationship of F_3 folding to both S_1 cleavage and F_2 folding precludes its placement as a separate deformational event predating any other. F_3 folds are, therefore, concluded to have formed early in the development of F_2 folds and to have preserved their original strain orientations despite external rotation.

In summary, all fabrics, even though rotational evidence is demonstrated, are of a single progressive deformational event. No single fold type or cleavage is independent of any other in its kinematic time of formation. F_1, F_2 and F_3 folding were all initiated simultaneously with each level of folding, ending when no longer supported by regional or local stresses. Cleavage forms a fanning, axial planar pattern to each size of fold, and its relative orientation depends on the scale at which it is studied.

CHAPTER V

MEGASCOPIC ANALYSIS

On a larger scale, the occurrence and position of solution cleavage was examined across the Ridge and Valley thrust belt. Two cross-sections from the North Carolina-Tennessee border to Pine Mountain were constructed through the study area. Evidence demonstrating that cleavage is fold-controlled and thus synkinematic with domal warping was crucial in regional interpretation in and around the Chapman Ridge anticline. Superimposed over the fold related cleavage is a system of cleavage and boudinaged bedding associated with the Dumplin Valley thrust emplacement. These kinematic relationships of cleavage and structure confirm earlier constructed balanced sections by Roeder, Gilbert and Witherspoon (1978).

Procedures

The principles and procedures used in construction and geometrical balancing of sections follow techniques presented by Roeder, Gilbert and Witherspoon (1978).

Cross-sections were constructed perpendicular to strike for easy correlation along strike. A scale of 1:125,000 was used in the original construction, and all recognized formations were accounted for. The Knox and carbonate portion of the Chickamagua Group were then combined and drawn as a massive black unit. Pre-Rome rocks involved in thrusting were drawn in as diagonally ruled areas. This method of simplification was employed for better correlation with sections by Roeder, Gilbert and Witherspoon (1978). All sections were then reduced for easier publication.

Sections were constructed from maps by Rodgers (1953, Plates 1, 2, 8 and 9) and geologic quadrangles by Cattermole (1958). Mesoscopic field examination and analysis were useful in controversial areas.

Stratigraphic formation thicknesses were constructed in compliance with the general stratigraphic wedge of Tennessee (Roeder, 1978) (Figure 5, pg. 11) and constructed thicknesses. Construction techniques for determining stratigraphic thicknesses are shown in Figure 38. Methods involve the construction of a line perpendicular to the formations with the same dip and dip direction into a single unit. The thickness of those beds would be the perpendicular thickness. Formation thicknesses were corrected for position within the thrust belt and also for estimated amounts of transport due to thrusting.

The base of each section is taken to be the Rome Formation. Depth to basement was obtained from Tegland (1978) and is correlatable with depth to basement determinations by Roeder, Gilbert and Witherspoon (1978).

Regional Occurrence of Solution Cleavage

Solution cleavage was confined to the anticline of the study area and is associated with frontal zone fabrics. Outcrops of the same lithology which have undergone simple thrusting without folding showed no signs of solution cleavage. Apparently, horizontal compression in the frontal zone was necessary for cleavage development in the Lenoir since outcrops associated with transport zone fabrics show no similar development. (See Figure 39 for an explanation of frontal zone and transport zone fabrics).

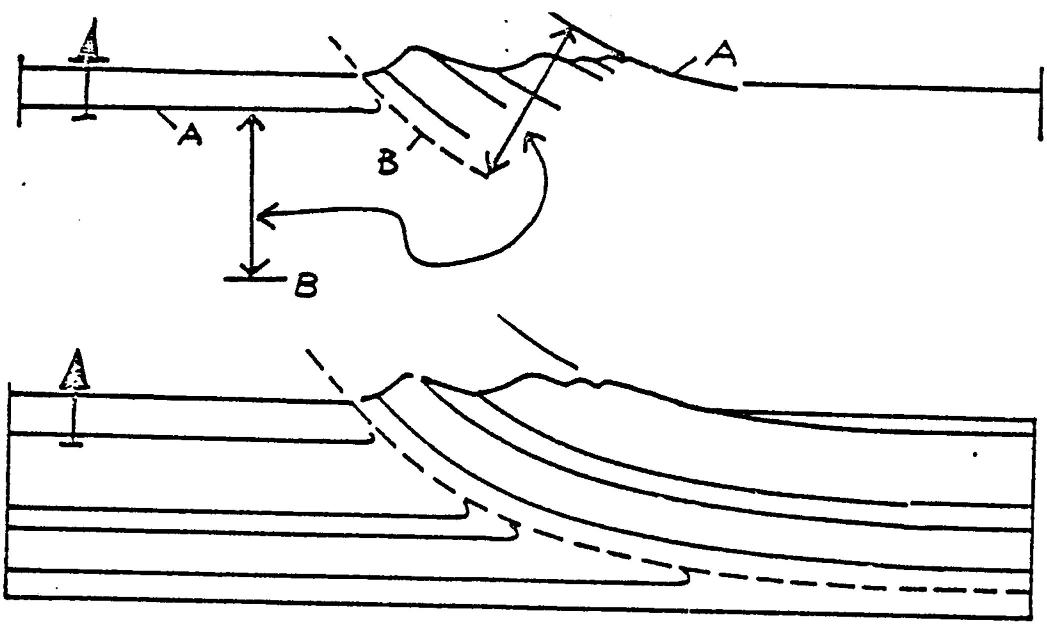

Figure 38. Structure section showing procedures used in balancing cross sections. Upper section: thickness of thrust unit is determined by constructing a perpendicular to bedding. Lower section: measure thickness is added stratigraphicly below known horizon (Roeder, 1978).

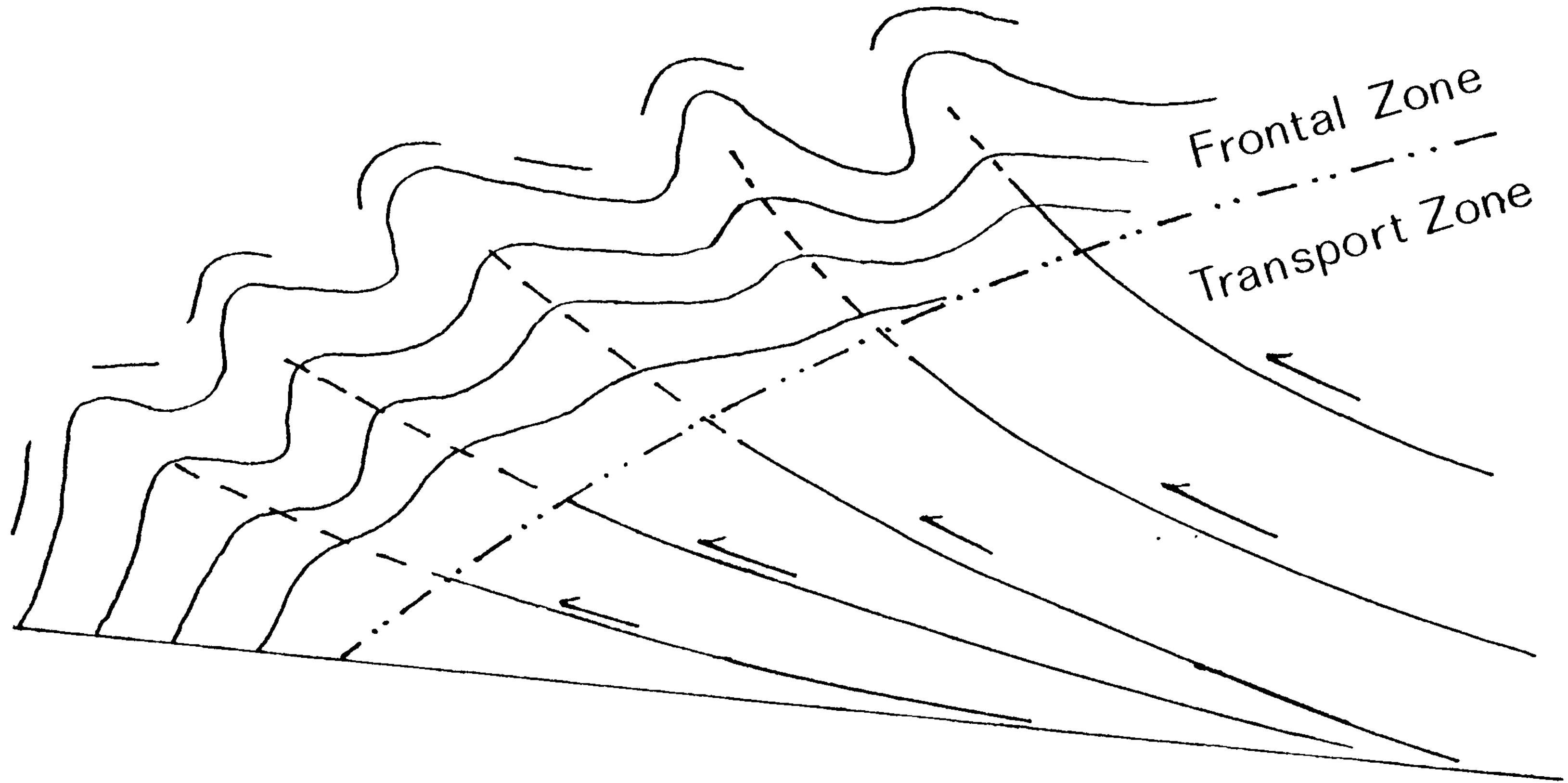

Figure 39. Schematic cross section of a thrust belt showing the transition from frontal zone folding to transport zone low angle thrust faulting.

Description of Cross Sections

Based on reflection seismic data (Tegland, 1978) and on stratigraphic constrictions (Roeder, Gilbert and Witherspoon, 1978), the basement top beneath the study area is located at a depth of about 5 km and dips at 2 to 3 degrees to the southeast.

Roeder, Gilbert and Witherspoon (1978) have determined a foreshortening of 53 to 59%. Similar shortening has resulted from the present study and a reasonable correlation along strike is possible with sections by Roeder, Gilbert and Witherspoon (1978).

Four zones can be distinguished in each section (Figure 40). The basis of distinction is on fabric type and kinematic age of development. A description of each zone is presented below: (Descriptions concern section B-B' (Plate 2) and can be correlated along strike with section A-A' (Plate 1).

Zone I comprises the Pine Mountain thrust sheet and marks the orogenic front (Plate 2). It is characterized by extensive bedding parallel decollements in shallow stratigraphic horizons. The Pine Mountain thrust shows simple ramping and a broad anticlinal structure.

Zone II comprises the evenly distributed imbricate thrusts between the Hunter thrust and the Saltville thrust. Three major thrusts are found in this zone: the Copper Creek thrust, the Hunter thrust and the Beaver Valley thrust. The Hunter thrust and the Beaver Valley thrust splay into two faults at the surface. Imbricate slices in this zone are shown to glide along the Rome Formation. Relative timing of emplacement of these thrusts are assumed to proceed from west to east with the final

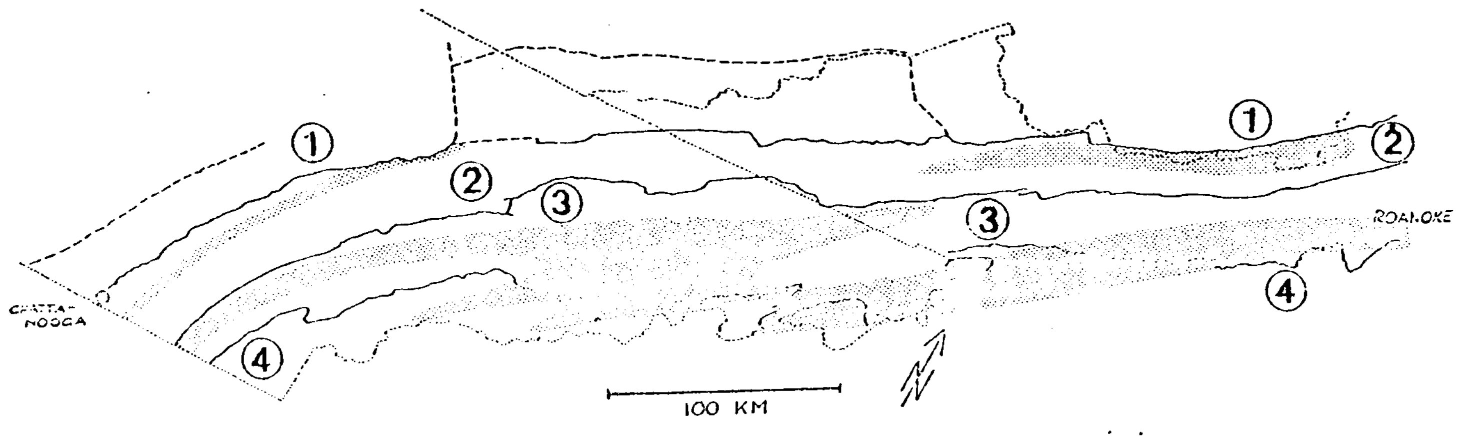

Figure 40. Structural map of deformation zones in the southern Appalachians. See text for explanation. Shaded area are belts of major polyphase redeformation of emplaced thrust sheets (Roeder, 1978).

thrust, the Beaver Valley fault, truncating the first two faults. Sole faults within the Rome are branches of the basal decollement (Roeder, Gilbert and Witherspoon, 1978).

Zone III, the most complex, extends between the Saltville thrust and the Blue Ridge-Great Smoky fault. Fabrics of this zone show both transport and frontal zone characteristics in a series of highly deformed folded-fault structures. This area marks a transition from low angle transport fabrics to frontal zone folded fabrics, possibly as a result of erosion lowering the confining pressure in the transport zone to the critical point where folding could occur (Figure 39).

The Saltville forms small splays near the surface with the oldest splay along the western extreme and the most recent splay at the eastern end. Bedding parallel transport occurs along the Rome, and a minor frontal-brow fold is formed near the surface.

Between the Saltville and Knoxville faults, a broad syncline is developed. Because this structure involves stratigraphic horizons of Cambrian age and because thrusting takes place predominantly in Cambrian rocks, the Saltville sole fault must be involved in folding at depth. Folded-fault structures such as this are associated with the frontal-fabric realm (Roeder, Gilbert and Witherspoon, 1978). The Saltville fault soles out in the basal decollement, and fold axes within the Saltville thrust sheet dip to the northwest.

The Knoxville fault overrides a small signoidal anticline drawn to fill a void created in balancing. This type of polyphase fold-fault structure is common at the front of major thrust sheets (Roeder, Gilbert and Witherspoon, 1978).

The Knoxville fault can be traced and seen to be folded by a domal folded-fault structure. This domal structure is recognizable at the surface by gentle northwest dipping strata and an anamalous divergence of the thrust fronts. The anticlinal expression of this domal structure contains the coarse set of axial plane cleavage described in this paper.

The Dumplin Valley fault involves ramping with extensive bedding parallel slippage along Middle Ordovician rocks for about 15 km. Surface splays of the Dumplin Valley fault show a younging to the east and well developed drag features. The Dumplin Valley fault is interpreted as a break-back fault. Associated with ramping is a large box shaped frontal-brow fold with a conjugate set of axial planes. Final emplacement of the Dumplin Valley fault and extensive bedding parallel transport are interpreted to be coeval with the development of cleavage and boudinaged bedding in the southeast limb of the Chapman Ridge anticline.

Zone IV extends eastward from the Great Smoky fault. Structures of this area vary from major low angle thrusting to steeply dipping polyphase thrusts and westerly dipping formations (Roeder, Gilbert and Witherspoon, 1978). Pre-Rome rocks, indicated by diagonally ruled areas, are involved in thrusting and associated with extensive transport. Substantial parts of deformation in this zone are Middle Ordovician in age (Rodger, 1970; Keller, 1980). Kinematically younger than the imbricate thrusts is a large domal structure, which does not break the surface in section I but forms a fenster to younger rocks in section 2 and many other sections along strike. Two deep imbricate thrusts with small increments of transport were constructed at depth to account for this structure.

Kinematic Sequence

Through the use of local cross-cutting relationships in the field and in balanced cross sections and by extending these relationships into the thrust sheet itself, a general kinematic sequence of deformational events can be established. Events within each thrust sheet can be further expanded to encompass the entire thrust belt.

Instrumental in establishing a kinematic sequence is the recognition of two distinct regions of a thrust belt: the transport zone and the frontal zone (Figure 39). The zones are designated on the basis of fabric types, which is a reflection of the confining pressure. Fabrics of the transport zone (lower zone) develop under greatly confining pressure and, combined with horizontal tectonic forces, develop predominantly low angle thrusting. Frontal zone fabrics (top zone) on the other hand, are subjected to less confining pressure and tectonic compressive forces in this realm lead to development of folded structures. Folded fault structures such as those described in zone III are the result of a movement from the transport zone to the frontal zone by a reduction of confining pressure. Such a reduction is caused by erosion during deformation. An increase in confining pressure would lead to the development of "faulted-fold structures" as fabrics move from the frontal zone to the transport zone. Such a transition is possible by deposition during deformation or extensive overthrusting.

Three major kinematic events are recognized in the development of the Chapman Ridge anticline. Fabrics of these events mark a shift from transport zone to frontal zone tectonics and correspond with zone III mentioned earlier. Age dating of these events is Middle to Late Pennsylvanian.

Event I consists of ramping and transport of the Knoxville thrust for nearly 14 km. Transport is along Middle Ordovician rocks and is placed at this kinematic setting because it is folded by domal warping.

Event 2 consists of domal warping resulting from ramping at depth. Two small imbricate thrusts transform the simple thrust faulting of zone III into the complex folded fault structure observed. Deformation associated with this event includes folding of the Saltville thrust sheet into a broad sigmoidal syncline, and warping of the Knoxville thrust fault to form the Chapman Ridge anticline. F_2 and F_3 folds with fanning axial planes and solution cleavage with fold controlled stress orientations are kinematically placed in this event of domal warping.

Event 3 consists of ramping and emplacement of the Dumplin Valley thrust sheet. Deformation of this event is reflected in the Chapman Ridge anticline by the most intensely developed solution cleavage on the southeast limb of the anticline (Area A, Figure 3, pg. 6). Boudinaged bedding is also associated with this area. Deformation of this event does not penetrate deeply into the anticline.

REFERENCES

REFERENCES

Alvarez, W., Engelder, T., and Geiser, T., 1978, Classification of solution cleavage in pelagic limestones: Geology, v. 6, p. 263-266.

Alvarez, W., Engelder, T. and Lowrie, W., 1976, Formation of spaced cleavage and folds in brittle limestone by dissolution: Geology, v. 4, p. 698-701.

Benedict, G. L. and Walker, K. R., 1978, Paleobathymetric analysis of Paleozoic sequences and its geodynamic significance: American Journ. Sci. V. 27.

Beutner, E. C., Jancon, M. D., and Simon, R. W., 1977, Dewatering origin of cleavage in light of deformed calcite veins and clastic dikes in Martinsburg Slate Delaware Water Gap. New Jersey: Geology, v. 5, p. 118-122.

Dean, S. L. and Kulander, B. R., 1977, Kinematic analysis of folding and pre-folding structures on the southwestern flank of the Williamsburg anticline, Greenbriar County, West Virginia: Geologic Society American Abs. with Programs, v. 9, No. 2, p. 132-133.

Dieterich, J. H., 1969, Origin of cleavage in folded rocks; American Journ. Sci., v. 267, p. 155-165.

Durney, D. W., 1972, Solution transfer and important geological deformation mechanism: Nature, v. 235, p. 315-317.

Elliott, D., 1973, Diffusion flow laws in metamorphic rocks: Geologic Society of America Bulletin, v. 84, p. 2645-2664.

Geiser, D. A., 1974, Cleavage in some sedimentary rocks of the central valley and ridge province, Maryland: Geologic Society of America Bulletin, v. 85, p. 1399-1414.

Gray, D. R., 1979, Microstructure of crenulation cleavages: an indicator of cleavage origin: Am. Journ. Sci., v. 279, p. 97-128.

Groshong, R. H. Jr. 1975, "Slip" cleavage caused by pressure solution in a buckle fold: Geology, v. 3, p. 411-413.

Groshong, R. H. Jr., 1976, Strain and pressure solution in the Martinburg Slate Delaware Water Gap, New Jersey: Am. Journ. Sci. v. 276, p. 1131-1146.

Hardeman, W. D., 1953, Geologic map of East Tennessee with explanatory text: Tennessee Division of Geology Bulletin 58, Part II.

Harris, L. D. and Milici, R. C., 1977, Characteristics of thin skinned style of deformation in the southern Appalacians and potential hydrocarbon traps: U. S. Geol. Survey Prof. Paper 1018, p. 40.

Hobbs, B. E., Means, W. D., and Williams, P. R., 1976, An outline of structural geology: John Wiley and Sons, Inc., New York, London, Sidney and Toronto, p. 571.

Hudson, J. D., 1975, Carbon isotope and limestone cement: Geology v. 3, p. 9-22.

Keller, F. B., 1980, Late Precambrian stratigraphy, depositional history and structural chronology of part of the Tennessee Blue Ridge: Yale Univ., New Haven, Conn., Ph. D. dissertation, p. 353.

Milici, R. C., 1975, Structural patterns in the southern Appalachians: evidence for a gravity slide mechanism for Alleghanian deformation: Geologic Society America Bulletin, v. 86, p. 1316-1320.

Nickelsen, R. P., 1972, Attributes of rock cleavage in some mudstones and limestones of the Valley and Ridge Province Pennsylvania: Pennsylvania Acad. Sci., v. 46, p. 107-112.

Ramsay, J. G., 1969, The measurement of strain and displacement in orogenic belts in Kent, P. E. (ed.) Time and place in orogeny: Geol. Soc. London, Spec. Pub. 3, p. 43-79.

Ramsay, J. G., 1976, A discussion on natural strain and geological structure Philosophical Trans. of the Royal Society, v. 283, p. 1-23.

Rodgers, John, 1953, Geological map of east Tennessee with explanatory text: Tennessee Division of Geology Bulletin 58, pt. 2., 168 p.

Rodgers, J., 1970, The tectonics of the Appalachians: New York Interscience Publishers, New York, N. Y., p. 271.

Roeder, D., Gilbert, O. E., and Witherspoon, W. D., 1978, Evolution and macroscopic structure of valley and ridge thrust belt, Tennessee and Virginia: Studies in Geology 2, The University of Tennessee, Knoxville, p. 25.

Silberman, J. D., 1971, Cambrian-Ordovician structural and stratigraphic relationships of a portion of the Rome trough in Hutchenson, D. W. (ed.), Proceedings of the technical session of the Kentucky Oil and Gas Association, Kentucky Geol. Survey Spec. Pub. 21, p. 35-45.

Sorby, H. C., 1854, On the direct correlation of mechanical and chemical forces: Royal Society of London Proceedings, v. 12, p. 538-550.

Stephensson, O., 1976, Finite element analysis of folds: Pub. Trans. R. Soc. Lond. A. 283, p. 153-161.

Turner, F. J., and Weiss, L. E., 1963, Structural analysis of metamorphic tectonites: McGrew-Hill, Inc., New York, p. 545.

Weiss, L. E., 1972, The minor structures of deformed rocks, Springer-Verlag, New York, p. 431.

Williams, P. F., 1972, Development of metamorphic layering and cleavage in low-grade metamorphic rocks in Bermaqui, Australia: Am. Journ. Scil, v. 272, p. 1-47.

APPENDIX

APPENDIX

A. Methods for Finite Strain Calculation

Groshong (1976) and Alvarez (1978) have shown that truncated fabrics, such as fossils or veins, can be used in measuring finite strain. Case I describes calculations for fabrics which are bisected and show apparent fault like offsets. Case II is for fabrics which are simply truncated and not bisected.

Case I

1. Project the original shape of the vein or fossil from either side of the bisected fabric (Figure 41, A, B and C).
2. Construct a line perpendicular to the average cleavage direction (S_1) at the point of intersection of the unprojected section and the cleavage plane. This is the assumed direction of shortening.
3. Construct a line parallel to S_1 where the projected image intersects the extending original segment, and label this "S".
4. The perpendicular distance from S_1 to S is equal to l_1. This is the total length lost to shortening.
5. The length of the observed marker measured perpendicular to S_1 is equal to l_2.
6. The original length equals $l_o = l_1 + l_2$.
7. The percent loss per selvage is determined from the following equation: $\% \text{ loss} = \frac{l_1}{l_1 + l_2} \times 100.$

Case II

1. Project the shape of the original fossil established from undeformed examples (Figure 41D).
2. Construct a perpendicular from the average cleavage direction S_1 to the point on the projected curve farthest from the selvage.
3. Draw a line at this point parallel to S_1 and label it S.
4. The distance from S_1 to S is equal to l_1.
5. The actual length of the fossil measured perpendicular to the average cleavage direction is equal to l_2.
6. The original length equals $l_0 = l_1 + l_2$.
7. The minimum percentage shortening per selvage is calculated as follows: $\% \text{ shortening} = \frac{l_1}{l_1 + l_2} \times 100$.

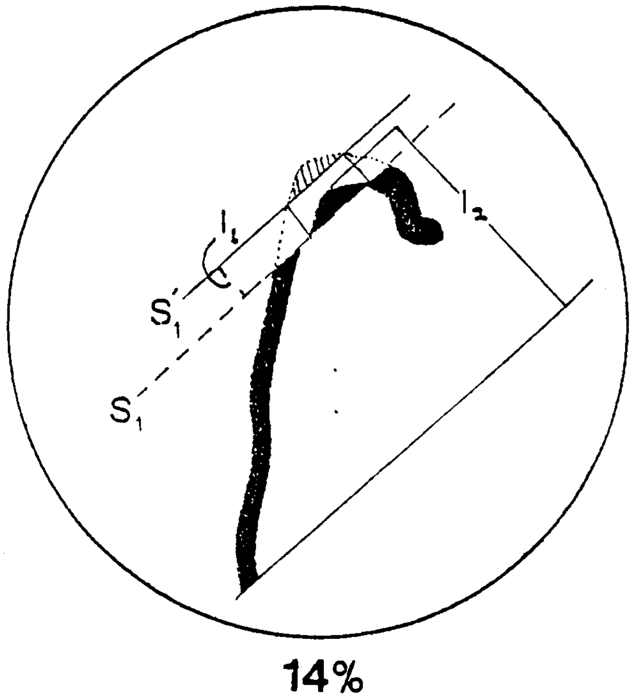

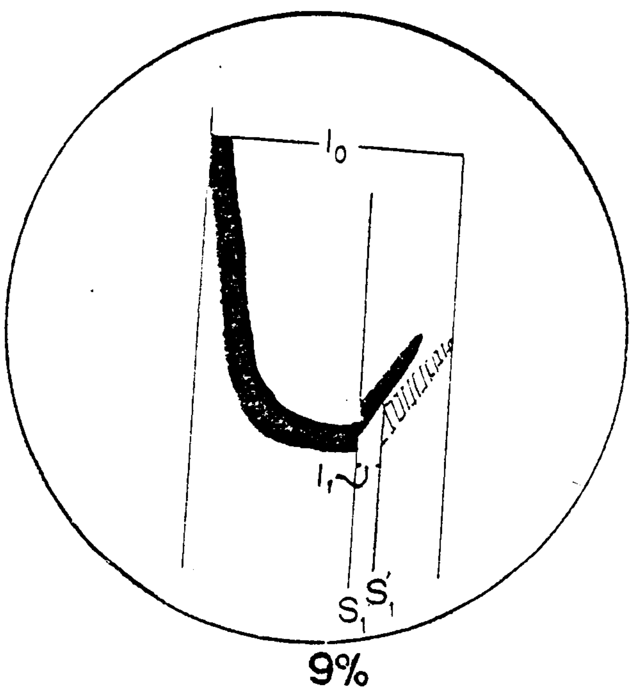

Figure 41. Scaled drawings of strain markers.

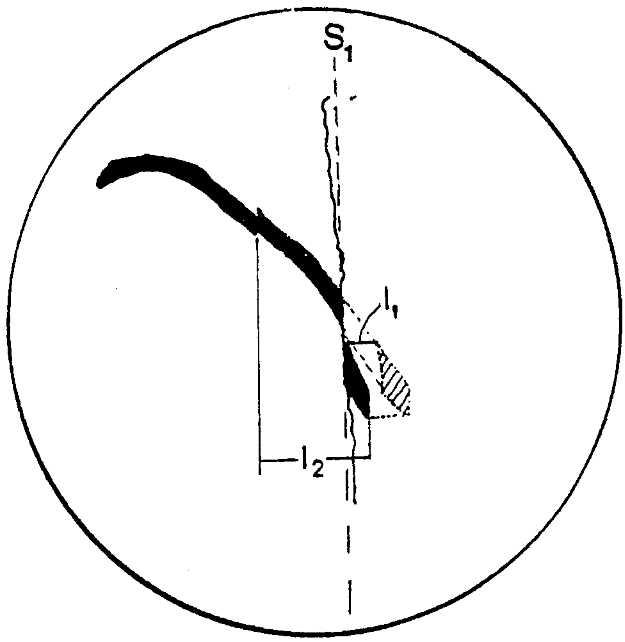

26%

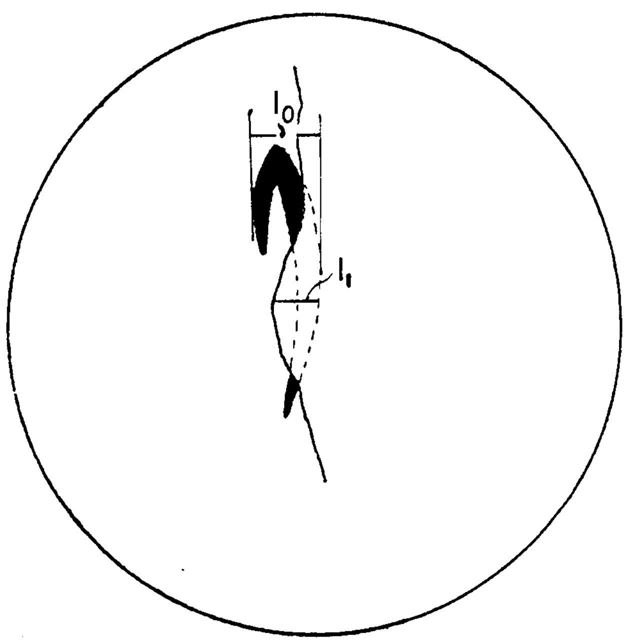

36%

Figure 41. (continued)

B. Components of Stress and Strain

Stress

Stress within a homogeneous field can be uniquely defined by three mutually orthogonal planes upon which the shear stresses are zero. These three planes are known as the principal planes of stress. Normals to these planes are the principal axes of stress. By convention, the normal stresses across the principal planes are denoted by sigma σ_1, σ_2 and σ_3 where $\sigma_1 > \sigma_2 > \sigma_3$. σ_1 is, therefore, the axis of maximum compression, σ_2. The intermediate principal stress axis and σ_3 the minimum principal stress axis (Hobbs, Means and Williams, 1976). Below is a stress ellipsoid with principal axes σ_1, σ_2, σ_3.

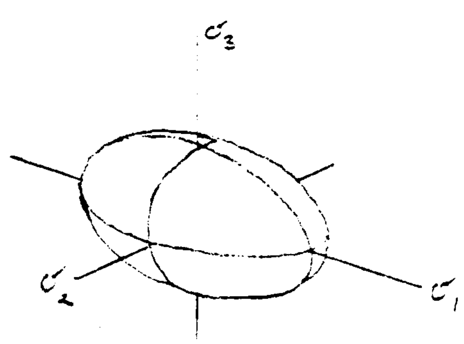

Strain

Strain is, by definition, the change in shape of a body compared to its original shape. The principal axes of strain are designated by the symbols λ_1, λ_2 and λ_3, corresponding to the maximum, intermediate and minimum principal axes, respectively. Lambda one λ_1, is the direction of maximum extension. Lambda three, λ_3, corresponds with the direction of maximum shortening. Lambda two, λ_2, is the intermediate strain axis and may be compressive or extensional. Figure A (below) is a strain ellipsoid with principal axes λ_1, λ_2 and λ_3. Figure B depicts the distribution of principal strain axes within a simple fold.

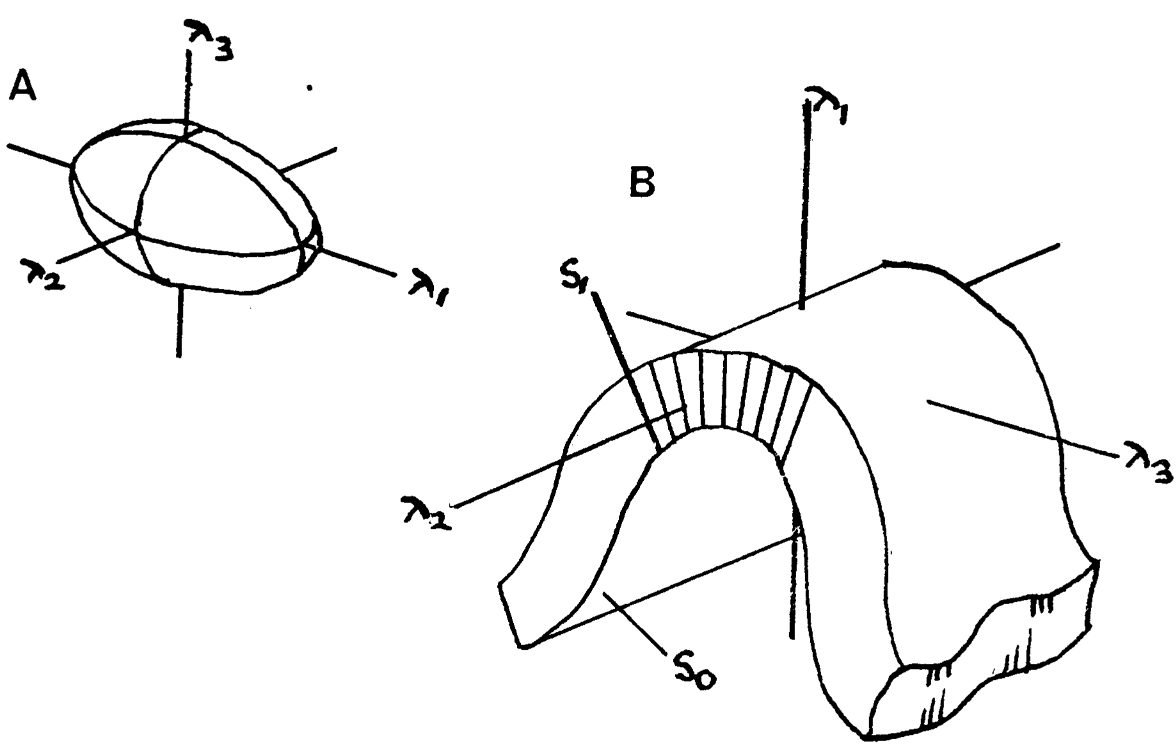

VITA

Thomas W. Wise was born in Kansas City, Missouri on October 7, 1955. He attended elementary schools in Wichita, Kansas; North Platte, Nebraska; Omaha, Nebraska; and Overland Park, Kansas and graduated from Ridgeway High School, Memphis, Tennessee in May 1974.

September 1974 he entered Memphis State University, transferring to The University of Tennessee, Knoxville in September 1975 where he received a Bachelor of Science degree in Geology in May 1978. He entered the University of Tennessee Graduate School on a graduate assistantship in September 1978.

The author is currently employed by the Geophysical Exploration Division of the Texaco Company in Denver, Colorado.

VALLEY AND RIDGE THRUST BELT

Plate 2

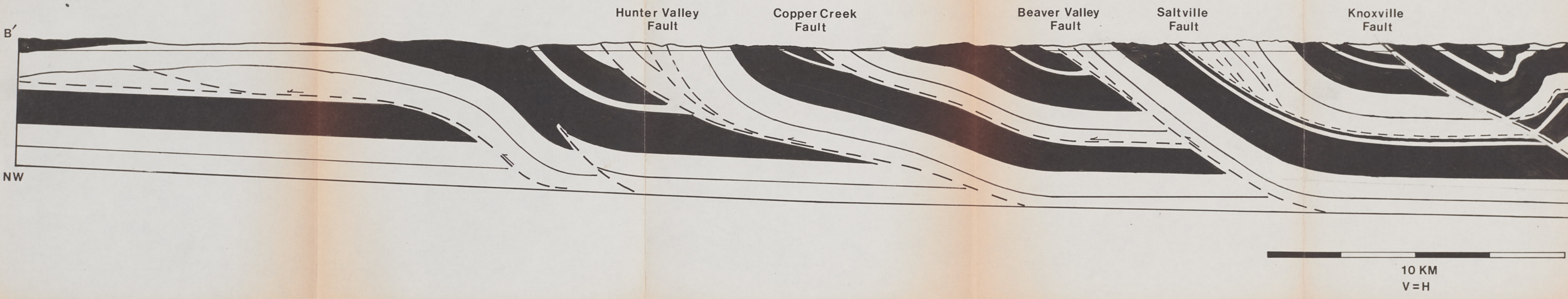

VALLEY AND RIDGE THRUST BELT

Plate 2